National Institute of Electricity and Electronics
INELEC - BOUMERDES
DEPARTMENT OF RESEARCH

THESIS

Presented in partial fulfilment of the requirements of the

DEGREE OF MAGISTER

in Electronic Systems Engineering

by

Samir DAHMANI

Hybrid-Mode Modeling of MIC's and MMIC's with Absorbing Boundaries

Defended on September 29, 1997 before the Jury :

President :	Dr. **A. FAREH**	(Maitre de Conference -ENP)
Supervisor:	Dr. **H. BOURDOUCEN**	(Maitre de Conference -INELEC)
Members :	Dr. **R. AKSAS**	(Maitre de Conference -ENP)
	Dr. **K. BENAISSA**	(Maitre de Conference -IAP-Boumerdes)
	Dr. **M. C. E. YAGOUB**	(Maitre de Conference -USTHB)

Registration number : 02/97

DEDICATION

This work is dedicated to :

- My parents,
- My Sisters, Brothers, and all family members.

ACKNOWLEDGMENTS

My sincere and deep gratitude to my supervisor Dr. H. BOURDOUCEN for his assistance, guidance, and valuable suggestions during the realization of this work.

My sincere gratitude is due to the president of the Jury, Dr. A. FARAH (Maitre de Conference-ENP-Algiers), and the members of the jury, Dr. R. AKSAS (Maitre de Conference-ENP-Algiers), Dr. A. BENAISSA (Maitre de Conference-IAP-Boumerdes), and Dr. M. C. E. YAGOUB (Maitre de Conference-USTHB-Algiers) for their kind acceptance to evaluate this work.

Special thank to Dr. K. HARICHE, the Head of the department of research, for his considerable support and help.

Special thank also to all my colleagues for their appreciated cooperation and encouragement in the achievement of this project, particularly, Mr. A. OUADI, the Semiconductors & Microwaves Laboratory team, and my home town English team.

I would like to acknowledge the INELEC staff particularly, the department of research staff, the Head of the planning department, and the library staff for their cooperation and support with the possible means and materials for the achievement of the present work.

ABSTRACT

The present work concerns the Full Wave analysis of open planar Microwave Integrated Circuits (MIC's) and Monolithic Microwave Integrated Circuits (MMIC's) based on Absorbing Boundary Conditions (ABC's), using the Method of Lines (MoL). The structures to be covered are of great interest in this field, such as, the single microstrip, the edge coupled lines, the broadside-coupled lines, the broadside-edge coupled lines and some other multi-strip waveguiding structures.

After introducing the two first chapters, about the MoL technique and the ABC operators, the matching of the Absorbing Boundary operators to the Method of Lines is carried out. Using the MoL modeling, the lateral equations are considered to satisfy the ABC operator. Hence, a system of ordinarily differential equations is obtained through the introduction of some appropriate transformations. Then, the complete characterization of zero thickness and finite thickness strips microwave structures is conducted for isotropic and anisotropic structures using both uniform and nonuniform discretization schemes. Finally, a software package has been implemented using this mathematical development to characterize the aforementioned structures.

TABLE OF CONTENTS

GENERAL INTRODUCTION

The field of microwaves, which extends over the gigahertz region of the electromagnetic spectrum corresponding to wavelength of a few decimeters to a few millimeters, was traditionally used for radars which require high directivity antennas and adequate reflections from obstacles. Later, the use of microwaves was extended to communications, in particular with satellites and faraway space probes. In the recent years, a strong core of application exists for microwave frequencies such as point to point multichanal links, microwave spectroscopy, mobile communication systems, microwave/millimeter-wave video distribution systems (MVDS), microwave transceivers for optical fiber transmission, microwave instrumentation, local area networks, medical and industrial microwave heating, and other numerous applications.

At microwave frequencies, the basic circuit elements are transmission lines. These are made of conducting strips deposited upon a dielectric substrate, they are called Microwave Integrated Circuits (MIC). In the case the substrate is made of semiconductors, in which active devices are fabricated by diffusion or ion implantation, the resulting structures are then called Monolithic Microwave Integrated Circuits (MMIC) [1]. The main advantages of using MIC and MMIC structures are reduced dimensions and weight, large scale fabrication, increased reliability by reducing the number of connections and precise reproducibility of the integrated system, modern and small sized structures.

The wide spread use of integration methods, combined with the development in GaAs technology and miniaturization have led to MIC and MMIC structures whose dimensions are much smaller than the signal wavelength. When MIC structures have dimensions which are smaller than the wavelength of the transmitted signal, then they can be satisfactorily analyzed on the basis of inline voltages and currents, or in short the Quasi Static Analysis. When the frequency goes higher, and therefore, the wavelength becomes smaller, it becomes necessary to set up a rigorous and complete electromagnetic field solution based on the Full Wave Analysis [2].

In parallel with this rapid development, numerical characterizations and modeling of guided-wave passive components have been a new challenge to electromagnetic field theoreticians. This is due to the complexity and development in millimeter wave integrated circuits and monolithic integrated circuits. It is no longer economical, or even feasible, to tune the circuits once they are fabricated. Therefore, extremely accurate characterization methods are needed to model the structures. Because most today's MIC and MMIC structures are not amenable to closed-form analytical expressions, almost all the mathematical techniques capable of rigorously predicting the basic circuit parameters are either numerical or pseudo-numerical techniques. These techniques can be qualified by means of a set of criteria such as computing efficiency, accuracy, ease of use, memory requirement, generality, and reliability.

Since the advent of microwave integrated circuits, a number of methods have been invented and the classical ones have been refined for these modern structures [3]. Some of the famous methods used in the analysis of MIC structures are the Finite Difference Method based on discretizing the structure into nodes, the Finite Element Method where the discretization are taken over small elements, the Mode Matching Technique and other methods such as the Conformal Mapping, the Matrix Inversion Method and the Integral Equation Technique are used. These methods present some deficiency and limitations such as the need of a prior knowledge of the field, the convergence is not assured, which lead to spurious solutions occurrence, the long calculation time required, and the large memory needed due to the nature of the discretization schemes used [3,4].

Another method that can be used is the Method of Lines [5,6]. One of the recent methods introduced in analyzing MIC and MMIC structures [7,8]. This method is semi-analytical, where the differential equations to be solved are discretized in all the variables letting only one in its analytical form. Hence, the solution is given along lines. This aspect leads to less discretization effort and a lesser number of equations, where precious time and memory requirements are gained over the previously stated methods. Furthermore, this method does not suffer from relative convergence or spurious solutions as it is the case in the Mode Matching Technique due to the Fourier series truncation as well as it does not necessitate the prior knowledge of the fields to be calculated.

This method has been extensively used in analyzing closed MIC and MMIC structures in both Quasi-Static [9,10] and Full Wave [11,35]. The former is used in structures supporting TEM waves operating at low frequency range and the latter is used at higher microwave and

millimeter wave frequencies, where the used wavelength is of the order of the structure spatial dimensions. It has been firstly used in two-dimensional wave propagation in waveguides in 1980 [7], then, it has been extended to three dimensional problems in 1984 [12]. After that, it has been applied to the parallel multi-conductor multi-layer structures and crossing conductors in both quasi static and full wave analysis, and to some other structures in 1987 [13] and in 1990 [14].

Generally, the analyzed MIC and MMIC structures are assumed to be enclosed within a metallic shielding. Therefore, the well known Closed Boundary conditions (Dirichlet-Neumman) are used. This requires not only the specifications of the microstrip and the characteristics of the dielectric, but one must precisely specify also the box dimensions.

The analysis and data are most often reported for open microstrips [15], with the usual assumption that both the substrate and the ground plane extend to infinity in the transverse direction, so that the characteristic impedance and the effective permittivity are not affected by the radiation effect of the walls. Hence, the larger are the dimensions of the closed structure in the simulation, the more accurate and realistic data could be achieved. But, increasing the size of the structure will lead to an increase in the problem simulation. This generates a disadvantage in both memory and time requirements.

To overcome this problems, and to analyze the actual open structures, one can use the concept of Absorbing Boundary Conditions (ABC), which are operators derived to simulate the existence of artificial boundaries that minimize reflections from the edges of the computational domain (i.e. an artificial box boundaries) [16,17].

Thus, the present work concerns the Full Wave analysis of open planar Microwave Integrated Circuits and Monolithic Microwave Integrated Circuits structures based on Absorbing Boundary Conditions (ABC), using the Method of Lines (MoL). The structures to be covered are of great interest in this field, such as, the single microstrip, the edge coupled lines, the broadside coupled lines, the broadside-edge coupled lines and some other multi-strip structures. The material covered in this thesis will be presented as follows:

Chapter one concerns the numerical tool to be used in the analysis of open microwave structures, which is the Method of Lines. The basic principles and the modeling procedure of this method is illustrated over a closed microwave structure in both uniform and non-uniform schemes.

The absorbing boundary conditions operators and their theory are introduced in chapter two. They are divided into two major classes. The first class is the mode annihilating operators which are based on annihilating higher order modes in the far field expansion of the wave solution. The second class consists of the one-way wave equation operators, which are differential equations describing wave propagation in a given direction. These two types of operators are used regarding the numerical method that best suits for their formulation. In using the Method of Lines, the one way-wave equation is shown to be most convenient.

After having introduced the two previous chapters, the matching of the Absorbing Boundary Condition operators to the Method of Lines is discussed in chapter three. The one-way wave equation operator is taken to describe the wave propagating outwards at the walls of an artificial enclosure of open microstrip structures. Using the Method of Lines modeling, the two limit equations are taken to satisfy the ABC operators. Hence, a system of ordinary differential equations is obtained through the introduction of some appropriate transformations.

Chapter four is devoted to the complete characterization of microwave structures having zero thickness strips. The field transfer relations between the dielectric layer interfaces are firstly deduced, and then, the field matching equations are studied for simple and complex structures where a final characteristic equation is established for each structure, from which the propagation constant is calculated. A wide set of microwave structures can be characterized using this development, such as, single microstrip, edge coupled, broadside coupled, broadside-edge coupled structure, and other multi-layer multi-conductor structures.

In current MMIC's, the metallization thickness cannot be neglected compared with the conductor width or the slot width. Thus, the consideration of the finite metallization thickness is presented in the last chapter, in which a new set of difference operators are introduced to describe the field behavior at the level of the intermediate finite metallization regions. In a similar manner to the zero thickness case, all of the fields transfer equations and fields matching equations are established. Nevertheless, using these results, the structures described for the zero thickness case can be efficiently handled.

Finally, a general conclusion about this work is presented, and the most important features of the frequency dependent characteristics of the aformentioned structures are discussed.

Chapter 1

THE METHOD OF LINES

1.1 INTRODUCTION

Many numerical methods are used in analyzing microwave and millimeter wave structures such as the Finite Difference Method, the Finite Element Method, and the Mode Matching Technique. The present work is based on a semi-analytical numerical method, the Method of Lines.

It is one of the powerful numerical tools used for the analysis of planar and quasi-planar waveguiding structures. It has been developed by mathematicians in order to solve partial differential equations [5,6]. In 1980 [7], it has been introduced in the field of microwave and millimeter-wave engineering by Pregla *et al* for the calculation of frequency dependent characteristics of single and multi-dielectric substrates with metallic interfaces. It was then generalized to discontinuities, interconnections, and finite thickness strips structures for constant and arbitrary cross sections in both Full-Wave and Quasi-Static approaches [9-14].

The Method of Lines has certain similarities with some of the existing methods such as the Mode Matching and the Finite Difference Methods. It has shown some extra features mainly, saving much computing time and assured optimal convergence, if the strip edges are located in the right position between the discretization lines. Using this method, the planar and quasi-planar waveguides can be analyzed accurately, and in an easy way, where the problems encountered with some other methods such as the convergence in the Mode Matching Technique does not occur [11].

The objective of this chapter is to introduce the relatives of the method of lines, their use, and its application for the analysis of microwave and millimeter wave structures. And, that is by applying the Method of Lines in both uniform and nonuniform discretization on structures subject to the known Closed Boundary conditions, Dirichlet or Neumann.

1.2 PRINCIPLE OF THE METHOD OF LINES

The method of lines consists of transforming a second order system of partial differential equations into a system of second order ordinary differential equations by applying the Finite Difference approximation to their partial differentials, letting only one variable in its analytical form. For the analysis of waveguides with constant cross section, this procedure has to be done only with respect to one coordinate direction.

The discretization of the partial differential equation, means that the field is considered on straight lines that are perpendicular to the interfaces between the different layers. These lines may be equidistant or nonequidistant over the cross section depending on the considered discretization procedure. In the case of a single microstrip, and because of symmetry, only a half of the cross section can be considered.

For instance, in the Quasi-Static analysis, only one line system discretization procedure is needed to represent the potential function over the whole structure. Whereas, for the Full Wave approach, which is of interest, a system of two-separate-lines is used to describe both the electric field e_z and the magnetic field h_z due to the Closed Boundary conditions that are immediately fulfilled if the lines are in the right positions with respect to the lateral boundaries.

For the Full Wave analysis, and in order to have the Dirichlet condition for example, it is better to put a line on the lateral boundary and set the corresponding field component to zero. In the subsequent calculation, it is not necessary to carry on along this field component. Also, the Neumann condition is easily satisfied by including a boundary between two consecutive lines and equating the fields components. The shifting two lines system has many other advantages than those related to the boundary mainly, optimal edge positioning, reduction of the discretization error, and ease of quantitative description that will be discussed in the following sections [11].

1.3 DESCRIPTION OF THE DISCRETIZATION SCHEME

To introduce the method of lines discretization scheme in solving partial differential equation, the second order differential equation which is the wave equation is taken as an example. Let us consider the closed boundary structure as shown in Fig. 1.1. The structure is composed of two dielectric layers within closed boundaries of a rectangular form, and a microstrip conductor is placed at the interface of the two dielectric layers.

If we consider the full wave analysis of this structure, the wave equation is given by the following second order partial differential equations

$$\begin{aligned} \frac{\partial^2 \Psi^e}{\partial x^2} + \frac{\partial^2 \Psi^e}{\partial y^2} + \frac{\partial^2 \Psi^e}{\partial z^2} + k^2 \Psi^e = 0 \\ \frac{\partial^2 \Psi^h}{\partial x^2} + \frac{\partial^2 \Psi^h}{\partial y^2} + \frac{\partial^2 \Psi^h}{\partial z^2} + k^2 \Psi^h = 0 \end{aligned} \qquad (1.1)$$

where :

$$k^2 = \varepsilon_r k_0^2 \quad ; \quad k_0 = \omega\sqrt{\mu_0 \varepsilon_0} \qquad (1.2)$$

which describe the behavior of the electric and the magnetic fields presented respectively by the related functions Ψ^e and Ψ^h within the (x, y) discretization plane of the closed structure. Using the Method of Lines, which is based on the discretization of all the existing variables in the differential equation letting only one variable in its analytical form. If we consider the two dimensional problem as shown in Fig. 1.1, the variable x is being discretized, while the variable y is let in its analytical form. The related electric and magnetic field functions will be given by the solutions of the wave equation along the discretization lines. Given Ψ^v, where v stands for either the electric or magnetic related function in the form,

$$\Psi^v = \Psi_0^v(x, y) e^{(-j k_z z)} \qquad (1.3)$$

where, the wave propagation is assumed to be in the z-direction. The discretization of equ.(1.3) allows the following transformation,

$$\Psi^v(x, y)\Big|_{x_i} \rightarrow \Psi_i^v(y) \qquad (1.4)$$

where x_i is the position of the line along the discretized axis.

In order to match the boundary conditions, the lateral electric field lines are put on the metallic enclosure, whereas its value is taken to be zero. On the other hand, the magnetic field lines are considered at the two adjacent left and right lines of the metallic enclosure with equal quantities. These lines must be continuous along the layers of the structure for the sake of field matching in the continuity study at the layers interfaces.

To get an expression of these field lines for the structure of Fig. 1.1, the Method of Lines can be used in either uniform or nonuniform discretization schemes.

1.4 UNIFORM DISCRETIZATION ANALYSIS

Using uniform discretization, the discretized variable, in our case the x variable, is divided into $n-1$ equidistant intervals h. For the electric field lines the position of the lines will be given according to the following relation:

$$x_i = ih \quad ; \quad i = 0,1,\ldots,n+1 \tag{1.5}$$

where x_{n-1} is the dimension of the structure, and the positions of the magnetic field lines are calculated to be in the middle between the electric field lines. See Fig. 1.1.

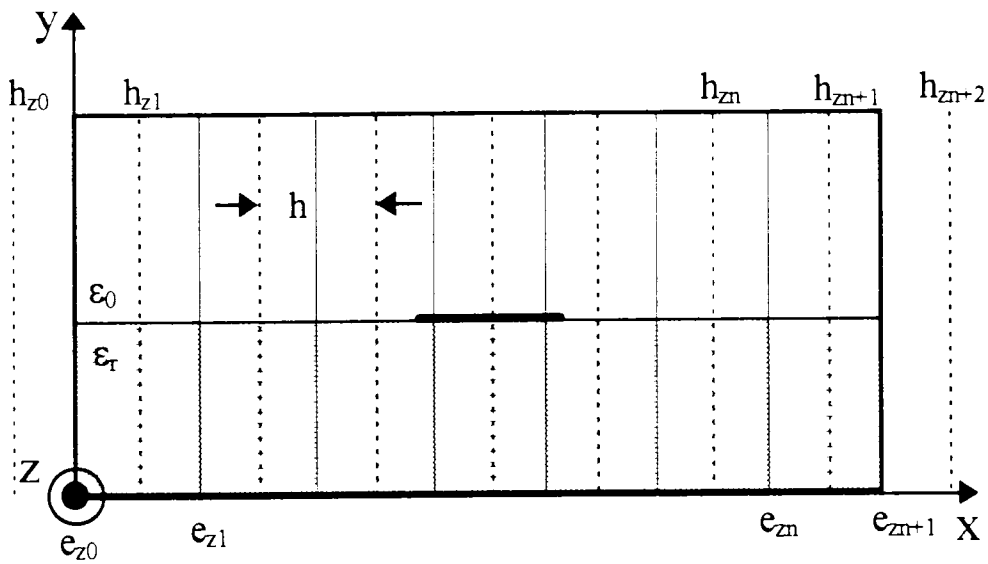

Fig. 1.1 Discretization scheme of a closed microstrip structure

Using equ.(1.3), the Helmholtz relation given by equ.(1.1) reduces to,

$$\left(\frac{\partial^2}{\partial x^2} + \frac{\partial^2}{\partial y^2} + (k^2 - k_z^2)\right)\Psi^v = 0 \tag{1.6}$$

By introducing the notation of equ.(1.4), which describes the discretized fields related solutions along the discretized lines, and applying the central difference approximation to the first order derivatives of the field functions at the i^{th} line of the discretization scheme, we get a relation for the electric field as:

$$\left.\frac{\partial \Psi^e}{\partial x}\right|_i = \frac{\Psi^e_{i-1} - \Psi^e_i}{h} \quad ; \quad i=0,\ldots,n \tag{1.7}$$

defined at the position of the magnetic field lines between the two electric field lines indexed by the subscripts (i, $i-1$). And similarly, for the magnetic field first derivatives approximation, we get

$$\left.\frac{\partial \Psi^h}{\partial x}\right|_i = \frac{\Psi^h_{i-1} - \Psi^h_i}{h} \quad ; \quad i=0,1,\ldots,n+1 \tag{1.8}$$

defined at the position of the electric field lines between the two magnetic field lines indexed by the subscripts (i, $i-1$). Where h is the discretization step for both electric and magnetic lines in the uniform discretization.

For the second order partial differentials, the first order finite difference approximation can be evaluated using the same idea as before, resulting into the following form:

$$\left.\frac{\partial^2 \Psi^e}{\partial x^2}\right|_i = \frac{\left.\frac{\partial \Psi^e}{\partial x}\right|_i - \left.\frac{\partial \Psi^e}{\partial x}\right|_{i-1}}{h} \quad ; \quad i=1,\ldots,n \tag{1.9}$$

when it is evaluated at the position i of the electric field line, and

$$\left.\frac{\partial^2 \Psi^h}{\partial x^2}\right|_i = \frac{\left.\frac{\partial \Psi^h}{\partial x}\right|_i - \left.\frac{\partial \Psi^h}{\partial x}\right|_{i-1}}{h} \quad ; \quad i=1,\ldots,n+1 \tag{1.10}$$

when evaluated at the position i of the magnetic field line.

If we proceed in rearranging this last two equations (1.9) and (1.10) by using the above results of the first order approximation in eqs.(1.7) and (1.8), we end up with a new second-order finite difference approximation with the following form,

$$\left.\frac{\partial^2 \Psi^e}{\partial x^2}\right|_i = \frac{\Psi^e_{i-1} - 2\Psi^e_i + \Psi^e_{i-1}}{h^2} \quad ; \quad i=1,\ldots,n \tag{1.11}$$

and

$$\left.\frac{\partial^2 \Psi^h}{\partial x^2}\right|_i = \frac{\Psi^h_{i-1} - 2\Psi^h_i + \Psi^h_{i-1}}{h^2} \quad ; \quad i=1,\ldots,n+1 \tag{1.12}$$

Now, substituting the last two eqs.(1.11) and (1.12) into the second order partial differential equation equ.(1.6), we get a new differential equation expressed in terms of finite difference approximations for the field functions with respect to the discretized variable x as,

$$\frac{\partial^2 \Psi^e_i}{\partial y^2} + \frac{\Psi^e_{i-1} - 2\Psi^e_i + \Psi^e_{i-1}}{h^2} + (k^2 - k_z^2)\Psi^e_i = 0 \quad ; \quad i=1,\ldots,n \tag{1.13}$$

and

$$\frac{\partial^2 \Psi^h_i}{\partial y^2} + \frac{\Psi^h_{i-1} - 2\Psi^h_i + \Psi^h_{i-1}}{h^2} + (k^2 - k_z^2)\Psi^h_i = 0 \quad ; \quad i=1,\ldots,n+1 \tag{1.14}$$

If we construct the complete system of differential equations for all the discretized lines, we get for the electric field related function

$$\frac{d^2 \Psi^e}{d y^2} + \left((k^2 - k_z^2)I - \frac{1}{h^2} P^e\right)\Psi^e = 0 \tag{1.15}$$

and for the magnetic related function

$$\frac{d^2 \Psi^h}{d y^2} + \left((k^2 - k_z^2)I - \frac{1}{h^2} P^h\right)\Psi^h = 0 \tag{1.16}$$

where

$$\begin{aligned} \Psi^e &= (\Psi^e_1, \ldots\ldots, \Psi^e_n)^t \\ \Psi^h &= (\Psi^h_1, \ldots\ldots, \Psi^h_{n-1})^t \end{aligned} \tag{1.17}$$

and the second-order difference operator matrices P^e and P^h are given according to the boundary conditions at the lateral limits of the structure. Accordingly, in the case of closed boundary structures, two possible conditions are possible at each lateral edge; either Neumann or Dirichlet conditions that fulfill the following condition

Electric wall: $e_z = 0$ (Dirichlet condition); $\frac{\partial h_z}{\partial n} = 0$ (Neumann conditions)

Magnetic wall: $h_z = 0$ (Dirichlet condition); $\frac{\partial e_z}{\partial n} = 0$ (Neumann conditions)

n is the direction of the normal on the corresponding wall

Since the matrix P^v is a tridiagonal matrix, then there exists a non-singular matrix T such that P^v can be transformed into a diagonal matrix as

$$\lambda^v = T_v^t P^v T_v \tag{1.18}$$

where λ_i are the eigen values of P^v, and T is the matrix of the corresponding eigen vectors, and T^t its transpose. Moreover, T and T^t satisfy the orthogonality relation ($T.T^t$=I), where I is the identity matrix.

Using these transformations, the systems (1.15) and (1.16) of coupled differential equations can be easily decoupled by premultiplying their both sides by T^t, to obtain

$$\frac{d^2}{dy^2}(T_e^t \Psi^e) + \left((k^2 - k_z^2)I - \frac{1}{h^2}(T_e^t P^e T_e)\right)(T_e^t \Psi^e) = 0 \tag{1.19}$$

and

$$\frac{d^2}{dy^2}(T_h^t \Psi^h) + \left((k^2 - k_z^2)I - \frac{1}{h^2}(T_h^t P^h T_h)\right)(T_h^t \Psi^h) = 0 \tag{1.20}$$

or simply, by making a change of variables, and get

$$\frac{\partial^2 \overline{\Psi}^v}{\partial y^2} - K_v^2 \overline{\Psi}^v = 0 \tag{1.21}$$

where

$$K_v^2 = -\left(\frac{\lambda^v}{h^2} + (k^2 - k_z^2)\right) \tag{1.22}$$

with

$$\overline{\Psi}^v = T_v^t \Psi^v \tag{1.23}$$

which are the transformed electric and magnetic related function vectors.

The general solution of the above second order ordinary canonical form of equ.(1.21) is given by

$$\overline{\Psi}^{v} = C_1^{v} \cosh\left(K_v y\right) + C_2^{v} \sinh\left(K_v y\right) \tag{1.24}$$

from which, the general solution for the i^{th} line is found to be

$$\overline{\Psi}_i^{v} = C_{1i}^{v} \cosh\left(k_{vi} y\right) + C_{2i}^{v} \sinh\left(k_{vi} y\right) \tag{1.25}$$

where C_i^{v} are arbitrary constants related to the boundary conditions.

The main disadvantage of the uniform discretization is the fact that the number of lines in regions with high field concentration is the same as in those with low field concentration. This problem affects significantly the accuracy of the results in the singularity regions, and particularly the fields at the edges of the conductor strips. In order to solve this problem, a nonuniform discretization procedure should be used.

1.5 EDGE POSITIONING CONDITIONS

As it has been mentioned previously in section.1.2, the line positioning is very important for convergence of the solution, as it is the main parameter in defining the rate of convergence [18]. In this section a brief overview about the positioning of the discretization lines at the edges of the strips for both electric and magnetic lines is presented.

In other methods such as the Mode Matching Technique, the solution may converge towards a wrong value known as the relative convergence if the edge condition of the metallic strips is violated [19,20]. On the contrary, the convergence using the Method of Lines is always assured. However, at the vicinity of the strip edges, where field singularities occur, large discretization errors may arise. To minimize this error, an optimal edge positioning of the metallic edge relative to the lines given by the edge parameter p or q must be examined [18]. (See Fig. 1.2.)

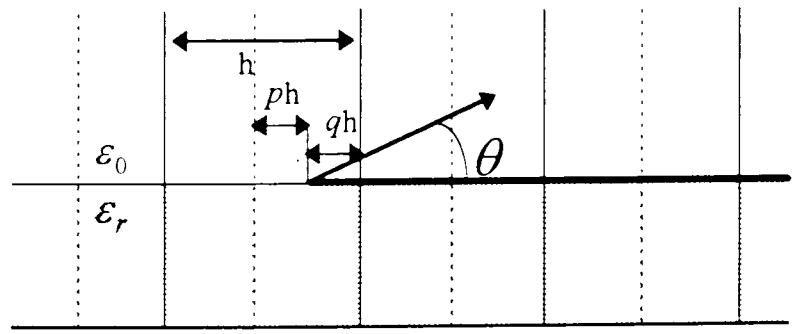

discretization lines : e_z —— h_z ·····

Fig. 1.2 Edge positioning

According to references [11,19], It is found that the solution for p and q conditions is p=q=0.25. This result proves one of the advantages of the two lines shifting system that is required for fast convergence. The value for the edge parameter found here is only valid for relatively infinite long edges. In the case of finite edge length, as *e.g.* for resonator structures, the edge parameter must be redetermined for each structure.

Finally, if the discretization lines are placed at the correct positions from the edges, the convergence of the solution is guaranteed with low computation effort. Whereas, if the edge parameter is not chosen optimally, the solution always converges, but with a bit more of computational effort. Hence, in the case of uniform discretization, it is recommended that the first discretization line on the strip is at a distance equal to 0.25h from the edge of the strip (h is the interval width for the uniform discretization). The same thing holds for the nonuniform discretization.

1.6 NON-UNIFORM DISCRETIZATION ANALYSIS

Due to the singularities in electromagnetic fields and current densities at the edges of the strip conductors, in the analysis of MIC and MMIC structures, the discretization step should be small enough to model accurately these singularities. When the uniform discretization is used, this small discretization step is generalized over the whole structure even in regions where no singularities are present. This leads to a great need in both time and memory due to the increase in the total number of lines. To solve this problem, the nonuniform discretization is proposed. It consists of discretizing the structure using different discretization steps. Hence, the step is very small at the edge of a conductor strip as compared to regions where no singularities occur[21], see Fig. 1.3.

The nonuniform modeling procedure is similar to the one described above for the uniform case. Consider the discretization scheme of Fig. 1.3, the intervals between two adjacent electric field lines are denoted by h_i and the intervals between two adjacent magnetic field lines by e_i.

The first order partial derivatives of the function Ψ^e are evaluated at the middle of the intervals h_i, whereas, the second order partial differentials of the function Ψ^e are evaluated at the middle of the intervals e_i. The same thing holds for the Ψ^h function, *i.e.* its first order partial derivatives are evaluated at the middle of the intervals e_i, whereas its second order partial differentials are evaluated at the middle of the intervals h_i, as it is shown in Fig. 1.3.

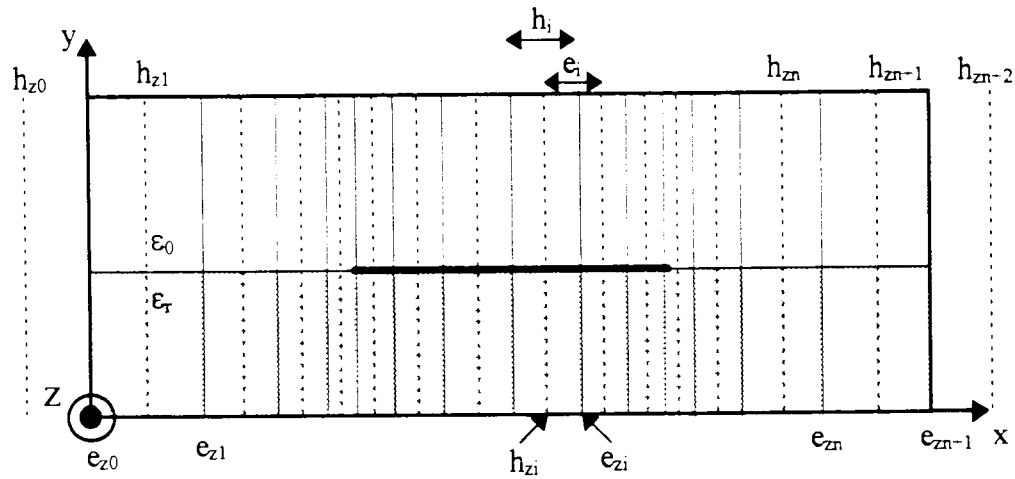

Fig. 1.3 Non-uniform discretization scheme

Using eqs.(1.3) and (1.4) for the discretized function representation, the first order partial differential can be transformed using the first order difference approximation as

$$\left.\frac{\partial \Psi^e}{\partial x}\right|_i = \frac{\Psi^e_{i-1} - \Psi^e_i}{h_i} \quad ; \quad i=0,\ldots,n \tag{1.26}$$

and

$$\left.\frac{\partial \Psi^h}{\partial x}\right|_i = \frac{\Psi^h_{i-1} - \Psi^h_i}{e_i} \quad ; \quad i=0,\ldots,n-1 \tag{1.27}$$

where, h_i and e_i are the interval widths for both electric and magnetic lines respectively, see Fig. 1.3.

For the second order partial differentials, the first order finite difference approximation can be evaluated, resulting to the following form

$$\left.\frac{\partial^2 \Psi^e}{\partial x^2}\right|_i = \frac{\left.\frac{\partial \Psi^e}{\partial x}\right|_i - \left.\frac{\partial \Psi^e}{\partial x}\right|_{i-1}}{e_i} \quad ; \quad i = 1,\ldots,n \tag{1.28}$$

and

$$\left.\frac{\partial^2 \Psi^h}{\partial x^2}\right|_i = \frac{\left.\frac{\partial \Psi^h}{\partial x}\right|_i - \left.\frac{\partial \Psi^h}{\partial x}\right|_{i-1}}{h_i} \quad ; \quad i =1,\ldots,n-1 \tag{1.29}$$

In the case of non-uniform discretization, we proceed in rearranging eqs(1.26) and (1.27) in order to get symmetrical operators to facilitate the diagonalization operation. Hence, we write the previous relations on the following form [21],

$$\sqrt{\frac{h_i}{h}}\left(h\left.\frac{\partial \Psi^e}{\partial x}\right|_i\right) = \sqrt{\frac{h}{h_i}}\,(\Psi^e_{i-1} - \Psi^e_i) \quad ; \quad i=0,\ldots,n \tag{1.30}$$

for the electric field, and

$$\sqrt{\frac{e_i}{h}}\left(h\left.\frac{\partial \Psi^h}{\partial x}\right|_i\right) = \sqrt{\frac{h}{e_i}}\,(\Psi^h_{i-1} - \Psi^h_i) \quad ; \quad i=0,\ldots,n+1 \tag{1.31}$$

for the magnetic field, where h is the equivalent interval in the case of a uniform discretization procedure.

If we consider a lateral boundary conditions for the structure to be analyzed such as the Dirichlet condition, we have the following condition on the two lateral boundaries

$$\Psi_0^e = \Psi_{n-1}^e = 0$$

Hence, the two first order differential equations of equ.(1.30) for the electric field at these two lateral electric walls can be expressed as

$$\sqrt{\frac{h_0}{h}}\left(h\frac{\partial \Psi^e}{\partial x}\bigg|_0\right) = \sqrt{\frac{h}{h_0}}\,\Psi_1^e \qquad ; \qquad i = 0 \tag{1.32}$$

and

$$\sqrt{\frac{h_n}{h}}\left(h\frac{\partial \Psi^e}{\partial x}\bigg|_n\right) = -\sqrt{\frac{h}{h_n}}\,\Psi_n^e \qquad ; \qquad i = \mathrm{n} \tag{1.33}$$

In the same way, we can apply eqs.(1.30) and (1.31) to the remaining first order differentials at each line for both electric and magnetic functions. Hence, the result for the set of equations can be expressed in a matrix form as

$$\begin{aligned} h\, r_h^{-1}\Psi_x^e &= r_h\, D\, \Psi^e \\ h\, r_e^{-1}\Psi_x^h &= -r_e\, D^t\, \Psi^h \end{aligned} \tag{1.34}$$

where

$$\begin{aligned} \Psi^e &= (\Psi_1^e, \ldots\ldots, \Psi_n^e)^t \\ \Psi^h &= (\Psi_1^h, \ldots\ldots, \Psi_{n-1}^h)^t \end{aligned} \tag{1.35}$$

are the electric and magnetic related vector functions.

The matrix operator D, is the first order difference operator and its form is related to the boundary conditions used at the lateral limits, whereas, the two normalizing operators r_h and r_e given by

$$r_h = diag\left(\sqrt{\frac{h}{h_i}}\right)$$
$$r_e = diag\left(\sqrt{\frac{h}{e_i}}\right) \qquad (1.36)$$

are diagonal matrices.

In the same way, and using the same procedure as above, the second order difference equations can be expressed as follows

$$\sqrt{\frac{e_i}{h}}\left(h\frac{\hat{c}^2\Psi^e}{\hat{c}x^2}\bigg|_i\right) = \sqrt{\frac{h}{e_i}}\left(\frac{\hat{c}\Psi^e}{\hat{c}x}\bigg|_i - \frac{\hat{c}\Psi^e}{\hat{c}x}\bigg|_{i-1}\right); \qquad i = 1,\ldots,n \qquad (1.37)$$

and

$$\sqrt{\frac{h_i}{h}}\left(h\frac{\hat{c}^2\Psi^h}{\hat{c}x^2}\bigg|_i\right) = \sqrt{\frac{h}{h_i}}\left(\frac{\hat{c}\Psi^h}{\hat{c}x}\bigg|_i - \frac{\hat{c}\Psi^h}{\hat{c}x}\bigg|_{i-1}\right); \qquad i = 1,\ldots,n+1 \qquad (1.38)$$

Similarly, equ.(1.34) and eqs.(1.37-38) can be applied to the whole discretized structure, and we end up with a system of equations for both electric and magnetic fields related functions that can be presented in a matrix form as follows

$$h\, r_e^{-1}\Psi^e_{xx} = -r_e\, D^t\, \Psi^e_x$$
$$h\, r_h^{-1}\Psi^h_{xx} = -r_h\, D\, \Psi^h_x \qquad (1.39)$$

where $\Psi^{e,h}_{xx}$ are the second order finite difference approximation vectors.

A second order difference operators can be found for the second order differentials of equ.(1.39). Using the following notation for the normalized first order difference operator

$$D_x = r_h\, D\, r_e \qquad (1.40)$$

and introducing the normalized electric and magnetic related vector functions

$$\Phi^{e,h} = r_{e,h}^{-1}\,\Psi^{e,h}$$
$$\Phi^{e,h}_{xx} = r_{e,h}^{-1}\,\Psi^{e,h}_{xx} \qquad (1.41)$$

eqs.(1.37) and (1.38) are rewritten using the above notation as

$$h^2 \Phi_{xx}^{e,h} = D_{xx}^{e,h} \Phi^{e,h} \tag{1.42}$$

with

$$\begin{aligned} D_{xx}^{e} &= -D_x^t D_x \\ D_{xx}^{h} &= -D_x D_x^t \end{aligned} \tag{1.43}$$

where, the new normalized electric and magnetic related functions Ψ^e and Ψ^h are given by

$$\Phi^e = \left(\frac{\Psi_1^e}{\sqrt{\frac{h}{e_1}}}, \ldots\ldots, \frac{\Psi_n^e}{\sqrt{\frac{h}{e_n}}} \right)^t \tag{1.44}$$

$$\Phi^h = \left(\frac{\Psi_1^h}{\sqrt{\frac{h}{h_0}}}, \ldots\ldots, \frac{\Psi_{n+1}^h}{\sqrt{\frac{h}{h_{n-1}}}} \right)^t \tag{1.45}$$

To solve the Helmholtz equation (1.6) using the non-uniform discretization procedure, the discretization is considered in only one direction (the x-direction). Using the relation given by equ.(1.42), its second order differential derivatives will be transformed into a second order ordinary differential equation as

$$\frac{d^2 \Phi^{e,h}}{dy^2} + \frac{D_{xx}^{e,h} \Phi^{e,h}}{h^2} + (k^2 - k_z^2) \Phi^{e,h} = 0 \tag{1.46}$$

Note that the operators $D_{xx}^{e,h}$ are real and symmetric. On the other hand, these operators are tridiagonal, which means, that the electric and magnetic related vector components are coupled to each other. By an appropriate orthogonal transformation, the system of equations (1.46) can be decoupled by transforming the two operators $D_{xx}^{e,h}$ into two diagonal matrices of eigen values defined as

$$\lambda^{e,h} = T_{e,h}^t D_{xx}^{e,h} T_{e,h} \tag{1.47}$$

where

$$\lambda^{e,h} = diag(\lambda_i^{e,h}) \tag{1.48}$$

Taking into account the transformations expressed by equ.(1.47), the systems of the coupled differential equations (1.46) are transformed into a decoupled system of differential equations as

$$\frac{d^2\overline{\Phi}^{e,h}}{dy^2} + \left(\frac{\lambda^{e,h}}{h^2} + (k^2 - k_z^2)\right)\overline{\Phi}^{e,h} = 0 \tag{1.49}$$

where the transformed electric and magnetic related functions $\overline{\Phi}^{e,h}$ are given by

$$\overline{\Phi}^{e,h} = T_{e,h}^{t}\Phi^{e,h} \tag{1.50}$$

Now, letting

$$K_{e,h}^2 = -\left(\frac{\lambda^{e,h}}{h^2} + (k^2 - k_z^2)\right) \tag{1.51}$$

the system (1.49) will be presented in the following canonical form of a second order differential equations

$$\frac{d^2\overline{\Phi}^{e,h}}{dy^2} - K_{e,h}^2\overline{\Phi}^{e,h} = 0 \tag{1.52}$$

where the general solution of the above system (1.52) is given by equ.(1.24).

1.7 NON-UNIFORM DISCRETIZATION ALGORITHM

In order to get a minimum error due to the discretization procedure, the intervals between the lines have to be small enough in regions where the variations of the function are considerable, whereas larger intervals will be selected in regions where the function variations are small.

To that purpose, there are two main procedures to establish the nonuniform discretization to describe the spatial variation of the discretization function, which are the sinusoidal and the geometrical discretizations. For the first type, the sinusoidal discretization [21,13], the lines are distributed sinusoidally on the intervals h_i given by the relation

$$h_i = x_{i-1} - x_i \tag{1.53}$$

where

$$x_i = \sin\left(\frac{2i - M_n}{2M_n}\pi\right) \tag{2.54}$$

with M_n is the total number of lines on the n^{th} strip or slot.

This discretization procedure leads to a maximum number of lines near the strips edges due to the fields singularity. Hence, for a strip width of w_a=x_b-x_a placed at the interface y=0, the field lines will be having the following coordinates

$$x_i = \frac{x_b + x_a}{2} + \frac{x_b - x_a}{2}\sin\left(\frac{2i - M_n}{2M_n}\pi\right) \quad ; \qquad i = 1,\ldots,M_n \tag{1.55}$$

This distribution applies for the regions situated between the strips as well.

Given the width of the smallest interval found numerically by considering all the strips and the slots as,

$$\Delta = h_i = x_{M\,min} - x_{M\,min-1} \tag{1.56}$$

the number of lines on each strip or slot can be deduced from the relation (1.54) [13] as:

$$M_n = Int\left(\frac{2\pi}{\pi - 2\sin^{-1}\left(1 - \frac{2\Delta}{x_b - x_a}\right)}\right) \tag{1.57}$$

where *Int* designates the integer part.

The intervals h_i between the lines are calculated from equ.(1.55). On the other hand, the external slots which are bounded by the lateral walls are treated in the same way. To reduce the influence of the walls, we put them at distances double to that of the real width of these slots. Consequently, the intervals h_i will have their maximum value near the lateral walls of the metallic box.

The convergence rate of the method depends on the position of the lines that are located near the strip/slot edges. At each strip/slot edge, the last line associated to the slot preceding this strip and the first line on the strip are located respectively at $0.75h_i$ and $0.25h_i$. To take into account these conditions, and the considerable variations of the field functions near the strip

edges, the width of the intervals h_i on the strips are decreased by a reduction factor α [13] given by:

$$\alpha = \frac{w - \frac{2\Delta}{3}}{w} \tag{1.58}$$

where $w=x_b-x_a$.

Using the reduction factor α in calculating the new strip lengths, the intervals between the lines located at the exterior of the slots are interpolated.

1.8 CONCLUSION

In this Chapter, one of the numerical methods used in the analysis of planar and quasi-planar waveguide structures has been investigated. The Method of Lines basic principles and modeling procedure are shown through its application on the known Closed Boundary Conditions.

It has shown a lot of features, such as simplicity of handling the analysis of different waveguide structures, requires less computational time, and less memory space needed due to the analysis done along lines and not on points, mainly when analyzing the open boundary structures that will be discussed in the following chapters. Also, the convergence behavior is always assured when the edge conditions are satisfied.

A general introduction of the use of this method in the Full-Wave analysis of planar microwave structures is covered, and then, the two types of discretization schemes, *i.e.* uniform and nonuniform discretizations, are also presented.

Chapter 2

THEORY OF ABSORBING BOUNDARY CONDITIONS

2.1 INTRODUCTION

Because of the problem of artificial reflections in the simulation of wave propagation phenomena, where these reflections are introduced by the limits of the computational domain, the Absorbing Boundary Conditions operators were derived to minimize artificial reflections from the edges of the computational domain.

The theory of ABCs was first developed by Lysmer and Kuhlemeyer (1969). Then, many authors got interest in this field and developed a set of operators, called Absorbing Boundary Condition (ABC) operators or Radiation Boundary Condition (RBC) operators. Among these authors who defined a variety of ABCs, Engquist and Majda (1977), Mur (1981), Wagatta (1983), Lindman (1975), Randall (1988), Bayliss and Turkel (1980), Gunzburger and Turkel (1982), and Liao (1984) [22].

The idea behind this ABC's is that, in order to generate solutions that are unique, boundary conditions have to be imposed on the surface limits of the structure. But, in many applications the media are of infinite extent, and in this case, imposing boundary conditions on the surface of the structure may give rise to reflections that are not in the actual physical situations. Consequently, to simulate an infinite geometry, Absorbing Boundary Conditions are imposed at the surface limits to diminish these reflections, which reduces memory requirements as the size of the surface is made smaller.

For all the existing ABC's theories, we can distinguish two basic types of radiation boundary operators.

1-mode annihilating approximations.

2-one-way wave equation approximation.

Each of these two radiation boundary operators possesses different characteristics and forms.

2.2 MODE ANNIHILATING OPERATORS

The mode annihilating Absorbing Boundary Condition operator is based on the idea of annihilating the higher order terms in the far field series expansion, which is the expansion of the outward propagating solutions of the wave equation, by applying the Sommerfeld radiation condition at the boundary.

In this section, we start by introducing the first order boundary condition operator by applying the Sommerfeld radiation condition on the far field series expansion of a time harmonic solution, and then, we extend the boundary operators to higher order operators in both one and two dimensional cases.

2.2.1 Far-Field Expansion and the Sommerfeld Radiation Condition

In this part, the first order radiation operator is deduced by applying the Sommerfeld radiation condition on the far field expansion of the wave equation solutions.

Consider the solutions $u(R,\theta,\phi,t)$ of the Helmholtz equation given in operator form as

$$\nabla^2 u - u_{tt} = 0 \tag{2.1}$$

Equ.(2.1) can be rewritten, in the case where the solutions are considered to be a time-harmonic function, as

$$\nabla^2 u + k^2 u = 0 \tag{2.2}$$

where the solution has an exponential $e^{-j\omega t}$ time dependency.

According to reference [23], the radiating solutions of the wave equation, propagating in directions which are outward from the origin of a spherical coordinate system, can be expanded in a general convergent series of the form

$$u(R,\theta,\phi,t) = \sum_{i=0}^{\infty} \frac{f_i(t-R,\theta,\phi)}{R^i} \tag{2.3}$$

In the case where the function u is considered to be time-harmonic equ.(2.2), the expansion relation (2.3) can be extended to the time case [23] as

$$u(R,\theta,\phi) = \frac{e^{jkR}}{R}\sum_{i=0}^{\infty}\frac{f_i(\theta,\phi)}{R^i} \tag{2.4}$$

It is found that equ.(2.4) is a convergent expansion for the scalar wave functions that satisfy the Sommerfeld radiation condition [24], which is given by

$$\lim_{R\to\infty} R(u_R + u_t) = 0 \;\Leftrightarrow\; \lim_{R\to\infty} R(u_R - jku) = 0 \tag{2.5}$$

The Sommerfeld radiation condition is an operator, when applied to the far-field expansion of the time-harmonic function u, gives the following far-field asymptotic result

$$\left(\frac{\partial}{\partial R} - jk\right)u = o(R^{-2}) \tag{2.6}$$

in the limit $R \to \infty$.

The Sommerfeld radiation condition preserves the terms that are not greater than $o(R^{-2})$ in the expansion, whereas, the higher order terms are put equal to zero at the far-field limit. Hence, it can be considered as the first order Radiation Boundary Condition which describes the field behavior at the far-field limit. A more exact form of the Sommerfeld radiation condition is given by [16] as

$$\lim_{R\to\infty}\iint_{y=R}\left|\frac{\partial u}{\partial R} - iku\right|^2 ds = 0 \tag{2.7}$$

where the integral is over spherical shells centered at R=0.

2.2.2 Higher Order Operators

After having defined the first order Boundary Condition operator described by the asymptotic result of the far-field series expansion using the Sommerfeld radiation condition, higher order operators can be derived using the same series expansion. To achieve that, operators, that annihilate terms up to any order in the far-field expansion of u, were developed for the

expansion given by equ.(2.3) as a sequence of operators B_n, as given in reference [25]. Similar sequence of operators can be developed for time harmonic solutions in two dimensions [26]. The derivation of higher order operators B_n starts by multiplying a slightly modified version of $u(R,\theta,\phi)$ of equ.(2.4) by R^n and then, splitting the sum as follows

$$R^n u(R,\theta,\phi) = \sum_{i=0}^{n} R^{n-i} e^{jkR} F_i(\theta,\phi) + \sum_{i=n+1}^{\infty} R^{n-i} e^{jkR} F_i(\theta,\phi) \qquad (2.8)$$

Given the first order operator defined in equ.(2.6) as

$$L = \frac{\partial}{\partial R} - jk \qquad (2.9)$$

Applying the L^n operator to both sides of equ.(2.8) annihilates the first sum of the expression and makes the leading order term of the second sum to be $o(R^{-n-1})$. As a result to that, we get a new operator of the form

$$L^n (R^n u) = o(R^{-n-1}) \qquad (2.10)$$

which annihilates the first n-terms of the far field expansion of equ.(2.4). The operator in equ.(2.10) can be developed further to be expressed as a single operator acting on the function u only. Hence, applying the operator given by equ.(2.10) for the first order n=1, we get

$$\begin{cases} L^n (R^n u) = \left(\dfrac{\partial}{\partial R} - jk\right) R u = o(R^{-2}) \\ \Leftrightarrow R\left(\dfrac{\partial}{\partial R} - jk\right) u + u = o(R^{-2}) \\ \Leftrightarrow \left(\dfrac{\partial}{\partial R} - jk + \dfrac{1}{R}\right) u = o(R^{-3}) \end{cases} \qquad (2.11)$$

And, the first order operator in the sequence to be

$$B_1 = L + \frac{1}{R} \qquad (2.12)$$

which, when applied to both sides of the expansion of equ.(2.4), annihilates the first term of the expansion. Similarly, applying the second order operator for n=2, we get

$$B_2 = \left(L + \frac{3}{R}\right)\left(L + \frac{1}{R}\right) \tag{2.13}$$

which, when applied to both sides of the expansion of equ.(2.4), annihilates the first two terms of the expansion. In general, a recursive relation can be obtained to produce the higher order operators. For instance, the n^{th} order

$$B_n = \left(L + \frac{2n-1}{R}\right) B_{n-1} \tag{2.14}$$

produces an operator which annihilates the first n-terms of the expansion in equ.(2.4).
This sequence of operators, which is given as a single operator acting on the function u, gives

$$B_n\, u = o(R^{-2n-1}) \tag{2.15}$$

for any function u satisfying the expansion in equ.(2.4). This last result presented as a single operator B_n, of order n, has been used as a Boundary Condition operator in simulating wave behavior, that is,

$$B_n\, u = 0 \tag{2.16}$$

for the wave function u.
It is apparent that this condition becomes more accurate as the order of the operator increases, and as a limit $n \to \infty$.

Analogously to the procedure described above for the one dimensional wave propagation, a two dimensional wave propagation operators can be developed. Considering the wave functions $u(r,\theta,t)$ in two space dimensions, in the time harmonic case, a similar expansion to the wave solution presented in (2.3) is presented in reference [27], and the far-field asymptotic expansion is expressed [28] as

$$u(r,\theta) = \sqrt{\frac{2}{\pi k r}}\, e^{j(kr-\frac{\pi}{2})} \sum_{i=0}^{\infty} \frac{f_i(\theta)}{r^i} \tag{2.17}$$

Similarly, and following the same procedure as above, a recursive sequence of boundary operators is defined for this far field expansion as that one described in equ.(2.14) [25],

$$B_n = \left(L + \frac{4n-3}{2r} \right) B_{n-1} \tag{2.18}$$

where the initial operators are given by

$$\begin{aligned} B_1 &= L + \frac{1}{r} \\ L &= \frac{\partial}{\partial r} - jk \end{aligned} \tag{2.19}$$

The operator B_n annihilates the first n-terms of the expansion and yields to an expression of the order

$$B_n\, u = o(r^{-2n-\frac{1}{2}}) \tag{2.20}$$

Applying the results of eqs.(2.19) and (2.20), the first two operators can be calculated and expressed as

$$\begin{aligned} B_1 &= L + \frac{1}{r} \\ B_2 &= \left(L + \frac{5}{2r} \right) \left(L + \frac{1}{r} \right) \end{aligned} \tag{2.21}$$

These two sequences of higher order operators are very useful in field radiation and wave scattering problems and mainly, in truncating the computational domain for modeling the outward propagation of waves to infinity.

2.3 ONE-WAY WAVE EQUATION OPERATORS

The second type of Absorbing Boundary Conditions operators is the one-way wave equation operator. This type is expressed as a partial differential equation that allows wave propagation in only a given direction, where the boundary must permit propagating waves to exit [23].

Hence, If we consider the computational domain shown in Fig. 2.1 limited by the outer boundary $\partial\Omega$, only numerical wave motion, that is outward from Ω, is permitted. The boundary must permit outward propagating numerical waves to exit Ω as if the simulation were performed on a computational domain of infinite extent. A scheme which passes as one-way wave equation on $\partial\Omega$ for this purpose is called a Radiation Boundary Condition or an RBC.

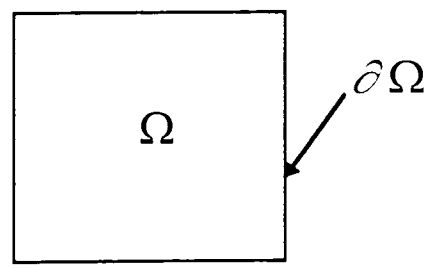

Fig. 2.1 Computational domain

The derivation of these one-way wave equation ABC operators whose purpose is to absorb numerical waves incident upon the outer boundary, can be deduced either in terms of operator factoring or dispersion relation.

2.3.1 Derivation by Wave Equation Factoring

In this section, the one-way wave equation absorbing boundary conditions operators are deduced using the wave equation factoring. The idea is to describe the wave fields propagation behavior at the limits of the computational domain by using an appropriate approximation to the wave equation.

Consider the following two-dimensional Helmholtz equation in Cartesian coordinates,

$$u_{xx} + u_{yy} - u_{tt} = Lu = 0 \tag{2.22}$$

with the partial differential operator L given by

$$L = D_x^2 + D_y^2 - D_t^2 \tag{2.23}$$

where,

$$D_x^2 = \frac{\partial^2}{\partial x^2} \; ; \; D_y^2 = \frac{\partial^2}{\partial y^2} \; ; \; D_t^2 = \frac{\partial^2}{\partial t^2} \tag{2.24}$$

The wave operator in (2.23) can be written [16] as

$$L u = L^+ L^- u = 0 \tag{2.25}$$

where the suboperators $L^{\pm}$ are defined as,

$$L^{\pm} = D_x \pm D_t \sqrt{1 - s^2} \tag{2.26}$$

with

$$s = \frac{D_y}{D_t}$$

It is shown, according to Majda [16], that at a boundary, say at x=0, the application of the L^- operator to the wave function u will exactly absorb the plane waves incident at any angle and traveling in the negative x-direction. Thus,

$$L^- u = 0 \tag{2.27}$$

Applied at $x = 0$, operates as an exact analytical Absorbing Boundary Condition operator, which absorbs wave motion from the interior of the spatial domain Ω. The same thing goes for L^+ operator at the positive x-direction.

Actually, the numerical implementation of an RBC is not that exact due to the fact that a small amount of reflection does develop at the boundary. However, higher order ABC's can be designed to minimize the reflections over a wide range of incident angles [29]. The RBC that can be derived uses a two-term Taylor series approximation for the radical as follows

$$\sqrt{1 - s^2} \cong 1 + \tfrac{0}{1!} s - \tfrac{1}{2!} s^2 + \ldots\ldots \cong 1 - \tfrac{1}{2} s^2 \tag{2.28}$$

Taking the first two terms of equ.(2.28), leads to the following approximate analytical RBC which can be numerically implemented at the boundary $x = 0$ as

$$u_{xt} + \tfrac{1}{2} u_{yy} - u_{tt} = 0 \tag{2.29}$$

A generalization of (2.26) presented in reference [30] showed that the construction of numerically useful absorbing boundary conditions reduces to approximation of the radical on the interval [-1 , 1] by the rational function,

$$r(s) = \frac{p_m(s)}{q_n(s)} \tag{2.30}$$

where p and q are polynomials of degree m, n and $r(s)$ is said to be of type (m,n). By specifying $r(s)$ as a general type (2,0) approximation, the radical is approximated by an interpolating polynomial of the form :

$$\sqrt{1-s^2} \cong p_0 + p_2 s^2 \tag{2.31}$$

resulting in the general second-order approximate analytical RBC, as

$$u_{xt} - p_2 u_{yy} - p_0 u_{tt} = 0 \tag{2.32}$$

The choice of p_i is determined by the method of interpolation used. Many of the standard techniques of interpolation such as Chebyshev, least-squares, or Padé approximations are applied to produce an approximate RBC whose performance is quite good over a wide range of incident wave angles. As an example, using the general type (2,2) rational function approximation,

$$\sqrt{1-s^2} \cong \frac{p_0 + p_2 s^2}{q_0 + q_2 s^2} \tag{2.33}$$

leads to the general third-order approximate analytical Absorbing Boundary Condition operator, which gives

$$q_0 u_{xtt} + q_2 u_{xyy} - p_2 u_{tyy} - p_0 u_{ttt} = 0 \tag{2.34}$$

appropriate selection of the subscript p_i and q_i coefficients in equ.(2.33) produces various families of Radiation Boundary Conditions. For example, according to references [29,30] for

$q_0 = p_0 = 1$, $p_2 = -3/4$, $q_2 = -1/4$ gives a Padé (2,2) approximation with resulting RBC function better than the previous (2,0) for numerical waves impacting the boundary near normal incidence.

Other types of approximating polynomials tune the RBC to absorb numerical waves incident at specified angles other than normal, and are considered to be a means to improve wide-angle performance[29].

2.3.2 Derivation by Dispersion Relation

An alternate procedure for obtaining a one-way wave equations is the derivation by dispersion relation, instead of wave equation factoring, as it is presented in refernces [29,30]. It is well known that if the dispersion relation for a linear constant-coefficient partial differential equation is known, then, the equation itself is specified. Thus, if one can obtain the dispersion relation for a one-way wave equation then, an RBC appropriate for use on $\partial\Omega$ is obtained.

As an example, if a plane wave solution is described by

$$u(x,y,t) = e^{j(\omega t - \xi x - \eta y)} \tag{2.35}$$

is substituted into equ.(2.22), then, we get

$$\omega^2 = \xi^2 + \eta^2 \tag{2.36}$$

which is the dispersion relation for the wave equation which permits wave propagation in all the directions of the (x, y) plane. The wave in equ.(2.35) has a velocity that can be given as

$$V = v_x \hat{x} + v_y \hat{y} \tag{2.37}$$

where

$$\begin{cases} v_x = -\frac{\xi}{\omega} = -\cos(\theta) \\ v_y = -\frac{\eta}{\omega} = -\sin(\theta) \end{cases} \tag{2.38}$$

θ is being the counter clockwise angle measured from the $(-x)$ axis. By rewriting equ.(2.36) as

$$\frac{\xi}{\omega} = \pm\sqrt{1-s^2} \quad \text{with} \quad s = \frac{\eta}{\omega} \tag{2.39}$$

The wave motion from the interior of the computational domain Ω will be absorbed at the boundary $x = 0$, if an equation having the dispersion relation,

$$\xi = \omega\sqrt{1-s^2} \quad : \textit{pseudo-differential equation} \tag{2.42}$$

is applied at that boundary.

By approximating the radical in equ.(2.39), it is possible to obtain a dispersion relation which can be identified as a partial differential equation that operates as an approximate analytical RBC. Once a dispersion relation is obtained, which approximates the exact relation in equ.(2.42), the same RBC's are also derived. For example, the two term Taylor series approximation to the radical

$$\xi = \omega\sqrt{1-s^2} \tag{2.43}$$

leads to

$$\xi = \omega\left(1 - \frac{1}{2}\frac{\eta^2}{\omega^2}\right) \Leftrightarrow \xi\omega = \omega^2 - \tfrac{1}{2}\eta^2 \tag{2.44}$$

which is the dispersion relation of the differential equation given by

$$u_{xt} = u_{tt} - \tfrac{1}{2}u_{yy} \tag{2.45}$$

Note that the higher order RBC's can be deduced directly by using the radical approximation.

2.3.3 Reflection Coefficient Analysis

As it has been mentioned in the previous sections, RBCs derived from approximate analytical one-way wave equations are not exact because of the presence of a small amount of reflection. The higher the order of the operator is used, the more accurate the results will be in simulation. Hence, one way to quantify the performance of a given RBC is by defining a reflection coefficient R which gives the amount of the boundary wave reflections when an RBC is applied

on that boundary. The amount of reflection is dependent upon the angle of incidence θ, and so, a good RBC gives a small value of R over a wide range of θ.

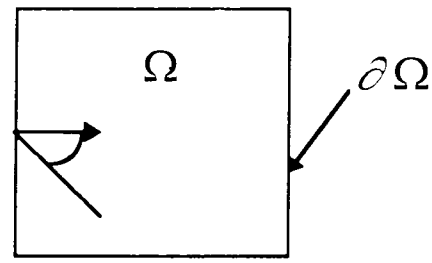

Fig. 2.2 Reflection scheme

Consider the out-going plane wave in Fig. 2.2, where the wave considered has the form,

$$u_{in} = e^{j(k\,t+k\,x\cos(\theta)-k\,y\sin(\theta))} \tag{2.46}$$

The total field at the boundary of the computational domain must satisfy its specific Radiation Boundary Condition. Postulating the existence of a reflected wave scattered back from the boundary, the total field at that boundary x=0 is the addition of both the incident and the reflected waves satisfying the form

$$u = e^{j(k\,t+k\,x\cos(\theta)-k\,y\sin(\theta))} + \mathrm{Re}^{j(k\,t-k\,x\cos(\theta)-k\,y\sin(\theta))} \tag{2.47}$$

where the reflection coefficient R can be determined by substituting the u directly into the equation for the Radiation Boundary Condition used at x=0 boundary. By substituting into one of the Radiation Boundary Conditions analytical expressions, for example the second and third order operators given by,

$$\begin{aligned} u_{xt} - p_2 u_{yy} - p_0 u_{tt} &= 0 \\ q_0 u_{xtt} + q_2 u_{xyy} - p_2 u_{tyy} - p_0 u_{ttt} &= 0 \end{aligned} \tag{2.48}$$

the reflection coefficient expressions as a function of incident angles are obtained for the general second-order and third-order RBCs. They are respectively,

$$R = \frac{\cos(\theta) - p_0 - p_2 \sin^2(\theta)}{\cos(\theta) + p_0 + p_2 \sin^2(\theta)} \tag{2.49}$$

for the second order RBCs operators and

$$R = \frac{q_0 \cos(\theta) + q_2 \cos(\theta)\sin(\theta) - p_0 - p_2 \sin(\theta)}{q_0 \cos(\theta) + q_2 \cos(\theta)\sin(\theta) + p_0 + p_2 \sin(\theta)} \tag{2.50}$$

for the third order RBCs [29].

Tabulated values for angles of incidence at which the RBC's are designed to exactly absorb numerical plane waves are generally used. In all the cases, the behavior of reflection coefficient for higher order RBCs is better than that of a lower order RBCs.

2.4 COMMON ABSORBING BOUNDARY CONDITIONS

The most popular ABCs that have been developed so far are firstly, Engquist-Majda ABC's, secondly, Lindman ABC's, thirdly, Bayliss-Turkel ABC's, and finally, Liao ABC's. They differ in the way of implementation, the ease of application to specific class of structures, and the corresponding numerical method that best suits for the analysis. All the theory of these ABC's is based on the two distinct basic types of radiation boundary operators previously described.

2.4.1 Engquist-Majda ABC's

Their idea is based on the fact that arbitrary waves can be expanded in terms of a spectrum of plane waves. Hence, ABCs can be derived primarily for plane waves of arbitrary incidence. If the ABC is made such that, it is independent of the angle of incidence and wavelength of plane waves, then, it can be used for an arbitrary wave [16].

2.4.2 Lindman ABC's

The Lindman ABC is just an extension for the Majda's ABC's. While the paraxial approximation breaks down when the angle of incidence is too large for the previous ABC, a better approximation is made for the paraxial expression in the Lindman ABC [22].

2.4.3 Bayliss-Turkel ABC's

In this case the analysis is conducted using the spherical coordinates. It is assumed that the wave has a form of a series of terms in the vicinity of the box boundary. The field expression is intuitive, where the far field from a source is expanded in terms of spherical harmonics [25].

2.4.4 Liao ABC's

The plane wave solution to the wave equation in the time domain is given a certain expression, where the direction of the plane wave makes an angle θ with the x-axis. The advantage of the Liao ABC is its ease in implementation, even at the corners of a given structure [22].

2.5 CONCLUSION

The Absorbing or the Radiation Boundary Conditions, ABC's or RBC's, are operators used in reducing nonphysical reflections from the outer boundary, which normally would permit most of the scattered energy to exit the computational domain. This nonphysical reflections contribute to the nonaccuracy of the modeling procedure. They are utilized Also, to truncate the computational domain in a manner which accurately models the propagation of the scattered waves to infinity.

In this chapter, the two types of the ABC operators are presented. The first, is the mode annihilating operator, which is based on annihilating terms in a far-field expansion of the wave equation solution. Its order is defined by the order of the terms to be annihilated. As the order increases a more accuracy is achieved. The second type, is the one-way wave equation operators, which is described by a differential equation that permits wave propagation in only one direction. It can be deduced by either Helmholtz operator factoring or by the dispersion relation of linear partial differential equations. Similarly to the first type, the higher the order is used, the smaller the error is induced.

Chapter 3

ANALYSIS USING ABSORBING BOUNDARY CONDITION FOR ISOTROPIC AND ANISOTROPIC MEDIA

3.1 INTRODUCTION

So far, we have introduced the two basic chapters, the Method of Lines and the Absorbing Boundary Conditions theory. In this chapter, the adaptation procedure of absorbing boundary condition operators to the method of lines is discussed. The one-way wave equation operator is used to describe the wave propagation outward the walls of an artificial enclosure for open microstrip structures. Using the method of lines modeling, the two lateral equations in the discretized system are taken to satisfy the ABC operator. Hence, a system of ordinary differential equations is obtained through the introduction of some appropriate transformations. The adaptation is considered for two different types of dielectric materials. First, the full wave analysis is carried out for both electric and magnetic fields for an open isotropic substrate, then, the procedure is extended to the anisotropic substrate case.

3.2 PROBLEM FORMULATION

Most of the numerical efforts in analyzing MIC and MMIC structures are based on the closed boundary conditions; the general Dirichlet-Neumann conditions, where the structure is assumed to be enclosed within a metallic boundaries. The analysis of structures located within a box requires not only the specifications of the microstrip and the dielectric permittivity, but one must also precisely indicate where the structure is located with respect to the enclosure walls, while the box dimensions must also be specified.

The analysis and data are most often reported for open microstrips, with the usual assumption that both the substrate and the ground plane extend to infinity in the transverse direction. Some rules are used to indicate how far the sides and the cover should be located for the data to be

applicable so that the characteristic impedance and the effective permittivity are not affected by the radiation effect of the walls [15], see Fig.3.1. For example, for alumina (ε_r=9.8), the height up to the cover should be more than eight times the substrate thickness, and the distance to walls should be more than five times the conductor thickness for the relations to be valid.

Therefore, the larger the closed structure dimensions in the simulation is, the more accurate and realistic data could be obtained. But, increasing the size of the structure leads to a complication of the problem simulation. This generates a disadvantage in both memory and time requirements. To overcome this problem, and to analyze the actual open structures, one can use the concept of Absorbing Boundary Conditions (ABC), which are operators derived to simulate the existence of an artificial boundaries that minimize artificial reflections from the edges of the computational domain[31,32].

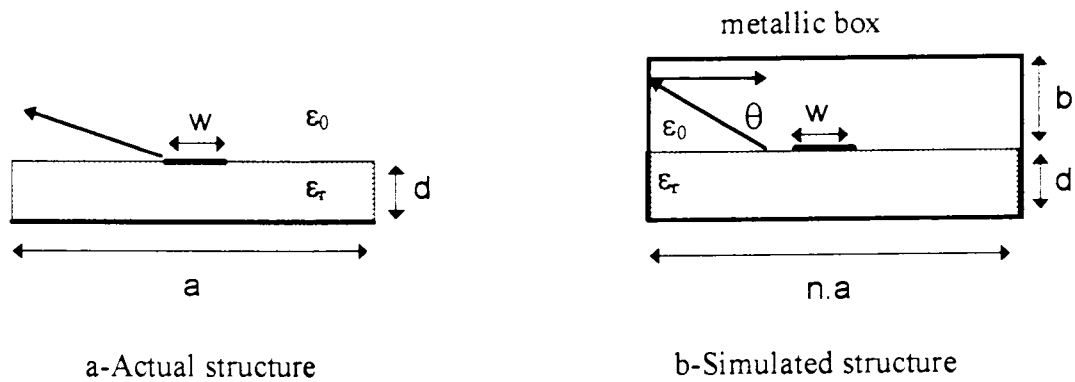

a-Actual structure

b-Simulated structure

Fig. 3.1 The open structures simulation model

Hence, our interest is oriented to the full-wave analysis of open microwave and millimeter wave structures, where the Helmholtz equation is the governing formula of wave propagation. The idea, in here, is to apply the semi-analytical numerical method, the Method of Lines, to solve the wave equation given by (3.1) for open microwave planar and quasi-planar structures subject to Absorbing Boundary Condition operators.

3.3 PRELIMINARIES

The discretization scheme of the open MIC structure is similar to that shown in chapter.1 for the closed boundary structure. Artificial boundaries are assumed to exist at the limits of the computational domain, *i.e.* the area of the open structure. The left limit is overlapped by the first electric field line e_{z0} , and the right limit on the e_{zn-1} electric field line similar to the metallic boxing discretization, see Fig. 3.2.

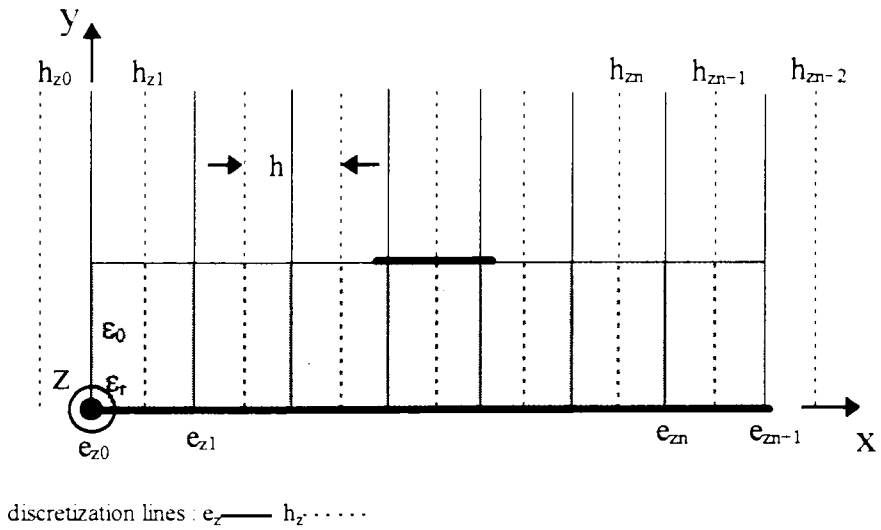

Fig. 3.2 Discretization scheme of an open microstrip structure

Consider the Helmholtz equation which is given by equ.(1.1) for an isotropic medium as

$$\left(\frac{\partial^2}{\partial x^2}+\frac{\partial^2}{\partial y^2}+\frac{\partial^2}{\partial z^2}+k^2\right)\Psi^v = 0 \qquad (3.1)$$

Keeping the assumption that the wave propagation is in the z-direction according to equ.(1.3) and its discretization according to equ.(1.4), equ.(3.1) reduces to

$$\left(\frac{\partial^2}{\partial x^2}+\frac{\partial^2}{\partial y^2}+(k^2-k_z^2)\right)\Psi^v = 0 \qquad (3.2)$$

The permittivity relations as a function of the propagation constants, for both dielectric layer and structure cases can be given as

$$\varepsilon_{re} = \frac{k_z^2}{k_0^2} \quad ; \quad \varepsilon_r = \frac{k^2}{k_0^2} \quad ; \quad \varepsilon_d = \varepsilon_r - \varepsilon_{re} \tag{3.3}$$

where k_0 is the air propagation constant.

Normalizing equ.(3.2) with respect to the air propagation constant k_0^2, and using the permittivity relations of equ.(3.3), we get

$$\left(\frac{\partial^2}{\partial \bar{x}^2} + \frac{\partial^2}{\partial \bar{y}^2} + (\varepsilon_r - \varepsilon_{re})\right)\Psi^v = 0 \tag{3.4}$$

where the normalized dimensions are obtained to be,

$$\bar{x} = k_0 x \quad ; \quad \bar{y} = k_0 y \tag{3.5}$$

If we let the new differential operators to be equal to

$$D_{\bar{x}} = \frac{\partial}{\partial \bar{x}} \quad ; \quad D_{\bar{y}} = \frac{\partial}{\partial \bar{y}} \tag{3.6}$$

Using the expressions (3.6), the normalized Helmholtz equation given by equ.(3.4) will result immediately to

$$\left(D_{\bar{x}}^2 + D_{\bar{y}}^2 + \varepsilon_d\right)\Psi^v = L\Psi^v = 0 \tag{3.7}$$

where the operator L is defined as,

$$L = D_{\bar{x}}^2 + D_{\bar{y}}^2 + \varepsilon_d \tag{3.8}$$

The wave equation operator in equ.(3.8), which describes the wave behavior, is defined for wave propagation in isotropic medium. The aim of the forgoing analysis is to match this operator to the MoL technique using the ABCs operator approximations. In a later section, the propagation in an anisotropic medium will be treated.

3.4 ISOTROPIC MEDIUM

As shown in the previous chapter, in the analysis of Absorbing Boundary Conditions, the Operator in equ.(3.8) is that mentioned in One-Way wave equation operator factoring. Hence, we can proceed the analysis using the Helmholtz Operator Factoring method. The solutions for open isotropic dielectric media are considered first, and then, an extension to the anisotropic case will be performed.

A medium is said to be isotropic if its properties do not vary with the direction of propagation of an electromagnetic wave at a given point. Since both electric and magnetic fields in isotropic medium are expressed by the same relation described by equ.(3.7), the adaptation procedure of the method of line to absorbing boundaries is identical for both fields related functions. Hence, considering the Helmholtz equation described by equ.(3.7), and by splitting the operator L into two different suboperators based on the idea of One-way wave equation operator and the direction of propagation, and according to equ.(2.25), the expression of the two suboperators L^- and L^+ are defined as follows,

$$L^{\pm} = D_{\tilde{x}} \pm j\sqrt{\varepsilon_d}\sqrt{1+s^2} \tag{3.9}$$

with

$$s^2 = \frac{1}{\varepsilon_d} D_{\tilde{y}}^2 \tag{3.10}$$

Applying the second order paraxial approximation in equ.(2.28) to the radix of the expression in equ.(3.9) we get,

$$\sqrt{1+s^2} \cong p_0 + p_2 s^2 \tag{3.11}$$

where the term s is within the interval [-1,1].

From the theory of Absorbing Boundaries the suboperators of L are defined to be the Absorbing Boundary Condition Operators at the two lateral limits depending on the wave propagation direction. Hence,

$$L^{+}\Psi^{e} = 0 \qquad \text{at right boundary}$$
$$L^{-}\Psi^{e} = 0 \qquad \text{at left boundary} \tag{3.12}$$

Developing the two suboperators of equ.(3.9), at the right and the left artificial walls of the structure, using the paraxial approximation given by equ.(3.11), we end up by the second order Absorbing Boundary Operator that describes the wave propagation phenomenon at the boundaries of the computational domain, given by

$$\left(D_{\bar{y}}^{2} \pm \frac{j\sqrt{\varepsilon_d}}{p_2} D_{\bar{x}} + \frac{p_0}{p_2}\varepsilon_d \right)\Psi^{e} = 0 \tag{3.13}$$

3.4.1 Tangential Fields solutions

3.4.1.1 Electric Field

Applying the Method of Lines discretization procedure in a shifted two lines system on the two ABC operators at the two lateral boundaries as it is described earlier in the Method of Lines preliminaries, we get

$$D_{\bar{y}}^{2} e_{zi} \pm \frac{j\sqrt{\varepsilon_d}}{p_2}\frac{1}{k_0}\left(\frac{e_{z(i+1)} - e_{z(i-1)}}{2h}\right) + \frac{p_0}{p_2}\varepsilon_d e_{zi} = 0 \tag{3.14}$$

where the plus sign in equ.(3.14) stands to the ABC operator at the left boundary and the minus sign to the ABC operator at the right boundary.

Introducing the notation,

$$\bar{h} = k_0 h \quad ; \quad n_d = \bar{h}\sqrt{\varepsilon_d} \tag{3.15}$$

and substituting it into equ.(3.14), the Helmholtz equation for the two lateral boundaries will be reduced to,

$$D_{\bar{y}}^2 e_{zi} \pm \frac{jn_d}{2p_2}\left(\frac{e_{z(i+1)} - e_{z(i-1)}}{\bar{h}^2}\right) + \frac{p_0}{p_2}\varepsilon_d e_{zi} = 0 \qquad (3.16)$$

Discretizing the Helmholtz equation along the whole structure to be analyzed, in a shifted one line system, this differential equation will be given in its general format as

$$D_{\bar{y}}^2 e_{zi} + \left(\frac{e_{z(i+1)} - 2e_{z(i)} + e_{z(i-1)}}{\bar{h}^2}\right) + \varepsilon_d e_{zi} = 0 \qquad (3.17)$$

Finally, using eqs.(3.16) and (3.17), we construct the complete system of partial differential equations for the structure under consideration, that describes the wave behavior along the *n*-lines of the discretization scheme presented in Fig. 3.2.

$$\begin{cases} \text{for } i = 1 \begin{cases} D_{\bar{y}}^2 e_{z1} + \dfrac{jn_d}{2p_2}\left(\dfrac{e_{z(2)} - e_{z0}}{\bar{h}^2}\right) + \dfrac{p_0}{p_2}\varepsilon_d e_{z1} = 0 \\ D_{\bar{y}}^2 e_{z1} + \left(\dfrac{e_{z0} - 2e_{z1} + e_{z2}}{\bar{h}^2}\right) + \varepsilon_d e_{z1} = 0 \end{cases} \\ \vdots \\ \text{for } i > 1 \ : \ D_{\bar{y}}^2 e_{zi} + \left(\dfrac{e_{z(i-1)} - 2e_{z(i)} + e_{z(i+1)}}{\bar{h}^2}\right) + \varepsilon_d e_{zi} = 0 \\ \vdots \\ \text{for } i = n \begin{cases} D_{\bar{y}}^2 e_{zn} - \dfrac{jn_d}{2p_2}\left(\dfrac{e_{z(n-1)} - e_{z(n+1)}}{\bar{h}^2}\right) + \dfrac{p_0}{p_2}\varepsilon_d e_{zn} = 0 \\ D_{\bar{y}}^2 e_{zn} + \left(\dfrac{e_{z(n-1)} - 2e_{z(n)} + e_{z(n+1)}}{\bar{h}^2}\right) + \varepsilon_d e_{zn} = 0 \end{cases} \end{cases} \qquad (3.18)$$

Concerning the two lateral walls, we eliminate the zero terms, corresponding to the couple of equations at i=1 and $i = n$, by combining the two lateral equations in the system of equ.(3.18) for both two-line and one-line shifted discretization procedures. Hence, for i=1 (left boundary), we solve for the electric field component at the line zero e_{z0} from the first equation in the system of equ.(3.18) and substituting it into the second equation, we end up with

$$D_{\bar{y}}^2 e_{z1} + (-\bar{h}^{-2})\left(2 - 2\frac{2p_2 + (p_0 - p_2)n_d^2}{2p_2 + jn_d}\right)e_{z1} + (-\bar{h}^{-2})\left(-1 + \frac{2p_2 - jn_d}{2p_2 + jn_d}\right)e_{z2} + \varepsilon_d e_{z1} = 0 \qquad (3.19)$$

the previous expression may be further simplified by introducing the notation,

$$\begin{cases} a = -2\dfrac{2p_2 + (p_0 - p_2)n_d^2}{2p_2 + jn_d} \\ b = -\dfrac{2p_2 - jn_d}{2p_2 + jn_d} \end{cases} \qquad (3.20)$$

Using this notation, equ.(3.19) can be rewritten as:

$$D_{\bar{y}}^2 e_{z1} + (-\bar{h}^{-2})(2 + a)e_{z1} + (-\bar{h}^{-2})(-1 - b)e_{z2} + \varepsilon_d e_{z1} = 0 \qquad (3.21)$$

Following the same procedure as presented above, for $i = n$ (right boundary), we solve for the electric field component at the line e_{zn-1} from the n^{th} equation in the system of (3.18) and substituting it into the second equation, we end up with

$$D_{\bar{y}}^2 e_{zn} + (-\bar{h}^{-2})(2 + a)e_{zn} + (-\bar{h}^{-2})(-1 - b)e_{z(n-1)} + \varepsilon_d e_{zn} = 0 \qquad (3.22)$$

Replacing the two lateral equations in the system of (3.26) by the two equations in (3.21) and (3.22), a new system of n second order differential equations is obtained, where each differential equation corresponds to the solution of the electric field at the appropriate line index as

$$\begin{cases} i = 1: \quad D_{\bar{y}}^2 e_{z1} + (-\bar{h}^{-2})(2 + a)e_{z1} + (-\bar{h}^{-2})(-1 - b)e_{z2} + \varepsilon_d e_{z1} = 0 \\ \qquad\qquad \vdots \\ i > 1 \quad : \quad D_{\bar{y}}^2 e_{zi} + \left(\dfrac{e_{z(i-1)} - 2e_{z(i)} + e_{z(i+1)}}{\bar{h}^2}\right) + \varepsilon_d e_{zi} = 0 \\ \qquad\qquad \vdots \\ i = n \quad : \quad D_{\bar{y}}^2 e_{zn} + (-\bar{h}^{-2})(2 + a)e_{zn} + (-\bar{h}^{-2})(-1 - b)e_{z(n-1)} + \varepsilon_d e_{zn} = 0 \end{cases} \qquad (3.23)$$

Generally, to characterize a system, *i.e.* defining its relative permittivity, we transform the system of equ.(3.23) into a matrix notation to reduce the problem of solving n differential

equations into only one vector field differential equation. Thus, the system of differential equations (3.23) is presented in a matrix form as

$$\left[D_{\bar{y}}^2 - (-\bar{h}^{-2})P_e + \varepsilon_d I\right]\Psi^e = 0 \tag{3.24}$$

where the (n : n) second order difference operator matrix P_e and the electric field column vector Ψ^e follow immediately as

$$P_e = \begin{bmatrix} p_{11} & p_{12} & & & 0 \\ -1 & 2 & -1 & & \\ & \ddots & \ddots & \ddots & \\ & & -1 & 2 & -1 \\ 0 & & & p_{12} & p_{11} \end{bmatrix} \tag{3.25}$$

with

$$p_{11} = 2 + a \qquad p_{12} = -1 - b \qquad \text{and} \qquad \Psi^e = \begin{bmatrix} e_{z1} \\ \vdots \\ e_{zi} \\ \vdots \\ e_{zn} \end{bmatrix} \tag{3.26}$$

where e_i is the electric field at the i^{th} line of the discretization scheme.

The system of equ.(3.23) is in its normalized form, hence, a nonnormalized system can be obtained simply by using the original dimensions. Given that,

$$\bar{h} = k_0 h \quad ; \quad n_d = \bar{h}\sqrt{\varepsilon_d} = k_0 h\sqrt{\varepsilon_d} \tag{3.27}$$

and multiplying equ.(3.23) by k_0^2, we get the original system of differential equations

$$\begin{cases} i=1 \;:\; D_y^2 e_{z1} + (-h^{-2})(2+a)e_{z1} + (-h^{-2})(-1-b)e_{z2} + k_0^2 \varepsilon_d e_{z1} = 0 \\ \qquad\qquad \vdots \\ i>1 \;:\; D_y^2 e_{zi} + \left(\dfrac{e_{z(i-1)} - 2e_{z(i)} + e_{z(i+1)}}{h^2} \right) + k_0^2 \varepsilon_d e_{zi} = 0 \\ \qquad\qquad \vdots \\ i=n \;;\; D_y^2 e_{zn} + (-h^{-2})(2+a)e_{zn} + (-h^{-2})(-1-b)e_{z(n-1)} + k_0^2 \varepsilon_d e_{zn} = 0 \end{cases} \tag{3.28}$$

Equivalently, the system (3.28) can be written in a matrix form as

$$\left[D_y^2 - (-h^{-2}) P_e + k_0^2 \varepsilon_d I \right] \Psi^e = 0 \tag{3.29}$$

By doing some manipulations on equ.(3.29), the system of coupled differential equations can be written in the form,

$$\left[D_y^2 - k_0^2 \left(\frac{P_e}{k_0^2 h^2} - \varepsilon_d I \right) \right] \Psi^e = 0 \tag{3.30}$$

Equ.(3.30) is a system of a set of coupled difference equations. The solution of such a system is not possible, unless we transform it into an uncoupled one. In order to get an uncoupled second-order differential equations system of equ.(3.30), the tridiagonal matrix P_e must be diagonalized using an appropriate transformation matrix T_e in the case of the electric field function. The uncoupled system will have the form:

$$\left[D_y^2 - k_0^2 \left(\frac{\lambda_e}{k_0^2 h^2} - \varepsilon_d I \right) \right] \overline{\Psi}^e = 0 \tag{3.31}$$

where the electric field vector and the eigenvalue matrix λ_e of the matrix P_e are transformed into the transformed domain via the matrix T_e as,

$$\begin{aligned} \overline{\Psi}^e &= T_e^{-1} \Psi^e \\ \lambda_e &= T_e^{-1} P_e T_e \end{aligned} \tag{3.32}$$

Equ.(3.31) can be further reduced to a simpler form as,

$$\left[D_y^2 - K_e^2\right]\overline{\Psi}^e = 0 \tag{3.33}$$

where,

$$k_e^2 = k_0^2\left(\frac{\lambda_e}{k_0^2 h^2} - (\varepsilon_r - \varepsilon_{re})I\right) \tag{3.34}$$

3.4.1.2 Magnetic Field

Equivalently, the same procedure, as described above for the electric field function Ψ^e, can be applied to the magnetic field function Ψ^h that satisfies equ.(3.7). The same operator L, given in equ.(3.8) in the case of the electric field, is to be factored at the lateral boundaries of the structure for the magnetic field discretization scheme giving rise to the two lateral equations in the shifted two lines systems,

$$\left(D_{\bar{y}}^2 \pm \frac{j\sqrt{\varepsilon_d}}{p_2} D_{\bar{x}} + \frac{p_0}{p_2}\varepsilon_d\right)\frac{\partial \Psi^h}{\partial x} = 0 \tag{3.35}$$

Eliminating the zero terms corresponding to equations at i=1 and i=n+1 by combining the operator (3.35) at the boundaries with the lateral equations of one-line shifted system. Thus, for i=1, *i.e.* left boundary, we solve for the magnetic field h_0 from the Absorbing Boundary operator and substituting it into the first equation of the one shifted system. The same thing goes for i=$n-1$ at the right boundary. Finally, we end up by a system of differential equations that can be represented in a matrix form as

$$\left[D_y^2 - (-h^{-2})P_h + k_0^2\varepsilon_d I\right]\Psi^h = 0 \tag{3.36}$$

where the (n+1 : n+1) second order difference operator matrix P_h is deduced to be equal to

$$P_h = \begin{bmatrix} p_{11} & p_{12} & p_{13} & & 0 \\ -1 & 2 & -1 & & \\ & \ddots & \ddots & \ddots & \\ & & -1 & 2 & -1 \\ 0 & & p_{13} & p_{12} & p_{11} \end{bmatrix} \tag{3.37}$$

with the subvariables defined as

$$\begin{cases} p_{11} = 1 + a \\ p_{12} = -1 - b - a \\ p_{13} = b \end{cases} \quad \text{and} \quad \Psi^h = \begin{bmatrix} h_{z1} \\ \vdots \\ h_{zi} \\ \vdots \\ h_{zn+1} \end{bmatrix} \tag{3.38}$$

where a and b are as defined previously by equ.(3.20). The magnetic field column vector Ψ^h in equ.(3.38) is just the representation of the discreet magnetic field elements, where h_{zi} is the discretized magnetic field at the i^{th} line.

Following the same procedure used earlier in solving equ.(3.30), the system of equations (3.36) can be transformed into an uncoupled system of the form,

$$\left[D_y^2 - K_h^2\right]\overline{\Psi}^h = 0 \tag{3.39}$$

with,

$$k_h^2 = k_0^2\left(\frac{\lambda_h}{k_0^2 h^2} - (\varepsilon_r - \varepsilon_{re})I\right) \tag{3.40}$$

where, the magnetic field vector and the eigen value matrix λ_h of the matrix P_h are transformed into the transformed domain via the matrix T_h as,

$$\begin{aligned} \overline{\Psi}^h &= T_h^{-1}\,\Psi^h \\ \lambda_h &= T_h^{-1}\,P_h\,T_h \end{aligned} \tag{3.41}$$

From the systems described in eqs.(3.29), and (3.36), and using the second order difference operator matrices P_e and P_h given in eqs.(3.25) and (3.37) successively as described above, one

can define the first order difference operator matrices, similarly to those defined in the case of the closed boundary structure. Hence,

$$h\frac{\partial e_z}{\partial x} \rightarrow D_e E_z$$
$$h\frac{\partial h_z}{\partial x} \rightarrow -D_h H_z \tag{3.42}$$

where the two difference matrices D_e and D_h are the first order difference matrices for the electric and magnetic lines discretization scheme. Thus,

$$D_e = \begin{bmatrix} 1+a & -b & & 0 \\ -1 & 1 & & \\ & \ddots & \ddots & \\ & & -1 & 1 \\ 0 & & +b & -1-a \end{bmatrix} \tag{3.43}$$

is the (n+1 : n) equivalent system difference matrix in the case of the electric field, and

$$D_h = \begin{bmatrix} 1 & -1 & & 0 \\ & 1 & \ddots & \\ & & \ddots & -1 \\ 0 & & 1 & -1 \end{bmatrix} \tag{3.44}$$

is the (n : n+1)equivalent system difference matrix in the case of the magnetic field.

The second order difference matrices, for both the electric field system P_e and the magnetic field system P_h, can be represented as a product of the first order difference operators D_e and D_h , as in the case of the closed boundary structure analysis. Thus,

$$P_e = D_h D_e \tag{3.45}$$

which is the product form in the case of the electric field, and

$$P_h = D_e D_h \tag{3.46}$$

in the case of the magnetic field. This implies that P_e is of order (n : n) and P_h is of order (n+1:n+1) due to the dimensions of the two first order difference operators D_e and D_h.

The solution of the uncoupled system of differential equations discussed previously for equ.(3.33) and equ.(3.39) is given by equ.(1.24), which is

$$\overline{\Psi}^{v} = C_1^{v} \cosh(k_v y) + C_2^{v} \sinh(k_v y) \tag{3.47}$$

The transformation matrices T_e and T_h can be calculated analytiaclly in the case of uniform discretization scheme, and are related through the following formula [11]

$$T_h = \begin{bmatrix} \dfrac{1}{\sqrt{N+1}} & \\ \vdots & D_e T_e \lambda_e^{-1} \\ \dfrac{1}{\sqrt{N+1}} & \end{bmatrix} \tag{3.48}$$

$$\lambda_h^2 = \begin{bmatrix} 0 & \\ & \lambda_e^2 \end{bmatrix}$$

Using the above equations, the normalized quasi-diagonal difference matrices ($\bar{\delta}_e, \bar{\delta}_h$) are calculated in the following way,

$$\bar{\delta}_e = T_h^{-1} D_e T_e (k_0 h)^{-1} = \begin{bmatrix} \cdots & 0 & \cdots \\ & \bar{\lambda}_e & \end{bmatrix}$$

$$\bar{\delta}_h = T_e^{-1} D_h T_h (k_0 h)^{-1} = \begin{bmatrix} \vdots & \\ 0 & \bar{\lambda}_e \\ \vdots & \end{bmatrix} \tag{3.49}$$

For the characterization of microwave structures, the components needed to be calculated are mainly, the field components and their derivatives at the two interfaces of the layer in order to study the continuity, and thus, identifying the set of constants of the discretization lines [11]. Thus, the relation that links the field function to their derivatives can be deduced to give the following relation,

$$\begin{bmatrix} \overline{\Psi}^{v\,\prime}(y_1) \\ \overline{\Psi}^{v\,\prime}(y_2) \end{bmatrix} = K_v^2 \begin{bmatrix} \gamma_v & \alpha_v \\ \alpha_v & \gamma_v \end{bmatrix} \begin{bmatrix} -\overline{\Psi}^{v}(y_1) \\ \overline{\Psi}^{v}(y_2) \end{bmatrix} \tag{3.50}$$

with

$$\overline{\Psi}^{v\prime} = \frac{1}{k_0}\frac{d}{dy}\overline{\Psi}^{v}$$

$$\gamma_v = diag(k_{vi}\tanh(k_{vi}d))^{-1}$$

$$\alpha_v = diag(k_{vi}\sinh(k_{vi}d))^{-1} \qquad (3.51)$$

$$K_v = diag\left(\frac{k_{vi}}{k_0}\right)$$

for any arbitrary layer with thickness dimension d, refer to Fig. 3.3.

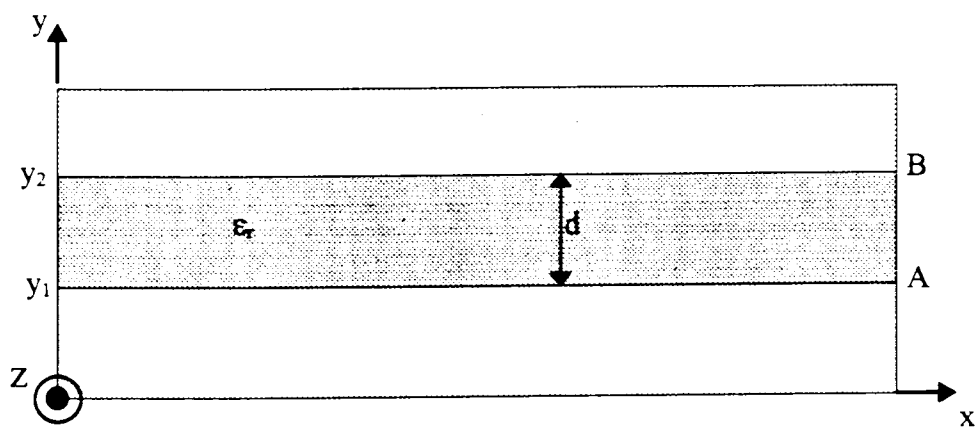

Fig. 3.3 Field matching at the layer interfaces

This complete analysis is conducted in the case of isotropic medium, whereas for an anisotropic one, the magnetic field has the same form, but there is a slight change in the final expression of the electric field.

3.4.2 Formulation of the Field Components by the MoL

With the solution of the transformed components E_z and H_z, the other field components can also be determined for each dielectric layer. For this purpose, the equations which relate the z components to the x and y components that are given by equ.(3.52) and equ.(3.53) are discretized and transformed using the MoL. To determine the effective dielectric constant, only the tangential components are necessary to begin with [11]. Thus, knowing the two field components e_z and h_z that satisfy the Helmholtz equations, the other field components can be found using the following relations [33,34]

$$\left(\frac{\partial^2}{\partial z^2}+k^2\right)\begin{bmatrix}e_x\\ e_y\end{bmatrix}=\begin{bmatrix}\dfrac{\partial^2}{\partial x\partial z} & -jk\eta\dfrac{\partial}{\partial y}\\ \dfrac{\partial^2}{\partial y\partial z} & jk\eta\dfrac{\partial}{\partial x}\end{bmatrix}\begin{bmatrix}e_z\\ h_z\end{bmatrix} \tag{3.52}$$

$$\left(\frac{\partial^2}{\partial z^2}+k^2\right)\begin{bmatrix}h_x\\ h_y\end{bmatrix}=\begin{bmatrix}j\dfrac{k}{\eta}\dfrac{\partial}{\partial y} & \dfrac{\partial^2}{\partial x\partial z}\\ -j\dfrac{k}{\eta}\dfrac{\partial}{\partial x} & \dfrac{\partial^2}{\partial y\partial z}\end{bmatrix}\begin{bmatrix}e_z\\ h_z\end{bmatrix} \tag{3.53}$$

with

$$\eta=\sqrt{\mu_0/\varepsilon}=\eta_0/\sqrt{\varepsilon_r}\quad;\quad \eta_0=\sqrt{\frac{\mu_0}{\varepsilon_0}} \tag{3.54}$$

Manipulating the two equations in such a way to get the x and y components as a function of e_z and h_z components, we end up with a system of equations for the whole structure using the Method of Lines formulation as

$$k_0\varepsilon_d\begin{bmatrix}E_x\\ \eta_0 H_x\end{bmatrix}=j\begin{bmatrix}-\sqrt{\varepsilon_{re}}h^{-1}D_e & -I\dfrac{\partial}{\partial y}\\ \varepsilon_r I\dfrac{\partial}{\partial y} & \sqrt{\varepsilon_{re}}h^{-1}D_h\end{bmatrix}\begin{bmatrix}E_z\\ \eta_0 H_z\end{bmatrix} \tag{3.55}$$

in the same way, we can deduce the relations for the other two field components in the y direction as

$$k_0\varepsilon_d\begin{bmatrix} E_y \\ \eta_0 H_y \end{bmatrix} = -j\begin{bmatrix} \sqrt{\varepsilon_{re}}\, I\dfrac{\partial}{\partial y} & h^{-1}D_h \\ \varepsilon_r h^{-1}D_e & \sqrt{\varepsilon_{re}}\, I\dfrac{\partial}{\partial y} \end{bmatrix}\begin{bmatrix} E_z \\ \eta_0 H_z \end{bmatrix} \tag{3.56}$$

The above relations (3.55) and (3.56) are expressed in the original domain. To handle the analysis in the transformed domain, the above systems of equations are transformed via the appropriate transformation matrices T_e or T_h into an equivalent system of the transformed field components. Hence, by transforming the difference operators D_e and D_h into the quasi-diagonal matrices δ_e and δ_h, the transformed systems of field components result in,

$$\varepsilon_d\begin{bmatrix} \overline{E}_x \\ \eta_0 \overline{H}_x \end{bmatrix} = j\begin{bmatrix} -\sqrt{\varepsilon_{re}}\,\overline{\delta}_e & -I\dfrac{1}{k_0}\dfrac{\partial}{\partial y} \\ I\dfrac{\varepsilon_r}{k_0}\dfrac{\partial}{\partial y} & \sqrt{\varepsilon_{re}}\,\overline{\delta}_h \end{bmatrix}\begin{bmatrix} \overline{E}_z \\ \eta_0 \overline{H}_z \end{bmatrix} \tag{3.57}$$

for the x components; and

$$\varepsilon_d\begin{bmatrix} \overline{E}_y \\ \eta_0 \overline{H}_y \end{bmatrix} = -j\begin{bmatrix} I\dfrac{\sqrt{\varepsilon_{re}}}{k_0}\dfrac{\partial}{\partial y} & \overline{\delta}_h \\ \varepsilon_r\overline{\delta}_e & I\dfrac{\sqrt{\varepsilon_{re}}}{k_0}\dfrac{\partial}{\partial y} \end{bmatrix}\begin{bmatrix} \overline{E}_z \\ \eta_0 \overline{H}_z \end{bmatrix} \tag{3.58}$$

for the y components. With the transformed fields by

$$E_x = T_h\overline{E}_x \;;\quad E_y = T_e\overline{E}_y \;;\quad E_z = T_e\overline{E}_z$$
$$H_x = T_e\overline{H}_x \;;\quad H_y = T_h\overline{H}_y \;;\quad H_z = T_h\overline{H}_z$$

3.4.3 Formulation of the Fields at a Layer Interfaces

If we consider the two interfaces of a dielectric layer A and B (see Fig. 3.3), one can establish a system of equations which relates the field components of the two interfaces of this dielectric layer [11,35]. Hence, by doing some manipulations on equ.(3.57) and using equ.(3.50), we obtain a system of equations for the tangential field components as

$$\eta_0 \begin{bmatrix} -j\overline{H}_{zA} \\ \overline{H}_{xA} \\ -j\overline{H}_{zB} \\ \overline{H}_{xB} \end{bmatrix} = \begin{bmatrix} -\varepsilon_d\gamma_h & \gamma_h\widetilde{\delta}_e & -\varepsilon_d\alpha_h & \alpha_h\widetilde{\delta}_e \\ \widetilde{\delta}_h\gamma_h & \gamma_E & \widetilde{\delta}_h\alpha_h & \alpha_E \\ -\varepsilon_d\alpha_h & \alpha_h\widetilde{\delta}_e & -\varepsilon_d\gamma_h & \gamma_h\widetilde{\delta}_e \\ \widetilde{\delta}_h\alpha_h & \alpha_E & \widetilde{\delta}_h\gamma_h & \gamma_E \end{bmatrix} \begin{bmatrix} \overline{E}_{xA} \\ -j\overline{E}_{zA} \\ -\overline{E}_{xB} \\ j\overline{E}_{zB} \end{bmatrix} \tag{3.59}$$

where,

$$\widetilde{\delta}_v = \sqrt{\varepsilon_{re}}\,\overline{\delta}_v \;\; ; \;\; \begin{bmatrix} \alpha_E \\ \gamma_E \end{bmatrix} = (\overline{\lambda}_e - \varepsilon_r I)\begin{bmatrix} \alpha_e \\ \gamma_e \end{bmatrix} \tag{3.60}$$

and α_e , α_h , γ_e and γ_h are defined above in equ.(3.51). Using the following abreviations in the system of equations (3.59), we get

$$\overline{y}_1 = \begin{bmatrix} -\varepsilon_d\gamma_h & \gamma_h\widetilde{\delta}_e \\ \widetilde{\delta}_h\gamma_h & \gamma_E \end{bmatrix} \;\; ; \overline{y}_2 = \begin{bmatrix} -\varepsilon_d\alpha_h & \alpha_h\widetilde{\delta}_e \\ \widetilde{\delta}_h\alpha_h & \alpha_E \end{bmatrix} \tag{3.61}$$

and

$$\overline{H}_{A,B} = \eta_0 \begin{bmatrix} -j\overline{H}_{zA,B} \\ \overline{H}_{xA,B} \end{bmatrix} \;\; ; \;\; \overline{E}_{A,B} = \begin{bmatrix} \overline{E}_{xA,B} \\ -j\overline{E}_{zA,B} \end{bmatrix} \tag{3.62}$$

Equ.(3.59) can be further simplified to give

$$\begin{bmatrix} \overline{H}_A \\ \overline{H}_B \end{bmatrix} = \begin{bmatrix} \overline{y}_1 & \overline{y}_2 \\ \overline{y}_2 & \overline{y}_1 \end{bmatrix} \begin{bmatrix} \overline{E}_A \\ -\overline{E}_B \end{bmatrix} \tag{3.63}$$

The fields in the right and left terms of equ.(3.63) are expressed for both A and B interfaces. In order to transform the tangential field components from one interface to the other in the case of layered substrates, the system (3.63) has to be converted in such a way to relate the field components at one interface plane to the field components at the second interface plane as

$$\begin{bmatrix} \overline{E}_B \\ \overline{H}_B \end{bmatrix} = \begin{bmatrix} \overline{V} & \overline{Z} \\ \overline{Y} & \overline{V} \end{bmatrix} \begin{bmatrix} \overline{E}_A \\ \overline{H}_A \end{bmatrix} \tag{3.64}$$

where the new block matrices in equ.(3.64) are calculated to be,

$$\begin{cases} \overline{V} = \overline{y}_2^{-1}\overline{y}_1 = \overline{y}_1\overline{y}_2^{-1} \\ \overline{Y} = \overline{y}_2 - \overline{y}_1\overline{y}_2^{-1}\overline{y}_1 \\ \overline{Z} = -\overline{y}_2^{-1} \end{cases} \tag{3.65}$$

and equivalently, if we inverse the system of equations in (3.64), we obtain the inverse relationship between the two layer interfaces as

$$\begin{bmatrix} \overline{E}_A \\ \overline{H}_A \end{bmatrix} = \begin{bmatrix} \overline{V} & -\overline{Z} \\ -\overline{Y} & \overline{V} \end{bmatrix} \begin{bmatrix} \overline{E}_B \\ \overline{H}_B \end{bmatrix} \tag{3.66}$$

Till now, this way of analysis using direct electric and magnetic field equations is valid only for structures based on isotropic homogeneous dielectric layers. Another way of describing the fields behavior is by introducing the Hertzian potential functions. This is used mainly in handling other types of substrates such as anisotropic ones.

3.4.4 Hertzian Potential Functions Description

In order to treat the homogeneous isotropic substrates using the Hertzian potential function description, it is advisable to choose two Hertzian potentials A and B, which possess only one component in the propagation direction, the z-direction in the present case, so that the boundary conditions can be easily established (see Fig. 3.2). Within each layer, the fields can be written in terms of these potentials [33,34] as,

$$\begin{aligned} e &= \frac{1}{j\omega\varepsilon}\nabla\times\nabla\times A - \nabla\times B \\ h &= \nabla\times A + \frac{1}{j\omega\mu}\nabla\times\nabla\times B \end{aligned} \tag{3.67}$$

where the two Hertzian potential functions are expressed as

$$\begin{aligned} A &= \Psi^e(x,y)e^{-jk_z z}\hat{a}_z \\ B &= \Psi^h(x,y)e^{-jk_z z}\hat{a}_z \end{aligned} \tag{3.68}$$

and the associated Helmholtz equations for these two potential functions are those given by equ.(3.1). The solution of the wave equation is derived directly from the procedure described in section 3.3.1. It is obvious that in each layer, the electromagnetic field may be expressed in

terms of the obtained solution as given by equ.(3.47). The electromagnetic field can be carried out using equ.(3.67) [33-35] as

$$\begin{bmatrix} e_x \\ h_x \end{bmatrix} = \begin{bmatrix} -j\frac{\eta}{k}\frac{\partial^2}{\partial x \partial z} & -\frac{\partial}{\partial y} \\ \frac{\partial}{\partial y} & -\frac{j}{k\eta}\frac{\partial^2}{\partial x \partial z} \end{bmatrix} \begin{bmatrix} \Psi^e \\ \Psi^h \end{bmatrix} \tag{3.69}$$

$$\begin{bmatrix} e_y \\ h_y \end{bmatrix} = \begin{bmatrix} -j\frac{\eta}{k}\frac{\partial^2}{\partial y \partial z} & \frac{\partial}{\partial x} \\ -\frac{\partial}{\partial x} & -\frac{j}{k\eta}\frac{\partial^2}{\partial y \partial z} \end{bmatrix} \begin{bmatrix} \Psi^e \\ \Psi^h \end{bmatrix} \tag{3.70}$$

$$\begin{bmatrix} e_z \\ h_z \end{bmatrix} = \begin{bmatrix} -j\frac{\eta}{k}\left(\frac{\partial^2}{\partial z^2} + k^2\right) & 0 \\ 0 & -\frac{j}{k\eta}\left(\frac{\partial^2}{\partial z^2} + k^2\right) \end{bmatrix} \begin{bmatrix} \Psi^e \\ \Psi^h \end{bmatrix} \tag{3.71}$$

Assuming the potential functions defined as harmonic wave type variation along the z-direction, and discretizing these equations in the same way as done previousely for the Hertzian potential functions, equ.(3.69-71) becomes

$$\begin{bmatrix} E_x \\ \eta_0 H_x \end{bmatrix} = \begin{bmatrix} -\frac{\sqrt{\varepsilon_{re}}}{\varepsilon_r} h^{-1} D_e & -I\frac{\partial}{\partial y} \\ I\frac{\partial}{\partial y} & \sqrt{\varepsilon_{re}} h^{-1} D_h \end{bmatrix} \begin{bmatrix} \eta_0 \Psi^e \\ \Psi^h \end{bmatrix} \tag{3.72}$$

$$\begin{bmatrix} E_y \\ \eta_0 H_y \end{bmatrix} = -\begin{bmatrix} \frac{\sqrt{\varepsilon_{re}}}{\varepsilon_r} I\frac{\partial}{\partial y} & h^{-1} D_h \\ h^{-1} D_e & \sqrt{\varepsilon_{re}} I\frac{\partial}{\partial y} \end{bmatrix} \begin{bmatrix} \eta_0 \Psi^e \\ \Psi^h \end{bmatrix} \tag{3.73}$$

$$\begin{bmatrix} E_z \\ \eta_0 H_z \end{bmatrix} = -j \begin{bmatrix} \frac{k_0}{\varepsilon_r} \varepsilon_d I & 0 \\ 0 & k_0 \varepsilon_d I \end{bmatrix} \begin{bmatrix} \eta_0 \Psi^e \\ \Psi^h \end{bmatrix} \tag{3.74}$$

This set of equations that describes the fields in the original domain can be expressed in the transformed domain via the following equations

$$\begin{bmatrix} \overline{E}_x \\ \eta_0 \overline{H}_x \end{bmatrix} = \begin{bmatrix} -\frac{\sqrt{\varepsilon_{re}}}{\varepsilon_r} h^{-1} \delta_e & -I \frac{\partial}{\partial y} \\ I \frac{\partial}{\partial y} & \sqrt{\varepsilon_{re}} h^{-1} \delta_h \end{bmatrix} \begin{bmatrix} \eta_0 \overline{\Psi}^e \\ \overline{\Psi}^h \end{bmatrix} \tag{3.75}$$

$$\begin{bmatrix} \overline{E}_y \\ \eta_0 \overline{H}_y \end{bmatrix} = -\begin{bmatrix} \frac{\sqrt{\varepsilon_{re}}}{\varepsilon_r} I \frac{\partial}{\partial y} & h^{-1} \delta_h \\ h^{-1} \delta_e & \sqrt{\varepsilon_{re}} I \frac{\partial}{\partial y} \end{bmatrix} \begin{bmatrix} \eta_0 \overline{\Psi}^e \\ \overline{\Psi}^h \end{bmatrix} \tag{3.76}$$

$$\begin{bmatrix} \overline{E}_z \\ \eta_0 \overline{H}_z \end{bmatrix} = -j \begin{bmatrix} \frac{k_0}{\varepsilon_r} \varepsilon_d I & 0 \\ 0 & k_0 \varepsilon_d I \end{bmatrix} \begin{bmatrix} \eta_0 \overline{\Psi}^e \\ \overline{\Psi}^h \end{bmatrix} \tag{3.77}$$

Because the matching equations can not be easily established for the Hertzian potential functions, in that case, the electromagnetic fields represented by equ.(3.75-77) may be expressed in terms of the transformed E_z and H_z similar to those of eqs.(3.57) and (3.58). After handling these equations, the relationship between the two interfaces for a dielectric layer given by equ.(3.63) remains valid.

3.5 ANISOTROPIC MEDIUM

In this section the adaptation of the MoL to ABC's is performed for a uniaxial anisotropic medium. A medium is said to be anisotropic if its properties do vary with the direction of propagation of an electromagnetic wave at a given point.

If we take the dielectric layer of the microwave structure to be anisotropic, the mathematical formulation will differ slightly from that of the isotropic dielectric structure due to the permittivity relation, and hence, the phase propagation constant definition. Dielectrics that are characterized by a scalar permeability and a diagonal tensor permittivity defined as

$$\mu = \mu_0 \quad ; \quad \varepsilon = \varepsilon_0 \begin{bmatrix} \varepsilon_x & & 0 \\ & \varepsilon_y & \\ 0 & & \varepsilon_z \end{bmatrix} \tag{3.78}$$

are known as bi-axial anisotropic dielectrics if all the diagonal elements are different. When two of the principal dielectric constants are equal, such as the x and y components, then only a single optical axis exists, and the medium is said to be uniaxial.

According to references [33,34], for uniaxial anisotropic dielectric medium, the electric and the magnetic fileds can be derived from two electric and magnetic Hertzian potential functions having only a direction along the optical axis [35].

3.5.1 Hertzian Potential Functions Calculation

Let the two dielectric constants ε_x and ε_z to be equal, and consider an $e^{-jk_z z}$ electric and magnetic Hertzian wave propagation variation as described previously. Assuming an $e^{j\omega t}$ time-harmonic variation, the electromagnetic fields in each homogeneous anisotropic region are expressed in terms of the two electric and magnetic Hertzian potential functions [36] as

$$\begin{aligned} \vec{\Phi}_{e,h} &= \Phi^{e,h}(x,y)\, e^{-jk_z z}\, \hat{a}_y \\ \vec{e}(x,y,z) &= k_\perp^2 \vec{\Phi}_e + \nabla(\nabla \cdot \vec{\Phi}_e) - j\omega\mu_0 \nabla \times \vec{\Phi}_h \\ \vec{h} &= j\omega\varepsilon_0\varepsilon_\perp \nabla \times \vec{\Phi}_e + \nabla(\nabla \cdot \vec{\Phi}_h) + k_\perp^2 \vec{\Phi}_h \end{aligned} \tag{3.79}$$

with

$$k_\perp^2 = k_0^2 \varepsilon_\perp = (\omega^2 \varepsilon_0 \mu_0)\varepsilon_\perp$$
$$\varepsilon_\perp = \varepsilon_x = \varepsilon_z \tag{3.80}$$

where the potential functions $\Phi^{e,h}$ are the solutions for the following scalar wave equations

$$\left(\frac{\partial^2}{\partial x^2} + \frac{\varepsilon_y}{\varepsilon_\perp}\frac{\partial^2}{\partial y^2} + (k_y^2 - k_z^2)\right)\Phi^e = 0 \tag{3.81}$$

and

$$\left(\frac{\partial^2}{\partial x^2} + \frac{\partial^2}{\partial y^2} + (k_\perp^2 - k_z^2)\right)\Phi^h = 0 \tag{3.82}$$

defined for each region of the structure. The boundary conditions associated to the electric and magnetic Hertzian potentials are identical to those of the electric and magnetic fields respectively [37-40].

3.5.1.1 Magnetic Hertzian Potential Function

Equ.(3.82) which expresses the magnetic field related function is identical to equ.(3.2) for the isotropic medium. Using the same discretization scheme as presented above, the result of the magnetic field for the isotropic medium equ.(3.36) is identical to the solution of the magnetic field related function. Hence, the Absorbing Boundary analysis for the anisotropic structure leads to the following system

$$\left[D_y^2 - (-h^{-2})P_h + k_0^2 \varepsilon_d^h I\right]\Phi^h = 0 \tag{3.83}$$

with

$$\varepsilon_d^h = \varepsilon_\perp - \varepsilon_{re} \tag{3.84}$$

Using eqs.(3.84) and (3.20), the elements p_{ik} of the second order difference operator P_h are calculated to be,

$$\begin{cases} p_{11}^h = 1 + a^h \\ p_{12}^h = -1 - b^h - a^h \\ p_{13}^h = b^h \end{cases} \tag{3.85}$$

And the uncoupled system follows directly to be equal to

$$\left[D_y^2 - k_h^2\right]\overline{\Phi}^h = 0 \tag{3.86}$$

From which the magnetic field related function solution can be given by equ.(3.47) with

$$k_h^2 = k_0^2\left(\frac{\lambda_h}{k_0^2 h^2} - \varepsilon_d^h I\right) \tag{3.87}$$

3.5.1.2 Electric Hertzian Potential Function

To solve for the electric field related function in anisotropic medium, equ.(3.81), which describes the wave propagation at the limits of the computational domain, has to be factored using the one-way wave operator principle. This equation is rewritten in an operator form after applying the normalization procedure as

$$\left(n^2 D_{\bar{y}}^2 + D_{\bar{x}}^2 + \varepsilon_d^e\right)\Phi^e = L'\Phi^e = 0 \tag{3.88}$$

with

$$\begin{gathered} \varepsilon_d^e = \varepsilon_y - \varepsilon_{re} \\ \left(n^2 = \varepsilon_y / \varepsilon_{-}\right) \end{gathered} \tag{3.89}$$

and the factorization of the operator L' in equ.(3.88) leads to,

$$L'^{\pm} = D_{\bar{x}} \pm j\sqrt{\varepsilon_d^e}\sqrt{1+s^2} \tag{3.90}$$

with,

$$S^2 = \frac{n^2}{\varepsilon_d^e} D_{\bar{y}}^2 \tag{3.91}$$

which is identical to the operator of equ.(3.9) in the case of an isotropic medium. Hence, following the same ABC analysis and discretization procedure described for electric fields in isotropic media for both lateral limits of the computational domain, the following system of equations in matrix form results in,

$$\left[n^2 D_y^2 - (-h^{-2}) P_e + k_0^2 \varepsilon_d^e I\right] \Phi^e = 0 \tag{3.92}$$

where, the elements p_{ik} of the second order difference operator P_e are calculated using eqs.(3.20) and (3.89). Hence, we get

$$\begin{aligned} p_{11} &= 2 + a^e \\ p_{12} &= -1 - b^e \end{aligned} \tag{3.93}$$

The uncoupled system follows directly to be equal to

$$\left[n^2 D_y^2 - k_0^2 \left(\frac{\lambda_e}{k_0^2 h^2} - \varepsilon_d^e I\right)\right] \overline{\Phi}^e = 0 \tag{3.94}$$

by rearranging equ.(3.94), it becomes,

$$\left[D_y^2 - k_e^2\right] \overline{\Phi}^e = 0 \tag{3.95}$$

From which the electric field related function solution can be given by equ.(3.47) with

$$k_e^2 = \frac{k_0^2}{n^2} \left(\frac{\lambda_e}{k_0^2 h^2} - \varepsilon_d^e I\right) \tag{3.96}$$

3.5.2 Field Components Using Potential Functions

After having defined the two Hertzian potential functions in the transformed domain, the remaining field components are determined from the electric and magnetic Hertzian potentials as those described for the isotropic layered structures. By using equ.(3.79) [33-35], we have

$$\begin{bmatrix} e_x \\ h_x \end{bmatrix} = \begin{bmatrix} \dfrac{\partial^2}{\partial x \partial y} & j\omega\mu_0 \dfrac{\partial}{\partial z} \\ -j\omega\varepsilon_0\varepsilon_\perp \dfrac{\partial}{\partial z} & \dfrac{\partial^2}{\partial x \partial y} \end{bmatrix} \begin{bmatrix} \Phi^e \\ \Phi^h \end{bmatrix} \tag{3.97}$$

$$\begin{bmatrix} e_y \\ h_y \end{bmatrix} = \left(k^2 - \frac{\partial^2}{\partial x^2}\right) \begin{bmatrix} \dfrac{1}{n^2} I & 0 \\ 0 & I \end{bmatrix} \begin{bmatrix} \Phi^e \\ \Phi^h \end{bmatrix} \tag{3.98}$$

$$\begin{bmatrix} e_z \\ h_z \end{bmatrix} = \begin{bmatrix} \dfrac{\partial^2}{\partial z \partial y} & -j\omega\mu_0 \dfrac{\partial}{\partial x} \\ j\omega\varepsilon_0\varepsilon_\perp \dfrac{\partial}{\partial x} & \dfrac{\partial^2}{\partial z \partial y} \end{bmatrix} \begin{bmatrix} \Phi^e \\ \Phi^h \end{bmatrix} \tag{3.99}$$

The operator $\dfrac{\partial}{\partial z}$ is replaced by $-jk_z$ since an $e^{-jk_z z}$ type variation is assumed. Discretizing these field components by using the same procedure as the one developed for the isotropic case, these last equations become

$$\begin{bmatrix} E_x \\ \eta_0 H_x \end{bmatrix} = k_0 \begin{bmatrix} k_0^{-1} h^{-1} D_e \dfrac{\partial}{\partial y} & \sqrt{\varepsilon_{re}}\, I\, k_0 \\ -\sqrt{\varepsilon_{re}}\, k_0\, \varepsilon_\perp I & -k_0^{-1} h^{-1} D_h \dfrac{\partial}{\partial y} \end{bmatrix} \begin{bmatrix} \Phi^e \\ \eta_0 \Phi^h \end{bmatrix} \tag{3.100}$$

$$\begin{bmatrix} E_y \\ \eta_0 H_y \end{bmatrix} = k_0 \begin{bmatrix} \dfrac{k_0}{n^2}\left(\varepsilon_{re} I + \dfrac{h^{-2}}{k_0^2} D_e D_h\right) & 0 \\ 0 & k_0\left(\varepsilon_{re} I + \dfrac{h^{-2}}{k_0^2} D_h D_e\right) \end{bmatrix} \begin{bmatrix} \Phi^e \\ \eta_0 \Phi^h \end{bmatrix} \tag{3.101}$$

$$\begin{bmatrix} E_z \\ \eta_0 H_z \end{bmatrix} = jk_0 \begin{bmatrix} -\sqrt{\varepsilon_{re}}\, I\, k_0^{-1} \dfrac{\partial}{\partial y} & h^{-1} D_h \\ \varepsilon_\perp h^{-1} D_e & -\sqrt{\varepsilon_{re}}\, I \dfrac{\partial}{\partial y} \end{bmatrix} \begin{bmatrix} \Phi^e \\ \eta_0 \Phi^h \end{bmatrix} \tag{3.102}$$

These equations (3.100-102) can be written in the transformed domain as

$$\begin{bmatrix} \overline{E}_x \\ \eta_0 \overline{H}_x \end{bmatrix} = k_0^2 \begin{bmatrix} \overline{\delta}_e k_0^{-1} \dfrac{\partial}{\partial y} & \sqrt{\varepsilon_{re}}\, I \\ -\sqrt{\varepsilon_{re}}\, \varepsilon_\perp I & -\overline{\delta}_h k_0^{-1} \dfrac{\partial}{\partial y} \end{bmatrix} \begin{bmatrix} \overline{\Phi}^e \\ \eta_0 \overline{\Phi}^h \end{bmatrix} \tag{3.103}$$

$$\begin{bmatrix} \overline{E}_y \\ \eta_0 \overline{H}_y \end{bmatrix} = k_0^2 \begin{bmatrix} \dfrac{1}{n^2}\left(\varepsilon_{re} I + \overline{\lambda}_e\right) & 0 \\ 0 & \left(\varepsilon_{re} I + \overline{\lambda}_h\right) \end{bmatrix} \begin{bmatrix} \overline{\Phi}^e \\ \eta_0 \overline{\Phi}^h \end{bmatrix} \tag{3.104}$$

$$\begin{bmatrix} \overline{E}_z \\ \eta_0 \overline{H}_z \end{bmatrix} = jk_0^2 \begin{bmatrix} -\sqrt{\varepsilon_{re}}\, I k_0^{-1} \dfrac{\partial}{\partial y} & \overline{\delta}_h \\ \varepsilon_\perp \overline{\delta}_e & -\sqrt{\varepsilon_{re}}\, I k_0^{-1} \dfrac{\partial}{\partial y} \end{bmatrix} \begin{bmatrix} \overline{\Phi}^e \\ \eta_0 \overline{\Phi}^h \end{bmatrix} \tag{3.105}$$

3.5.3 Fields Formulation at a Layer Interfaces

Another possible and useful combination of these equations, which are necessary for the field matching at the interfaces, must be defined for the interfaces A and B as shown in Fig. 3.3. Substituting $\dfrac{\partial}{\partial y}\Phi^{e,h}$ by means of equ.(3.50) into eqs.(3.103) and (3.105), these last equations become

$$\begin{bmatrix} \overline{E}_{xA} \\ \overline{E}_{xB} \end{bmatrix} = k_0^2\, \overline{\delta}_e k_e^2 \begin{bmatrix} -\gamma_e & \alpha_e \\ -\alpha_e & \gamma_e \end{bmatrix} \begin{bmatrix} \overline{\Phi}_A^e \\ \overline{\Phi}_B^e \end{bmatrix} + \eta_0 \sqrt{\varepsilon_{re}}\, k_0^2 \begin{bmatrix} \overline{\Phi}_A^h \\ \overline{\Phi}_B^h \end{bmatrix} \tag{3.106}$$

$$\eta_0 \begin{bmatrix} \overline{H}_{xA} \\ \overline{H}_{xB} \end{bmatrix} = -k_0^2 \sqrt{\varepsilon_{re}}\, \varepsilon_\perp \begin{bmatrix} \overline{\Phi}_A^e \\ \overline{\Phi}_B^e \end{bmatrix} - \eta_0 k_0^2\, \overline{\delta}_h k_h^2 \begin{bmatrix} -\gamma_h & \alpha_h \\ -\alpha_h & \gamma_h \end{bmatrix} \begin{bmatrix} \overline{\Phi}_A^h \\ \overline{\Phi}_B^h \end{bmatrix} \tag{3.107}$$

$$\begin{bmatrix} j\overline{E}_{zA} \\ j\overline{E}_{zB} \end{bmatrix} = k_0^2 \sqrt{\varepsilon_{re}}\, k_e^2 \begin{bmatrix} -\gamma_e & \alpha_e \\ -\alpha_e & \gamma_e \end{bmatrix} \begin{bmatrix} \overline{\Phi}_A^e \\ \overline{\Phi}_B^e \end{bmatrix} - \eta_0 k_0^2\, \overline{\delta}_h \begin{bmatrix} \overline{\Phi}_A^h \\ \overline{\Phi}_B^h \end{bmatrix} \tag{3.108}$$

$$\eta_0\begin{bmatrix} j\overline{H}_{zA} \\ j\overline{H}_{zB} \end{bmatrix} = -k_0^2\,\varepsilon_\perp\,\overline{\delta}\begin{bmatrix} \overline{\Phi}_A^e \\ \overline{\Phi}_B^e \end{bmatrix} + \eta_0 k_0^2\sqrt{\varepsilon_{re}}\,k_h^2\begin{bmatrix} -\gamma_h & \alpha_h \\ -\alpha_h & \gamma_h \end{bmatrix}\begin{bmatrix} \overline{\Phi}_A^h \\ \overline{\Phi}_B^h \end{bmatrix} \tag{3.109}$$

The electromagnetic fields along the y-direction are given for both interfaces by means of equ.(3.104) as

$$\begin{bmatrix} \overline{E}_{yA} \\ \overline{E}_{yB} \end{bmatrix} = \frac{k_0^2}{n^2}\left(\varepsilon_{re} I + \overline{\lambda}_e\right)\begin{bmatrix} \overline{\Phi}_A^e \\ \overline{\Phi}_B^e \end{bmatrix} \tag{3.110}$$

$$\eta_0\begin{bmatrix} \overline{H}_{yA} \\ \overline{H}_{yB} \end{bmatrix} = k_0^2\left(\varepsilon_{re} I + \overline{\lambda}_h\right)\begin{bmatrix} \eta_0\overline{\Phi}_A^h \\ \eta_0\overline{\Phi}_B^h \end{bmatrix} \tag{3.111}$$

3.5.4 Fields Expressions Using Tangential Components

Since it is not possible to establish matching equations for the electric and magnetic Hertzian potentials Φ_e and Φ_h, it is of interest to replace them by two field components. Thus, Φ_e and Φ_h can be expressed in terms of E_x and E_z as

$$\begin{bmatrix} \overline{\Phi}_A^e \\ \overline{\Phi}_B^e \end{bmatrix} = k_0^{-2}\left(\overline{\lambda}_e + \varepsilon_{re} I\right)^{-1}\begin{bmatrix} -\gamma_e & \alpha_e \\ -\alpha_e & \gamma_e \end{bmatrix}\left\{\overline{\delta}_h\begin{bmatrix} \overline{E}_{xA} \\ \overline{E}_{xB} \end{bmatrix} + \sqrt{\varepsilon_{re}}\begin{bmatrix} j\overline{E}_{zA} \\ j\overline{E}_{zB} \end{bmatrix}\right\} \tag{3.112}$$

$$\eta_0\begin{bmatrix} \overline{\Phi}_A^h \\ \overline{\Phi}_B^h \end{bmatrix} = k_0^{-2}\left(\overline{\lambda}_h + \varepsilon_{re} I\right)^{-1}\left\{\sqrt{\varepsilon_{re}}\begin{bmatrix} \overline{E}_{xA} \\ \overline{E}_{xB} \end{bmatrix} + \overline{\delta}_e\begin{bmatrix} j\overline{E}_{zA} \\ j\overline{E}_{zB} \end{bmatrix}\right\} \tag{3.113}$$

Substituting eqs.(3.112) and (3.113) into eqs.(3.106-109), a relation between the tangential components in both interfaces A and B is obtained as

$$\begin{aligned} \eta_0\begin{bmatrix} \overline{H}_{xA} \\ \overline{H}_{xB} \end{bmatrix} = &\left(\widetilde{\delta}_h k_h^2\begin{bmatrix} \gamma_h & \alpha_h \\ \alpha_h & \gamma_h \end{bmatrix}\left(\overline{\lambda}_h + \varepsilon_{re} I\right)^{-1} + \varepsilon_-\left(\overline{\lambda}_e + \varepsilon_{re} I\right)^{-1}\begin{bmatrix} \gamma_e & \alpha_e \\ \alpha_e & \gamma_e \end{bmatrix}\widetilde{\delta}_h\right)\begin{bmatrix} \overline{E}_{xA} \\ -\overline{E}_{xB} \end{bmatrix} \\ &+\left(\overline{\delta}_h k_h^2\begin{bmatrix} \gamma_h & \alpha_h \\ \alpha_h & \gamma_h \end{bmatrix}\left(\overline{\lambda}_h + \varepsilon_{re} I\right)^{-1} - \varepsilon_{re}\varepsilon_-\left(\overline{\lambda}_e + \varepsilon_{re} I\right)^{-1}\begin{bmatrix} \gamma_e & \alpha_e \\ \alpha_e & \gamma_e \end{bmatrix}\right)\begin{bmatrix} -j\overline{E}_{zA} \\ j\overline{E}_{zB} \end{bmatrix} \end{aligned} \tag{3.114}$$

$$\begin{bmatrix} -j\bar{H}_{xA} \\ -j\bar{H}_{xB} \end{bmatrix} = \left(\varepsilon_{re} k_h^2 \begin{bmatrix} \gamma_h & \alpha_h \\ \alpha_h & \gamma_h \end{bmatrix} \left(\bar{\lambda}_h + \varepsilon_{re} I\right)^{-1} - \varepsilon_- \bar{\delta}_e \left(\bar{\lambda}_e + \varepsilon_{re} I\right)^{-1} \begin{bmatrix} \gamma_e & \alpha_e \\ \alpha_e & \gamma_e \end{bmatrix} \bar{\delta}_h \right) \begin{bmatrix} \bar{E}_{xA} \\ -\bar{E}_{xB} \end{bmatrix}$$
$$+ \left(\varepsilon_- \tilde{\delta}_e \left(\bar{\lambda}_e + \varepsilon_{re} I\right)^{-1} \begin{bmatrix} \gamma_e & \alpha_e \\ \alpha_e & \gamma_e \end{bmatrix} + k_h^2 \begin{bmatrix} \gamma_h & \alpha_h \\ \alpha_h & \gamma_h \end{bmatrix} \left(\bar{\lambda}_h + \varepsilon_{re} I\right)^{-1} \tilde{\delta}_e \right) \begin{bmatrix} -j\bar{E}_{xA} \\ j\bar{E}_{xB} \end{bmatrix} \tag{3.115}$$

The electromagnetic fields along y-direction are finally given by

$$\begin{bmatrix} \bar{E}_{yA} \\ \bar{E}_{yB} \end{bmatrix} = \begin{bmatrix} \gamma_e & \alpha_e \\ \alpha_e & \gamma_e \end{bmatrix} \bar{\delta}_h \begin{bmatrix} \bar{E}_{xA} \\ -\bar{E}_{xB} \end{bmatrix} + \varepsilon_{re} \begin{bmatrix} \gamma_e & \alpha_e \\ \alpha_e & \gamma_e \end{bmatrix} \begin{bmatrix} -j\bar{E}_{zA} \\ j\bar{E}_{zB} \end{bmatrix} \tag{3.116}$$

$$\eta_o \begin{bmatrix} \bar{H}_{yA} \\ \bar{H}_{yB} \end{bmatrix} = \sqrt{\varepsilon_{re}} \begin{bmatrix} I & 0 \\ 0 & -I \end{bmatrix} \begin{bmatrix} \bar{E}_{xA} \\ -\bar{E}_{xB} \end{bmatrix} - \bar{\delta}_e \begin{bmatrix} I & 0 \\ 0 & -I \end{bmatrix} \begin{bmatrix} -j\bar{E}_{zA} \\ -j\bar{E}_{zB} \end{bmatrix} \tag{3.117}$$

The relation between the tangential magnetic fields H_x and H_z and the tangential electric fields E_x and E_z, is now established, and has the form

$$\eta_o \begin{bmatrix} -j\bar{H}_{zA} \\ \bar{H}_{xA} \\ -j\bar{H}_{zB} \\ \bar{H}_{xB} \end{bmatrix} = \begin{bmatrix} -\tilde{\gamma}_H & \tilde{\delta}_e \bar{\gamma}_e + \tilde{\gamma}_h \tilde{\delta}_e & -\tilde{\alpha}_H & \tilde{\delta}_e \bar{\alpha}_e + \bar{\alpha}_h \tilde{\delta}_e \\ \bar{\gamma}_e \tilde{\delta}_h + \tilde{\delta}_h \tilde{\gamma}_h & \tilde{\gamma}_E & \bar{\alpha}_e \tilde{\delta}_h + \tilde{\delta}_h \bar{\alpha}_h & \tilde{\alpha}_E \\ -\tilde{\alpha}_H & \tilde{\delta}_e \bar{\alpha}_e + \bar{\alpha}_h \tilde{\delta}_e & -\tilde{\gamma}_H & \tilde{\delta}_e \bar{\gamma}_e + \tilde{\gamma}_h \tilde{\delta}_e \\ \bar{\alpha}_e \tilde{\delta}_h + \tilde{\delta}_h \bar{\alpha}_h & \tilde{\alpha}_E & \bar{\gamma}_e \tilde{\delta}_h + \tilde{\delta}_h \tilde{\gamma}_h & \tilde{\gamma}_E \end{bmatrix} \begin{bmatrix} \bar{E}_{xA} \\ -j\bar{E}_{zA} \\ -\bar{E}_{xB} \\ j\bar{E}_{zB} \end{bmatrix} \tag{3.118}$$

with the following abreviations,

$$\begin{aligned} \bar{\alpha}_e &= \varepsilon_- (\bar{\lambda}_e + \varepsilon_{re} I)^{-1} \alpha_e \;; & \tilde{\alpha}_E &= \bar{\delta}_h \bar{\alpha}_h \bar{\delta}_e - \varepsilon_{re} \bar{\alpha}_e \\ \bar{\gamma}_e &= \varepsilon_- (\bar{\lambda}_e + \varepsilon_{re} I)^{-1} \gamma_e \;; & \tilde{\gamma}_E &= \bar{\delta}_h \bar{\gamma}_h \bar{\delta}_e - \varepsilon_{re} \bar{\gamma}_e \\ \bar{\alpha}_h &= k_h^2 \alpha_h (\bar{\lambda}_h + \varepsilon_{re} I)^{-1} \;; & \tilde{\alpha}_H &= \bar{\delta}_e \bar{\alpha}_e \bar{\delta}_h - \varepsilon_{re} \bar{\alpha}_h \\ \bar{\gamma}_h &= k_h^2 \gamma_h (\bar{\lambda}_h + \varepsilon_{re} I)^{-1} \;; & \tilde{\gamma}_H &= \bar{\delta}_e \bar{\gamma}_e \bar{\delta}_h - \varepsilon_{re} \bar{\gamma}_h \\ \tilde{\delta}_v &= \sqrt{\varepsilon_{re}}\, \bar{\delta}_v \end{aligned} \tag{3.119}$$

Using the definition according to equ.(3.63), equ.(3.118) becomes

$$\begin{bmatrix} \bar{H}_A \\ \bar{H}_B \end{bmatrix} = \begin{bmatrix} \bar{y}_1 & \bar{y}_2 \\ \bar{y}_2 & \bar{y}_1 \end{bmatrix} \begin{bmatrix} \bar{E}_A \\ -\bar{E}_B \end{bmatrix} \tag{3.120}$$

with,

$$\bar{y}_1 = \begin{bmatrix} -\tilde{\gamma}_H & \tilde{\delta}_e \bar{\gamma}_e + \tilde{\gamma}_h \tilde{\delta}_e \\ \bar{\gamma}_e \tilde{\delta}_h + \tilde{\delta}_h \tilde{\gamma}_h & \tilde{\gamma}_E \end{bmatrix} \;;\; \bar{y}_2 = \begin{bmatrix} -\tilde{\alpha}_H & \tilde{\delta}_e \bar{\alpha}_e + \bar{\alpha}_h \tilde{\delta}_e \\ \bar{\alpha}_e \tilde{\delta}_h + \tilde{\delta}_h \bar{\alpha}_h & \tilde{\alpha}_E \end{bmatrix} \tag{3.121}$$

The representation of equ.(3.120) is identical to equ.(3.63) which was developed for isotropic layers. We note also that, the matrices $\bar{y}_1$ and $\bar{y}_2$ are diagonal or quasi-diagonal matrices depending on the lateral boundaries.

3.6 CONCLUSION

As a first step in analyzing MIC and MMIC structures, the behavior of fields within an open medium has to be identified. Hence, in this chapter, the solutions of the wave equation for both electric field and magnetic field related functions are presented. A brief presentation of the need to such analysis is firstly presented. Due to the order of the wave equation and the method of lines discretization procedure, it is found that the convenient ABC operator that suits for studying open structures is the one-way wave equation operators. This operator is based on the wave equation factoring for both left and right lateral limits of the computational domain. Secondly, the adaptation of this absorbing boundary operator to the method of lines at the limits of an isotropic medium is conducted for both field quantities. Finally, the analysis is extended to the uniaxial anisotropic case, where the solution of electric and magnetic Hertzian potential functions is deduced.

After having defined the systems of equations for both electric and magnetic fields in a given medium, the complete characterization of open MIC and MMIC structures is to be given in the next chapters.

Chapter 4

FULL WAVE ANALYSIS OF ZERO THICKNESS OPEN STRUCTURES WITH ISOTROPIC AND ANISOTROPIC SUBSTRATES

4.1 INTRODUCTION

In most analysis of planar microwave integrated circuits, the width of metallic strips is taken to be of vanishing thickness, *i.e.* of zero thickness dimensions. Keeping in mind this assumption, we will try to develop in this chapter the different mathematical tools and procedures to completely characterize a variety of planar structures that are subject to open boundary conditions.

The characterization to be achieved, a more rigorous procedure, similar to that of the closed boundaries in references [7-11], has to be established in order to get the effective dielectric constant of the structure. The field transfer relations between the dielectric layer interfaces are first deduced. Then, the field matching equations are studied for simple and complex structures where a final characteristic equation is formulated for each structure, and from which, the propagation constant can be calculated. A wide set of structures can be characterized using this development such as, single microstrip, edge coupled, broadside coupled, broadside-edge coupled structures, and many other multi-layer multi-conductor structures.

4.2 FIELD TRANSFER EQUATION

4.2.1 Field Transfer Equation Between Dielectric Interfaces

In order to transform the tangential field components from one interface plane to another interface plane of the same layer, for both isotropic and anisotropic, in the case of multi layered structures, we use equ.(3.64) which relates the field quantities at the two interfaces of each dielectric layer A and B (See Fig. 3.2) as follows

$$\begin{bmatrix} \overline{E}_B \\ \overline{H}_B \end{bmatrix} = \begin{bmatrix} \overline{V} & \overline{Z} \\ \overline{Y} & \overline{V} \end{bmatrix} \begin{bmatrix} \overline{E}_A \\ \overline{H}_A \end{bmatrix} \tag{4.1}$$

Where the block matrices in equ.(4.1) have been defined previously in equ.(3.65) to be equal to

$$\begin{cases} \overline{V} = \overline{y}_2^{-1}\overline{y}_1 = \overline{y}_1\overline{y}_2^{-1} \\ \overline{Y} = \overline{y}_2 - \overline{y}_1\overline{y}_2^{-1}\overline{y}_1 \\ \overline{Z} = -\overline{y}_2^{-1} \end{cases} \tag{4.2}$$

and inversely, the system in equ.(4.1) can be swapped as

$$\begin{bmatrix} \overline{E}_A \\ \overline{H}_A \end{bmatrix} = \begin{bmatrix} \overline{V} & -\overline{Z} \\ -\overline{Y} & \overline{V} \end{bmatrix} \begin{bmatrix} \overline{E}_B \\ \overline{H}_B \end{bmatrix} \tag{4.3}$$

Consider the structure of the multi-dielectric layers in Fig. 4.1

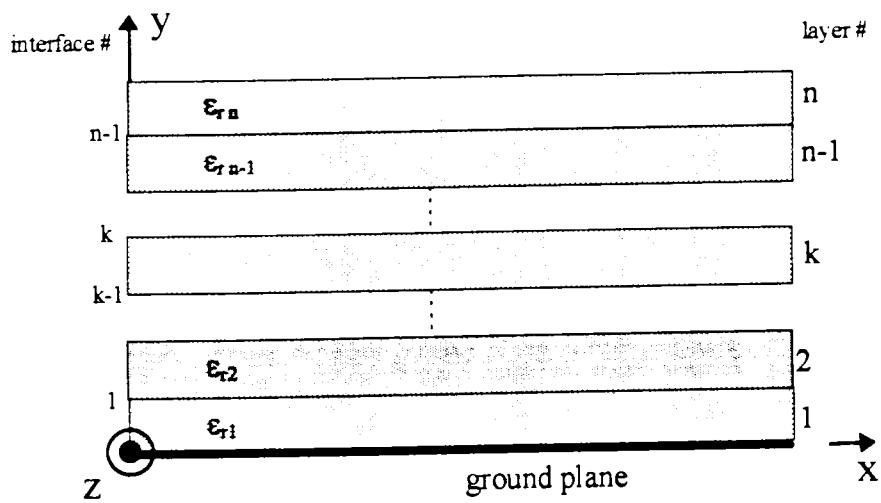

Fig. 4.1 Multi-dielectric layers structure

At the interface zero, corresponding to y=0, the ground plane, which is considered to be metallic, we have a zero electric field E_0=*0*, by applying equ.(4.1) to the first dielectric layer, we get

$$\begin{bmatrix} \overline{E}_1 \\ \overline{H}_1 \end{bmatrix} = \begin{bmatrix} \overline{V}_1 & \overline{Z}_1 \\ \overline{Y}_1 & \overline{V}_1 \end{bmatrix} \begin{bmatrix} \overline{E}_0 \\ \overline{H}_0 \end{bmatrix} \tag{4.4}$$

where E_1 and H_1 are the fields at the upper interface of the first layer. Considering the zero electric field condition due to the metallic shielding, as a result of this we can write,

$$\overline{H}_1 = \overline{Y}_t^1 \overline{E}_1 = \overline{V}_1 \overline{H}_0 = \overline{V}_1 \overline{Z}_1^{-1} \overline{E}_1 \tag{4.5}$$

where the transfer matrix $\overline{Y}_t^1$ at the interface 1 (see Fig. 4.1) is expressed by,

$$\overline{Y}_t^1 = \overline{V}_1 \overline{Z}_1^{-1} = -\overline{y}_1 \tag{4.6}$$

Equivalently, in the case of a magnetic wall at the lower shielding interface instead of the electric wall, where the magnetic field is equal to zero $H_0=0$, we get,

$$\overline{H}_1 = \overline{Y}_t^1 \overline{E}_1 = \overline{Y}_1 \overline{E}_0 = \overline{Y}_1 \overline{V}_1^{-1} \overline{E}_1 \tag{4.7}$$

where the transfer matrix $\overline{Y}_t^1$ is expressed by,

$$\overline{Y}_t^1 = \overline{Y}_1 \overline{V}_1^{-1} \tag{4.8}$$

Refering to the multi-layer structure described in Fig. 4.1, if we use the absorbing boundary conditions operators analysis, as it has been mentioned earlier, then, each dielectric layer in the structure will have its own transformation matrices, its first and second order difference operators, and hence, its diagonal and quasi-diagonal matrices. Automatically, any analysis should normally be in the same domain. Hence, at this level, it is not possible to carry on the analysis in the transformed domain. The previous layer parameters of each dielectric layer described by equ.(4.2) are transformed into the original (spatial) domain via its appropriate transformations T_e and T_h. The analysis is carried out in the original domain by matching the field parameters at the layers interfaces of the whole structure.

Following the procedure described above for the first layer field transformation equation, one can transform equ.(4.4) in the original domain to be

$$\begin{bmatrix} E_1 \\ H_1 \end{bmatrix} = \begin{bmatrix} V_1 & Z_1 \\ Y_1 & V_1 \end{bmatrix} \begin{bmatrix} E_0 \\ H_0 \end{bmatrix} \tag{4.9}$$

where E_1 and H_1 are the fields at the first layer upper interface in the original domain. Considering the zero electric field condition, equ.(4.5) will give

$$H_1 = Y_t^1 E_1 = V_1 H_0 = V_1 Z_1^{-1} E_1 \tag{4.10}$$

where, the transfer matrix y_t^1 is expressed by

$$Y_t^1 = V_1 Z_1^{-1} = -y_1 \tag{4.11}$$

For the second layer, in the multi-layer structure of Fig. 4.1, the field transfer equation can be expressed using the layer parameters as,

$$\begin{bmatrix} \overline{E}_{22} \\ \overline{H}_{22} \end{bmatrix} = \begin{bmatrix} \overline{V}_2 & \overline{Z}_2 \\ \overline{Y}_2 & \overline{V}_2 \end{bmatrix} \begin{bmatrix} \overline{E}_{21} \\ \overline{H}_{21} \end{bmatrix} \tag{4.12}$$

where $\overline{E}_{ij}$ and $\overline{H}_{ij}$ are the transformed fields at the layer interfaces of layer 2. The subscript i=2 stands for the second layer and j=1,2 stands for the numbering of the interfaces 1 or 2, respectively, in the case of the second layer. Transforming equ.(4.12) into the original domain, the field transfer equations will be given by

$$\begin{bmatrix} E_2 \\ H_2 \end{bmatrix} = \begin{bmatrix} V_2 & Z_2 \\ Y_2 & V_2 \end{bmatrix} \begin{bmatrix} E_1 \\ H_1 \end{bmatrix} \tag{4.13}$$

where E_i and H_i stand for the electric and magnetic fields at the interfaces 1 and 2. Developing equ.(4.13) for E_2 and H_2 and using equ.(4.10), the magnetic field at the second interface is written as a function of the electric field at the same interface as

$$H_2 = (Y_2 + V_2 Y_t^1)(V_2 + Z_2 Y_t^1)^{-1} E_2 \tag{4.14}$$

If we introduce the transfer matrix notation for the second layer as

$$Y_t^2 = (Y_2 + V_2 Y_t^1)(V_2 + Z_2 Y_t^1)^{-1} \tag{4.15}$$

equ.(4.15) will be written as

$$H_2 = Y_t^2 E_2 \tag{4.16}$$

In the same way, and following the same procedure, one can define a recursive relation between the magnetic field and the electric field as the one given by equ.(4.16). If we consider

the layer k in the multi-layer structure of Fig. 4.1, one can write the field transfer relation for that layer to be given by

$$\begin{bmatrix} \overline{E}_{kk} \\ \overline{H}_{kk} \end{bmatrix} = \begin{bmatrix} \overline{V}_k & \overline{Z}_k \\ \overline{Y}_k & \overline{V}_k \end{bmatrix} \begin{bmatrix} \overline{E}_{kk-1} \\ \overline{H}_{kk-1} \end{bmatrix} \tag{4.17}$$

where $\overline{E}_{ij}$ and $\overline{H}_{ij}$ are the transformed fields at the two layer interfaces of k^{th} layer (fields at interface k and k-1 respectively). Equ.(4.17) is transformed into the original domain as,

$$\begin{bmatrix} E_k \\ H_k \end{bmatrix} = \begin{bmatrix} V_k & Z_k \\ Y_k & V_k \end{bmatrix} \begin{bmatrix} E_{k-1} \\ H_{k-1} \end{bmatrix} \tag{4.18}$$

where E_k and H_k stand for the electric and magnetic fields at the interfaces k and k-1, see Fig.4.1. Developing equ.(4.18) for E_k and H_k and using the same relation as that of equ.(4.15) for the layer k-1, the magnetic field at the interface k is then written as a function of the electric field at the same interface by using the recurrence relation defined as,

$$H_k = Y_t^k E_k \tag{4.19}$$

with

$$Y_t^k = (Y_k + V_k Y_t^{k-1})(V_k + Z_k Y_t^{k-1})^{-1} \tag{4.20}$$

Note that the transfer matrix Y_t^k can be expressed as

$$Y_t^k = \begin{bmatrix} y_{11} & y_{12} \\ y_{21} & y_{22} \end{bmatrix} \tag{4.21}$$

A similar analysis can be handled if we start from the upper boundary interface of the structure. In open structures, as given in Fig. 4.1, we simulate the upper open boundary interface by an infinite distant bound; by taking the thickness of the layer to be infinite. In this case, instead of using the field transfer equation, we use its inverse described by equ.(4.3) as

$$\begin{bmatrix} \overline{E}_1 \\ \overline{H}_1 \end{bmatrix} = \begin{bmatrix} \overline{V}_1 & -\overline{Z}_1 \\ -\overline{Y}_1 & \overline{V}_1 \end{bmatrix} \begin{bmatrix} \overline{E}_0 \\ \overline{H}_0 \end{bmatrix} \tag{4.22}$$

Where in this case, the index $i=1$ stands for the first upper layer. Following the same analysis as the one described for the bottom layer starting condition, we end up with

$$\overline{H}_1 = -\overline{Y}_t^1 \overline{E}_1 \tag{4.23}$$

where the field transfer matrix is

$$\overline{Y}_t^1 = \overline{V}_1 \overline{Z}_1^{-1} \tag{4.24}$$

However, in the case of a magnetic wall upper boundary condition, this matrix can be written as

$$\overline{Y}_t^1 = \overline{Y}_1 \overline{V}_1^{-1} \tag{4.25}$$

where the subscript 1 stands for the lower interface of the first layer from the top. The upper starting condition leads to the same recurrence relation described above in the case of the bottom starting condition, so

$$H_L = -Y_t^L E_L \quad ; \quad \text{for } L=1,2.... \tag{4.26}$$

where L is the layer identifier and Y_t^L is the transfer matrix given by the recurrence equation,

$$Y_t^L = (Y_L + V_L Y_t^{L-1})(V_L + Z_L Y_t^{L-1})^{-1} \tag{4.27}$$

4.2.2 Field Transfer Equation at a Metallic Interface

If we consider the multi-layer structure of Fig. 4.2, that is composed of two or more dielectric layers deposited on a ground plane. This structure is subject to Absorbing Boundary conditions for both left and right lateral boundaries, and contains one metallic interface m composed of one or more zero thickness strips.

To study the continuity at the metallic interface m, the analysis has to be conducted in the original domain, since different transformations are used.

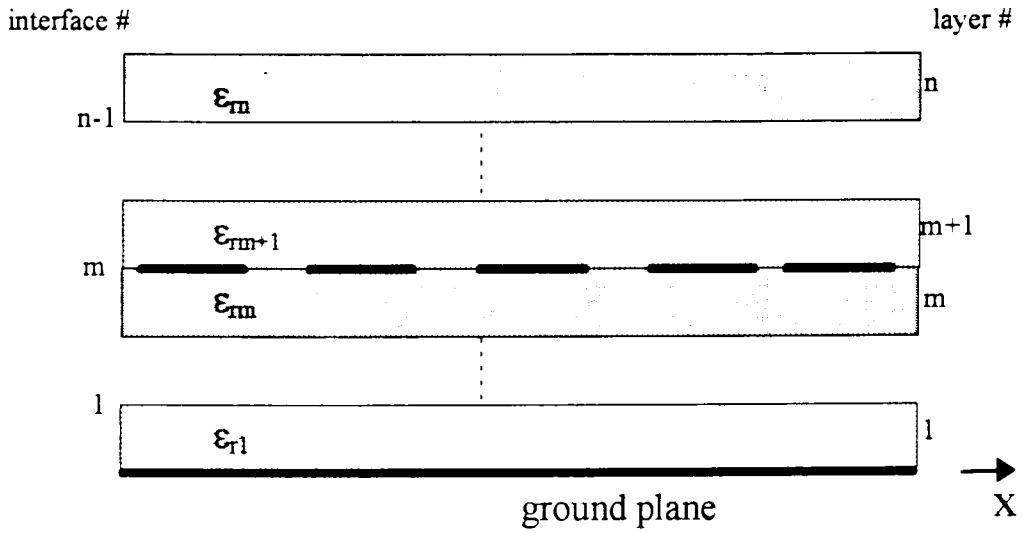

Fig. 4.2 Multi layer Single metallization Interface structure

For vanishing strips thickness, the continuity study reveals the existence of a current distribution that introduces a discontinuity in the tangential magnetic field at the interface *m*. This discontinuity is expressed in the spatial domain as

$$H_m^+ - H_m^- = -J_m \tag{4.28}$$

where

$$J_m = \eta_0 (jJ_x^t, J_z^t)^t \tag{4.29}$$

are the components of the current density, which introduces the magnetic field discontinuity. Note here that, only the tangential components of the current density are considered due to the zero thickness dimensions of the strips. Equ.(4.28) is valid only for zero thickness strips, whereas for finite thickness strips the analysis will be presented in the next chapter.

For the case where the structure consists of multiple layers as that described in Fig. 4.2, we can proceed our analysis by developing a recurrence relation similar to that given by equ.(4.20). Applying equ.(4.19) at the interface *m* of the multi-layer structure, we get

$$H_m = Y_t^m E_m \tag{4.30}$$

where Y_t^m is the transfer matrix for the bottom m layers.

Using equ.(4.30.), the magnetic field matching equation (4.28) at the strip level can be expressed in the following way

$$H_m^+ = H_m^- - J_m = Y_t^m E_m - J_m \tag{4.31}$$

At layer m+1 the field transfer equation between interface m and interface m+1 can be expressed as

$$\begin{bmatrix} E_{m+1} \\ H_{m+1} \end{bmatrix} = \begin{bmatrix} V_{m+1} & Z_{m+1} \\ Y_{m+1} & V_{m+1} \end{bmatrix} \begin{bmatrix} E_m \\ H_m \end{bmatrix} \tag{4.32}$$

developing equ.(4.32) for both electric and magnetic field functions and using the expression of the electric and magnetic field given by equ.(4.31) at the interface m, we have the expression magnetic field as a function of the electric field at the interface m+1 as

$$H_{m+1} = Y_t^{m+1} E_{m+1} - (Y_t^{m+1} Z_{m+1} - V_{m+1}) J_m \tag{4.33}$$

where the transfer matrix of the recursive equation is given by

$$Y_t^{m+1} = Y^{m+1} (V_{m+1} + Z_{m+1} Y_t^m)^{-1} \tag{4.34}$$

with

$$Y^{m+1} = Y_{m+1} + V_{m+1} Y_t^m \tag{4.35}$$

A similar analysis can be handled if we start from the upper boundary interface of the structure, exactly as the one described for the multi layer dielectric interface structure.

4.3 FIELD MATCHING RELATIONS

We have proceeded so far to the development of the necessary mathematical formulation to handle the complete analysis of a given MIC and MMIC open planar structures. Therefore, to characterize a given structure, a system of equations has to be established and should lead to the extraction of the structure effective permittivity.

We have defined previously the field transfer equations for both dielectric interface and a metallization interface. Hence, the matching equations of the fields, e.g. equ.(4.33), can be accurately elaborated to describe the behavior of microwave structures. As mentioned earlier, only two field components are needed to be identified in order to characterize the structure. In our case, as it has been used in the development of the layer parameters, the tangential components of the electric field $E = (E_x^t, -jE_z^t)^t$ are considered with the tangential components of the current densities described by equ.(4.29) as

$$J_m = \eta_0 (jJ_x^t, J_z^t)^t \tag{4.36}$$

The system which describes the complete structure is based upon a relation that links the tangential electric field components to the tangential current densities for different structures. Hence, in the following sections an algebraic relation will be defined for these different structures.

4.3.1 Multi-Layer Single-Metallization Interface

Consider the multi-layer single-metallization structure presented in Fig. 4.3 bellow. It is composed of one metallization interface *m* composed of an arbitrary number of strip conductors embedded below *l* and above *k* dielectric layers.

The two field transfer equations between the dielectric interfaces below and above the metallization interface given by eqs.(4.19) and (4.26) must be matched to each other. Consider the metallization interface shown in Fig. 4.3, at the upper interface of the substrate layer *k* and at the bottom interface of the substrate layer *l*, the matching equations of the electric fields and the magnetic fields are given by the following expressions

$$E_k = E_l = E_m \tag{4.37}$$

$$H_l - H_k = -J_m \tag{4.38}$$

where m denotes the metallization interface.

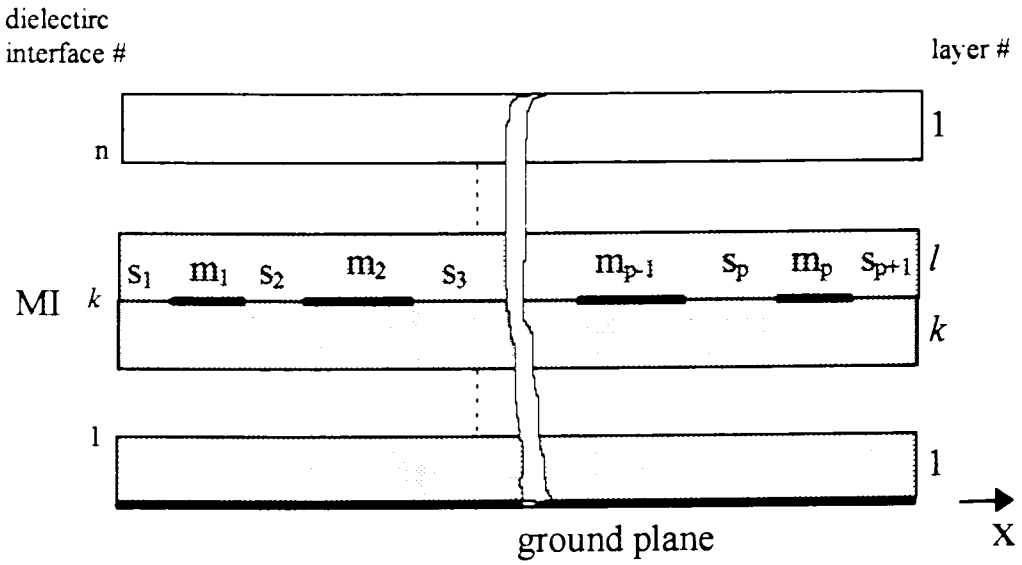

Fig. 4.3 Multi-layers Single-metallization Interface structure

Applying the field transfer equations (4.19) and (4.26) at the metallic interface m given by

$$H_k = Y_t^k E_k \tag{4.39}$$

for the field transfer equation for the bottom k layers. And

$$H_l = -Y_t^l E_l \tag{4.40}$$

for the field transfer equation for the upper l layers.

Using the magnetic field discontinuity equation (4.38) and substituting the magnetic fields by their corresponding expressions in eqs. (4.19) and (4.26), we get an algebraic relation that characterizes the structure. This is given by

$$(Y_t^l + Y_t^k)E_m = J_m \tag{4.41}$$

The above system of equations connects both the current distribution and the magnetic field. Thus, to solve this equation, we should consider the form of the metallic interface ***m***. If at the interface, the number of discretization lines on the slots are less than those on the strips, *i.e.* the width of the slots intervals are less than the width of the strips intervals, the system (4.41) will be used. This is due to the zero elements of the electric field vector E_m that will help in the solution of the system. Whereas, if the slots interval widths are greater than the strips widths, the inverse of the system above will be used, that is

$$(Y_t^k + Y_t^l)^{-1} J_m = E_m \tag{4.42}$$

The above systems (4.41) and (4.42), that characterize the microwave structure, have to be solved for the tangential electric field and the current density for the identification of the effective dielectric constant of the structure.

At the metallic interface *m*, the tangential electric field at the metallization strips and the current density at the slot regions are equal to zero. Considering the multi-layer single-metallization structure presented in Fig. 4.3, which is composed of p metallic strips and $p-1$ slot regions. The tangential electric field on the strips and the current density on the slots are given by

$$\begin{aligned} E_{xi} &= E_{zi} = 0 \\ J_{xk} &= J_{zk} = 0 \end{aligned} \tag{4.43}$$

where the subscript *i* denotes the strip number and the subscript *k* denotes the slot number. Constructing the electric field components E and the current density J expressions in vector form at the metallic interface *m* for p metallic strips, yields

$$J_{xM} = \begin{bmatrix} 0 \\ J_{xm1} \\ 0 \\ \vdots \\ J_{xmp} \\ 0 \end{bmatrix}; \quad J_{zM} = \begin{bmatrix} 0 \\ J_{zm1} \\ 0 \\ \vdots \\ J_{zmp} \\ 0 \end{bmatrix}; \quad E_{xM} = \begin{bmatrix} E_{xs1} \\ 0 \\ E_{xs2} \\ \vdots \\ 0 \\ E_{xsp+1} \end{bmatrix}; \quad E_{zM} = \begin{bmatrix} E_{zs1} \\ 0 \\ E_{zs2} \\ \vdots \\ 0 \\ E_{zsp+1} \end{bmatrix} \tag{4.44}$$

where the subscript *si* in E_x and E_z stands for slot identifier and the subscript *mi* in J_x and J_z stands for metallization identifier. Using equ.(4.41) or equ.(4.42), depending on the width of the slot or the strip regions, and substituting the field and current quantities. Assuming the slot regions width less than the strip regions width, equ.(4.41) can be written as

$$\begin{bmatrix} y_{11} & y_{12} \\ y_{21} & y_{22} \end{bmatrix} \begin{bmatrix} E_{xM} \\ -jE_{zM} \end{bmatrix} = \begin{bmatrix} jJ_{xM} \\ J_{zM} \end{bmatrix} \tag{4.45}$$

Where,

$$\begin{bmatrix} y_{11} & y_{12} \\ y_{21} & y_{22} \end{bmatrix} = (Y_t^l + Y_t^k) \tag{4.46}$$

Using the above quantities of equ.(4.44), equ.(4.45) will be expressed in the following form

$$\begin{bmatrix} y_{11} & y_{12} \\ y_{21} & y_{22} \end{bmatrix} \begin{bmatrix} E_{xs1} \\ 0 \\ E_{xs2} \\ \vdots \\ 0 \\ E_{xsp-1} \\ -jE_{zs1} \\ 0 \\ -jE_{zs2} \\ \vdots \\ 0 \\ -jE_{zsp-1} \end{bmatrix} = \begin{bmatrix} 0 \\ jJ_{xm1} \\ 0 \\ \vdots \\ jJ_{xmp} \\ 0 \\ 0 \\ J_{zm1} \\ 0 \\ \vdots \\ J_{zmp} \\ 0 \end{bmatrix} \tag{4.47}$$

To solve this system of equations, notice that those columns of the block matrices of y_{ik}, which, when multiplied with the electric vector E corresponding to the null subvectors, give no contribution and engender extra effort. Hence, it is of interest to not include them in the calculations in order to save time and memory. Eliminating the zero subvectors in the E vector and their corresponding columns in the $[y_{ik}]$ matrix, we end up with the so called reduced matrix representation of the form

$$\begin{bmatrix} y_{11}^{r} & y_{12}^{r} \\ y_{21}^{r} & y_{22}^{r} \end{bmatrix} \begin{bmatrix} E_{xs1} \\ \vdots \\ E_{xsp+1} \\ -jE_{zs1} \\ \vdots \\ -jE_{zsp+1} \end{bmatrix} = \begin{bmatrix} 0 \\ jJ_{xm1} \\ 0 \\ \vdots \\ jJ_{xmp} \\ 0 \\ 0 \\ J_{zm1} \\ 0 \\ \vdots \\ J_{zmp} \\ 0 \end{bmatrix} \tag{4.48}$$

where the subscript r stands for the reduced matrix representation.

It is apparent that this system can be further simplified since the current density vector contains zero subvectors. Hence, The system (4.48) can be partitioned into two subsystems according to zero and nonzero subvectors of the right hand side term J. Splitting the system into a homogeneous subsystem containing all the zero subvectors of the current density vector and a nonhomogeneous subsystem having the nonzero ones, we get

$$\begin{bmatrix} y_{11}^{rh} & y_{12}^{rh} \\ y_{21}^{rh} & y_{22}^{rh} \end{bmatrix} \begin{bmatrix} E_{xs1} \\ \vdots \\ E_{xsp+1} \\ -jE_{zs1} \\ \vdots \\ -jE_{zsp+1} \end{bmatrix} = [0] \tag{4.49}$$

and

$$\begin{bmatrix} y_{11}^{rn} & y_{12}^{rn} \\ y_{21}^{rn} & y_{22}^{rn} \end{bmatrix} \begin{bmatrix} E_{xs1} \\ \vdots \\ E_{xsp+1} \\ -jE_{zs1} \\ \vdots \\ -jE_{zsp+1} \end{bmatrix} = \begin{bmatrix} jJ_{xm1} \\ \vdots \\ jJ_{xmp} \\ J_{zm1} \\ \vdots \\ J_{zmp} \end{bmatrix} \tag{4.50}$$

where *rh* stands for the homogeneous reduced matrix system and *rn* for the nonhomogeneous reduced matrix system.

The homogeneous system (4.49) is an indirect eigenvalue problem, where the elements of the homogeneous reduced matrix are a function of the effective relative permittivity constant ε_{re}. To solve the indirect eigen value system which has nontrivial solutions only in the case where the determinant of the homogeneous reduced matrix is zero, the eigen value ε_{re} must be varied until the determinant of this system matrix vanishes to zero, which is given by

$$\det\left|Y_{rh}(\varepsilon_{re})\right| = 0 \tag{4.51}$$

The calculation of the eigen value, which is the effective dielectric constant ε_{re}, permits the calculation of the electric field vector using the homogeneous equation (4.66). Hence, the electric field vector is just the eigen vector corresponding to the eigen value ε_{re}. By evaluating these two previous quantities, the current density vector can be easily obtained using the nonhomogeneous system (4.50). Moreover, after having organized these vectors in their original form, all the other electric or magnetic field components are evaluated at the metallization interface, after which they can be evaluated at all other dielectric interfaces at any position along each discretization line of the structure.

In this part of analysis, we put the assumption that the slots width is less than the strips width. However, if the slots width is wider than the strips width, a similar analysis can be conducted following the same procedure, ending by the following homogeneous and nonhomogeneous system matrices,

$$\begin{bmatrix} z_{11}^{rh} & z_{12}^{rh} \\ z_{21}^{rh} & z_{22}^{rh} \end{bmatrix} \begin{bmatrix} jJ_{xm1} \\ \vdots \\ jJ_{xmp} \\ J_{zm1} \\ \vdots \\ J_{zmp} \end{bmatrix} = [0] \tag{4.52}$$

and

$$\begin{bmatrix} z_{11}^m & z_{12}^m \\ z_{21}^m & z_{22}^m \end{bmatrix} \begin{bmatrix} jJ_{xm1} \\ \vdots \\ jJ_{xmp} \\ J_{zm1} \\ \vdots \\ J_{zmp} \end{bmatrix} = \begin{bmatrix} E_{xs1} \\ \vdots \\ E_{xsp+1} \\ -jE_{zs1} \\ \vdots \\ -jE_{zsp+1} \end{bmatrix} \tag{4.53}$$

4.3.2 Multi-Layer Multi-Metallization Interfaces

Consider the general form of a multi-layer multi-metallization structure presented in Fig. 4.4 below. It is composed of an arbitrary number of metallization interfaces m, where each metallization interface contains an arbitrary number of metallization strips. Between each two successive metallization interfaces, there is an arbitrary number of dielectric layers N_l.

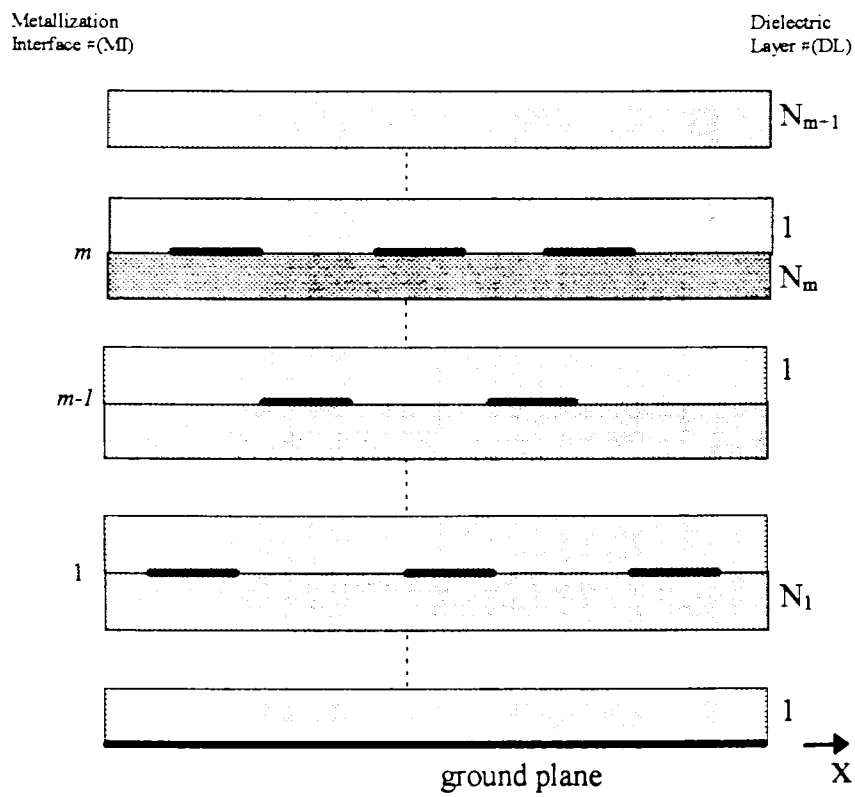

Fig. 4.4 Multi-Layer Multi-Metallization structure

In order to get the field transfer equations for N_1 and N_m dielectric layers below and above the two lateral metallization interfaces MI_1 and MI_m, the recursive relations, given by eqs.(4.19) and (4.26), are used. Hence, at the upper interface of the substrate layer N_1 and at the bottom interface of the substrate layer N_m, the matching equations of the electric and the magnetic fields are given by the following expressions

$$H_1^{n_1} = Y_t^{n_1} E_1 \tag{4.54}$$

and

$$H_m^{n_{m-1}} = -Y_t^{n_{m-1}} E_m \tag{4.55}$$

After defining the fields relations at the top and bottom of the first two metallization interfaces, we move towards the definition of a general relation that relates the tangential electric field components to the tangential magnetic field components between each two metallization interfaces MI_i and MI_{i-1} . See Fig. 4.5.

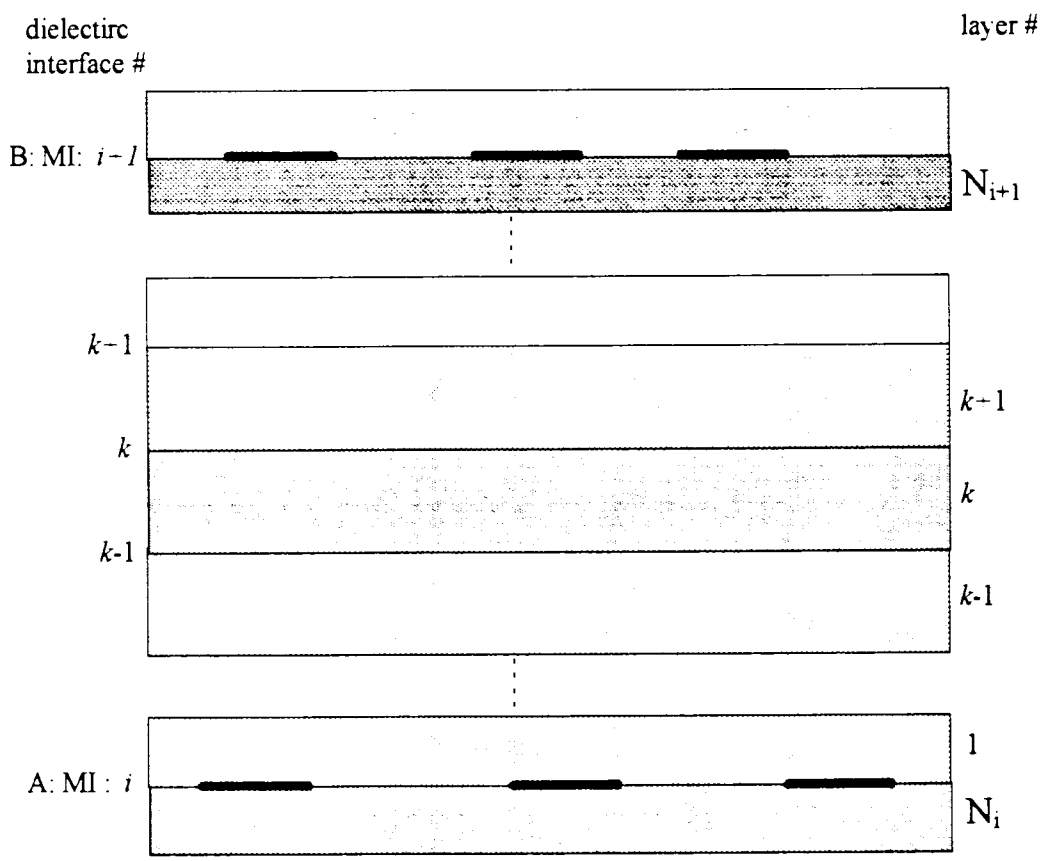

Fig. 4.5 Two successive metallization interfaces scheme

Consider N_{i-1} successive dielectric layers located between two metallization interfaces MI_i and MI_{i-1}. According to eqs.(3.63) or (3.120), the relationship between the tangential field components for any arbitrary layer k is

$$\begin{bmatrix} H_{k-1}^{-} \\ H_k \end{bmatrix} = \begin{bmatrix} y_1^k & y_2^k \\ y_2^k & y_1^k \end{bmatrix} \begin{bmatrix} E_{k-1} \\ -E_k \end{bmatrix} \tag{4.56}$$

Similarly, we can obtain the same relation for the layer $k-1$,

$$\begin{bmatrix} H_k \\ H_{k-1}^{+} \end{bmatrix} = \begin{bmatrix} y_1^{k+1} & y_2^{k+1} \\ y_2^{k+1} & y_1^{k+1} \end{bmatrix} \begin{bmatrix} E_k \\ -E_{k+1} \end{bmatrix} \tag{4.57}$$

where the notation (-) and (+) designate, respectively, the bottom and the top sides of the appropriate layer.

Introducing the continuity relations of the field components at the dielectric interface k, and using the above two relations (4.56) and (4.57), we obtain a relationship between the field components of the bottom interface of layer k and those of the top side layer $k+1$, see Fig. 4.5. The resulted equation can be described by the following general recurrence relation

$$\begin{bmatrix} H_{k-1}^{-} \\ H_{k+1}^{+} \end{bmatrix} = \begin{bmatrix} y_{11r}^{k+1} & y_{12r}^{k+1} \\ y_{21r}^{k+1} & y_{22r}^{k+1} \end{bmatrix} \begin{bmatrix} E_{k-1} \\ -E_{k+1} \end{bmatrix} \tag{4.58}$$

where

$$\begin{aligned} y_{11r}^{k+1} &= y_1^k - y_2^k (y_1^k + y_1^{k+1})^{-1} y_2^k \\ y_{12r}^{k+1} &= y_2^k (y_1^k + y_1^{k+1})^{-1} y_2^{k+1} \\ y_{21r}^{k+1} &= y_2^{k+1} (y_1^k + y_1^{k+1})^{-1} y_2^k \\ y_{22r}^{k+1} &= y_1^{k+1} - y_2^{k+1} (y_1^k + y_2^{k+1})^{-1} y_2^{k+1} \quad ; \quad k = 0,..N_{i+1} \end{aligned} \tag{4.59}$$

where N_{i-1} is the number of dielectric layers between two metallic interfaces as shown in Fig. 4.5.

Now, for all dielectric layers between two metallic interfaces, a general relation linking the tangential field components at these two metallization interfaces can be deduced using the

recurrence relation (4.58). Hence, for any two interfaces i and $i-1$ as indicated in Fig. 4.5, the following relation is obtained

$$\begin{bmatrix} H_A^i \\ H_B^i \end{bmatrix} = \begin{bmatrix} y_{11}^i & y_{12}^i \\ y_{21}^i & y_{22}^i \end{bmatrix} \begin{bmatrix} E_A^i \\ -E_B^i \end{bmatrix} \qquad (4.60)$$

where the block matrices y_{pq}^i are obtained using the recurrence relation (4.59).

In order to get a general relation between the tangential field components in the structure of an arbitrary number of metallization interfaces, a similar analysis to that described for single metallization interface will be conducted. Hence, considering three arbitrary successive metallization interfaces i-1, i, and i+1, similar relations to equ.(4.60) can be derived for the metallization interfaces i and i+1 as

$$\begin{bmatrix} H_l^i \\ H_h^i \end{bmatrix} = \begin{bmatrix} y_{11}^i & y_{12}^i \\ y_{21}^i & y_{22}^i \end{bmatrix} \begin{bmatrix} E_l^i \\ -E_h^i \end{bmatrix} \qquad (4.61)$$

$$\begin{bmatrix} H_l^{i+1} \\ H_h^{i+1} \end{bmatrix} = \begin{bmatrix} y_{11}^{i+1} & y_{12}^{i+1} \\ y_{21}^{i+1} & y_{22}^{i+1} \end{bmatrix} \begin{bmatrix} E_l^{i+1} \\ -E_h^{i+1} \end{bmatrix} \qquad (4.62)$$

where the subscripts l and h designate, respectively, the lower and upper sides of the dielectric regions. Using the field matching continuity equations described in eqs.(4.37) and (4.38) at the metallization interface i,

$$\begin{aligned} H_h^i - H_l^{i+1} &= J_i \\ E_h^i = E_l^{i+1} &= E_i \end{aligned} \qquad (4.63)$$

yields to the following recurrence relation for the i^{th} arbitrary metallization interface

$$L_i E_{i-1} + K_i E_i + R_i E_{i+1} = J_i \qquad i = 2,\ldots,m-1 \qquad (4.64)$$

where

$$
\begin{aligned}
L_i &= y_{21}^i \\
K_i &= y_{22}^i - y_{11}^{i+1} \\
R_i &= y_{12}^{i+1}
\end{aligned}
\tag{4.65}
$$

Equ.(4.64) can be extended for the lower and upper lateral regions by matching the fields using eqs.(4.54) and (4.55). Hence, the general recursive relation for the complete structure can be written as

$$
L_i E_{i-1} + K_i E_i + R_i E_{i+1} = J_i \qquad i = 1,2,....,m \tag{4.66}
$$

and

$$
\begin{aligned}
L_i &= \begin{cases} y_{21}^i & i = 2.....m \\ 0 & i = 1 \end{cases} \\
K_i &= \begin{cases} y_{22}^i - y_{11}^{i+1} & i = 2.....m-1 \\ y_{22}^i - y_i^m & i = m \\ y_i^1 - y_{11}^i & i = 1 \end{cases} \\
R_i &= \begin{cases} y_{12}^i & i = 1 \\ y_{12}^{i+1} & i = 2.....m-1 \\ 0 & i = m \end{cases}
\end{aligned}
\tag{4.67}
$$

where y_i^m and y_i^1 are respectively the field transfer matrices described by eqs.(4.54) and (4,55) in the case of metallic shielding where, $E_0 = E_{m-1} = 0$. The above relation can be written in a matrix form as

$$
\begin{bmatrix}
K_1 & R_1 & & & 0 \\
L_2 & K_2 & R_2 & & \\
 & \ddots & \ddots & \ddots & \\
 & & L_{m-1} & K_{m-1} & R_{m-1} \\
0 & & & L_m & K_m
\end{bmatrix}
\begin{bmatrix} E_1 \\ E_2 \\ \vdots \\ E_{m-1} \\ E_m \end{bmatrix}
=
\begin{bmatrix} J_1 \\ J_2 \\ \vdots \\ J_{m-1} \\ J_m \end{bmatrix}
\tag{4.68}
$$

where it can be expressed in a shorter form as

$$\overline{\overline{Y}}\,\overline{\overline{E}} = \overline{\overline{J}} \tag{4.69}$$

The above relation is used, as described previously, in the cases where the total slot regions are smaller than the strip regions for all the metallization interfaces. Whereas if the optimal regions are the strip regions, the system (4.69) will be inverted to become

$$\overline{\overline{Z}}\,\overline{\overline{J}} = \overline{\overline{E}} \tag{4.70}$$

where

$$\overline{\overline{Z}} = \overline{\overline{Y}}^{-1} \tag{4.71}$$

The system (4.70) can be expressed in other forms depending on the optimal regions in each individual metallization interface. Therefore, if the system contains metallization interfaces that are optimal for slot regions and some others for strip regions, system (4.70) can be written in a mixed vector components for both electric field components and current density components [11].

In a similar manner to the analysis conducted previously in the case of multi-layer single metallization interface, the systems (4.69) and (4.70), that characterize the microwave structure, have to be solved for the tangential electric field and the current density.

At the metallic interface i, two conditions still need to be fulfilled. We mean, both the tangential electric fields at the metallization strips and electric current density at the slot regions must be put to zero. Considering the multi-layer multi-metallization structure presented in Fig. 4.4, the tangential electric field E on the strips and the current density J on the slots are given by

$$\begin{aligned} E^{i}_{xj} &= E^{i}_{zj} = 0 \\ J^{i}_{xk} &= J^{i}_{zk} = 0 \end{aligned} \tag{4.72}$$

where the subscripts (i,j,k) are

i : the metallization interface

j : components of the vector on the metallic strip

k : components of the vector on the slot

Constructing the tangential electric fields E_{xi}, E_{zi} and the current densities J_{xi}, J_{zi} at each metallization interface i using equ.(4.44), and considering equ.(4.68), the electric filed and the current density vectors for each metallic interface will be given by

$$E_i = \begin{bmatrix} E_{xi} \\ -jE_{zi} \end{bmatrix}$$
$$J_i = \begin{bmatrix} jJ_{xi} \\ J_{zi} \end{bmatrix} \tag{4.73}$$

Following the same procedure as described above in the case of a single metallization interface, we eliminate the zero subvectors in the electric field E_i, corresponding to the field components at the strip regions, and letting only the electric field at the slot intervals designated by E_{si}. The same procedure goes with the current density J_i, at the slot regions, ending only with the nonzero subvectors on the strip conductors J_{mi}. Splitting the system (4.68) into two subsystems, as it is done for eqs.(4.49) and (4.50), homogeneous and non-homogeneous one, we get

$$\begin{bmatrix} K_1^{rh} & R_1^{rh} & & & 0 \\ L_2^{rh} & K_2^{rh} & R_2^{rh} & & \\ & \ddots & \ddots & \ddots & \\ & & L_{m-1}^{rh} & K_{m-1}^{rh} & R_{m-1}^{rh} \\ 0 & & & L_m^{rh} & K_m^{rh} \end{bmatrix} \begin{bmatrix} E_{s1} \\ E_{s2} \\ \vdots \\ E_{s_{m-1}} \\ E_{s_m} \end{bmatrix} = [0] \tag{4.74}$$

for the homogeneous equation and

$$\begin{bmatrix} K_1^m & R_1^m & & & 0 \\ L_2^m & K_2^m & R_2^m & & \\ & \ddots & \ddots & \ddots & \\ & & L_{m-1}^m & K_{m-1}^m & R_{m-1}^m \\ 0 & & & L_m^m & K_m^m \end{bmatrix} \begin{bmatrix} E_{s1} \\ E_{s2} \\ \vdots \\ E_{s_{m-1}} \\ E_{s_m} \end{bmatrix} = \begin{bmatrix} J_{m1} \\ J_{m2} \\ \vdots \\ J_{m_{m-1}} \\ J_{m_m} \end{bmatrix} \tag{4.75}$$

for the nonhomogeneous equation.

The homogeneous system (4.74) is an indirect eigen value problem, similar to the one described for a single metallization interface. We first solve the indirect eigen value system, which has an eigen value ε_{re}, then, the nonzero subvectors of the electric field vector are

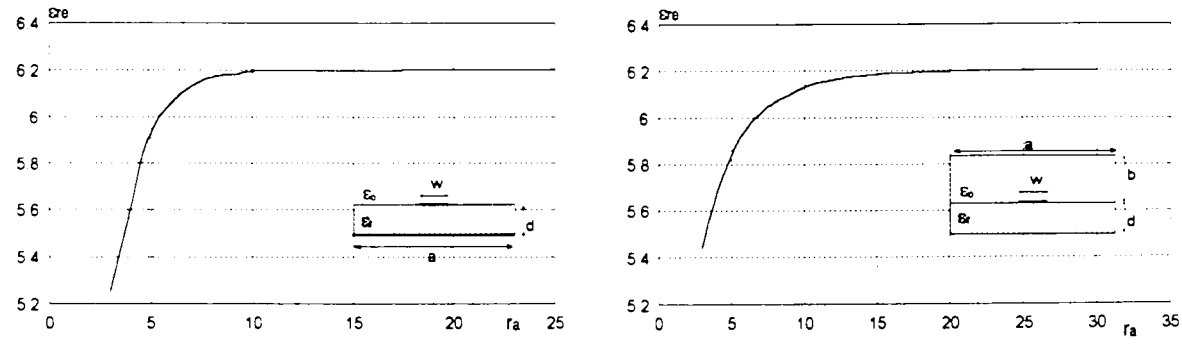

(a)

(b)

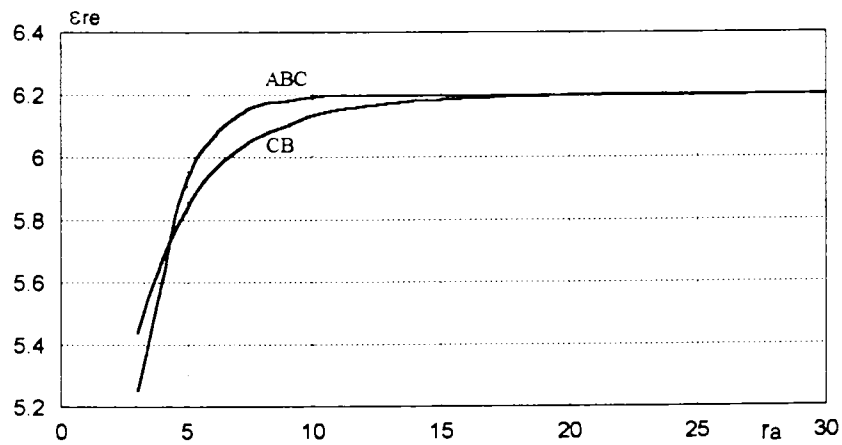

(c)

Fig. 4.6. Effective permittivity ε_{re} versus length ra=a/d. (a) ABC (b) CB (c) ABC and CB. d=1mm; rw=w/d=1; ε_r =8.875; M=5 lines; f=5GHz;

As it is clearly shown in the figure 4.6.c, the value of the effective permittivity at 5Ghz for the open case is greater than that of the closed one beyond a certain minimum value of **a**, for our case it is about 4.5mm. Also, for an error of 0.1% in the effective permittivity, the CB transverse dimension **a** is at least two times the ABC transverse dimension. This last result shows clearly that the size of the problem simulation can be further reduced using the ABC analysis since the dimension of the computational domain is made smaller, which saves a lot of time and memory.

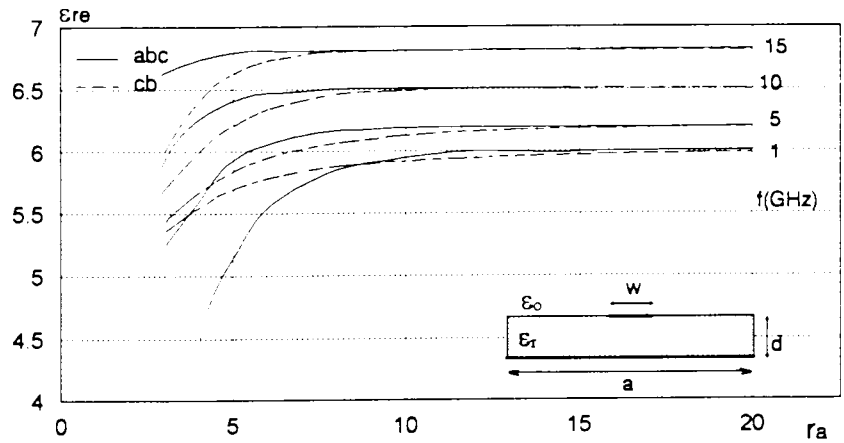

Fig. 4.7 Frequency effect on rapid convergence ABC-CB
d=1mm; rw=w/d=1; rb=b/d=50; ε_r=8.875

In order to see the effect of frequency on this minimum value of **a** which gives the same value for ε_{re} for both cases, the computations done for four frequencies 1, 5, 10, and 15GHz are reported in Fig. 4.7. We can see that the minimum value of **a** decreases with increasing frequency. We have also noticed during the simulation a high improvement in the convergence behavior.

2. Convergence

The convergence behavior is of great importance for the ABC analysis to see its stability, memory and time requirements. Consequently, this problem has been studied intensively and the results of the study are shown in Figs. 4.8 to 4.10. The effective permittivity as a function of the number of discretization lines on the strip using different edge parameters is presented in Fig. 4.8. The convergence is shown to be assured independently of the position of the first discretization line on the metallization strip, but with more effort if the edge condition is not satisfied. We can notice from this graph, that the optimal edge parameter can be deduced to be slightly greater than 0.25. The error in the effective dielectric constant as a function of the number M is presented in Fig. 4.9, which shows that, for the optimal edge positioning q=0.25, it becomes less than 0.5% with only two lines on the metallization strip M=2. This is a consequence of the line shifting discretization scheme which compensates very well the discretization error. The convergence as a function of the normalized discretization step h/d is

given in Fig. 4.10, where for an error of about 0.5% in the normalized wavelength parameter λ_g/λ_0, the minimum number of discretization lines M=2, in the case of optimal edge positioning, is included within that error interval. Similar results are obtained for closed boundaries in references [7,11].

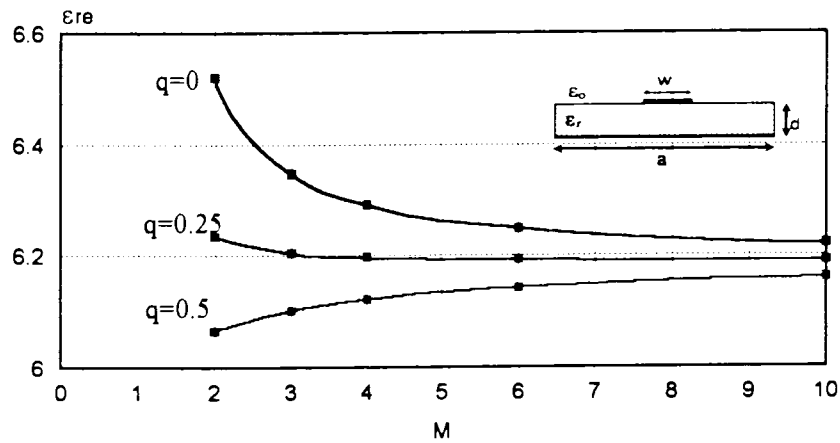

Fig. 4.8 Convergence behavior of ε_{re} for various edge parameters
d=1mm; rb=50; ra=10; rw=1; f=5GHz; ε_r =8.875.

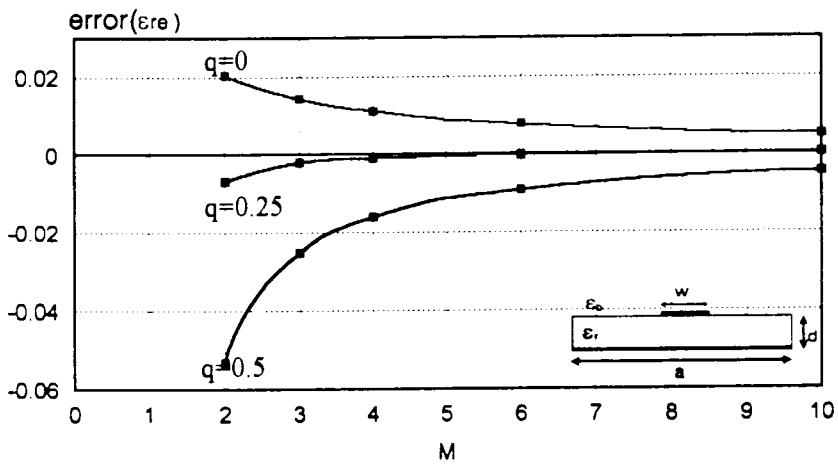

Fig. 4.9 Relative convergence error for ε_{re}
d=1mm; ra=10; rw=1; f=5GHz; ε_r =8.875

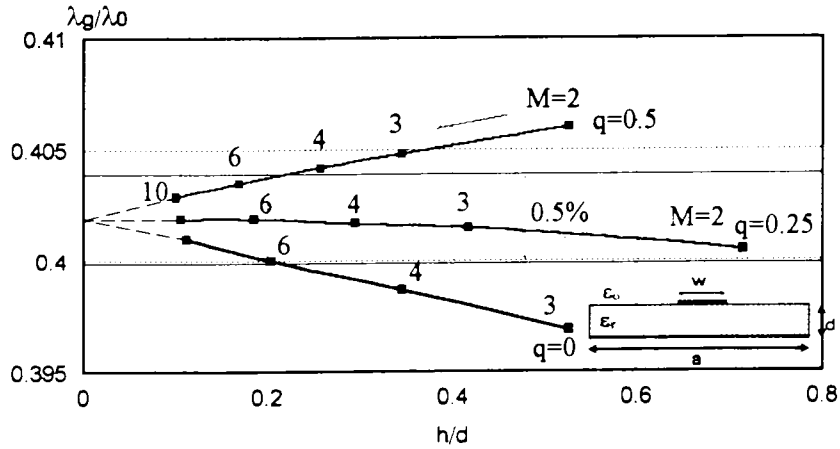

Fig. 4.10 Convergence behavior of the normalized wavelength λ_g/λ_0
d=1mm ; w=1mm; rb=50; ra=10; rw=1; f=5GHz; ε_r =8.875

3. Dispersion diagrams

The behavior of the effective permittivity ε_{re} as a function of frequency changes known as the dispersion diagram, for different substrate permittivities, exhibits the same behavior as compared to that of a closed boundary case.

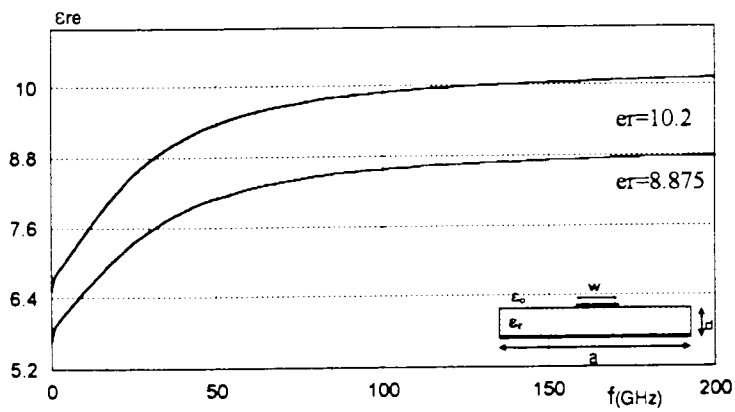

Fig. 4.11 Effective permittivity ε_{re} versus frequency
d=1mm; rw=1; ra=10; M=5 lines

In connection to this, Fig. 4.12 gives the dispersion curves as a function of the normalized substrate thickness d/λ_0 using different normalized strip metallization widths w/d. In Fig. 4.12.(a), the normalized metallization strip width is shown to be proportional to the effective

permittivity, whereas in Fig. 4.12.(b) it is inversely proportional to the characteristic impedance. The results shown in Figs. 4.11 and 4.12 are in total accordance with the existing graphical data published in reference [45] using the Spectral Domain approach.

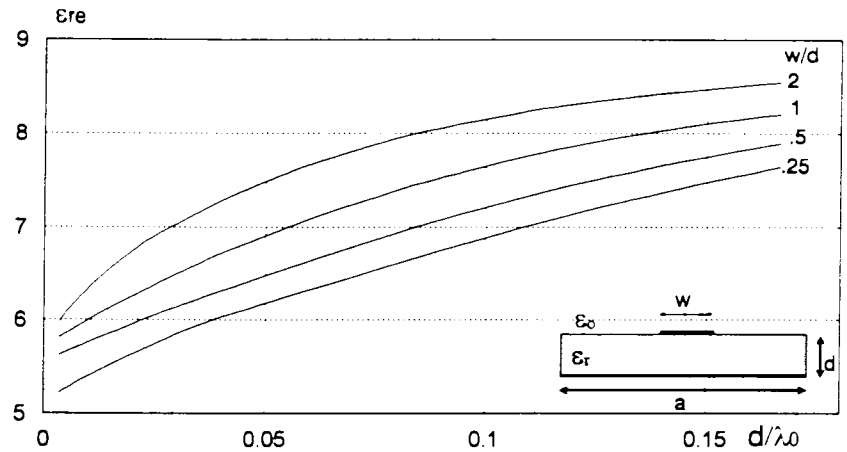

(a)

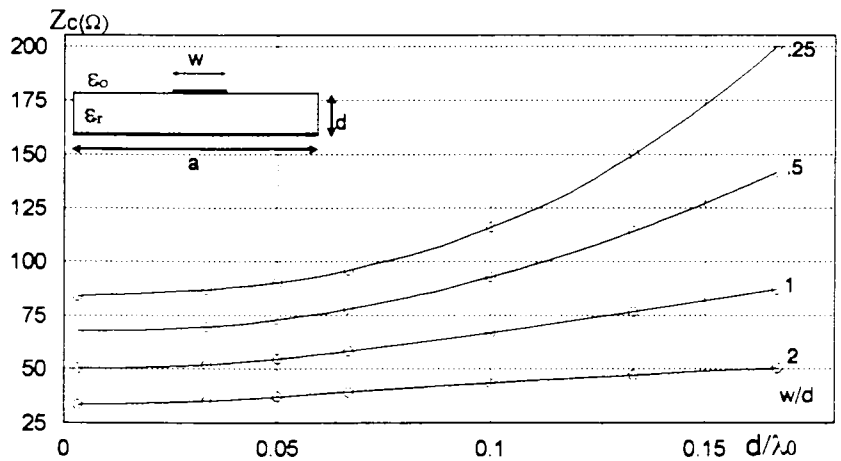

(b)

Fig. 4.12 Dispersion diagram versus normalized substrate thickness d/λ_0.
(a) Effective permittivity ε_{re} (b) Characteristic impedance Z_c
d=1mm; rb=50; ra=7; ε_r =9;

4. Effect of anisotropy

Dielectric anisotropy is another important effect in the analysis of microstrip-based MIC and MMIC's. It has been considered in our analysis for all the studied structures.

In fact, Fig. 4.13 presents a comparison in the effective permittivity characteristics of structures based on anisotropic substrates for both open and closed types. The sapphire substrate, for which $\varepsilon_{\perp} = 9.4$ and $\varepsilon_{\theta} = 11.6$, is taken as an example. It is shown that for different normalized substrate thickness w/d, the behavior of ε_{re} with respect to frequency changes is identical for both structures. The variation of the dispersion characteristics by ignoring the anisotropy when considering an equivalent isotropic substrate of $\varepsilon_r = 9.4$ is given in Fig. 4.14. The obtained results are verified using the references [35,40] for closed boundary conditions with different dimensions **ra,** and they are found to agree very well with the published ones.

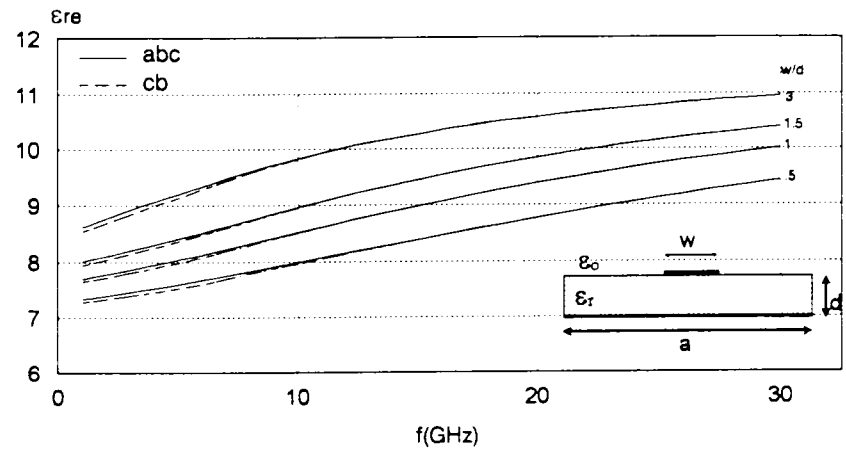

Fig. 4.13 Effective permittivity versus the frequency for sapphire substrate
d=1 mm; ra=12; $\varepsilon_{\perp} = 9.4$ and $\varepsilon_{\theta} = 11.6$

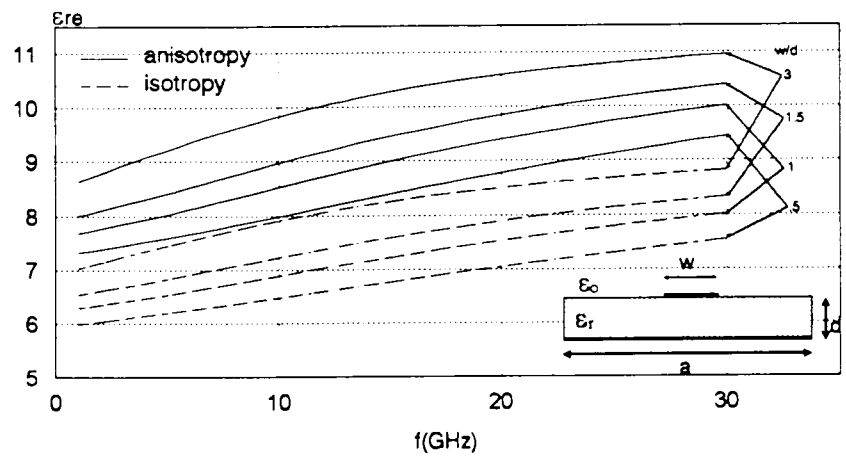

Fig. 4.14 Dispersion curve for both isotropic and anisotropic substrates
d=1 mm; ra=12; $\varepsilon_r = 9.4$; $\varepsilon_r = [\varepsilon_{\perp} = 9.4$ and $\varepsilon_{\theta} = 11.6]$

5. Effect of the upper boundary

The stripline dispersion characteristics are depicted in Figs. 15 and 16, where the effect of the upper boundary is illustrated as a function of frequency. It reveals that the dielectric constant is proportional to the upper normalized dimension b/d. When this ratio exceeds 15, the stripline exhibits the same behavior as an open upper boundary structure. A comparison with the closed boundary case is shown in Fig. 4.16, where the dispersion characteristics are shown to be significant when decreasing the value of b/d.

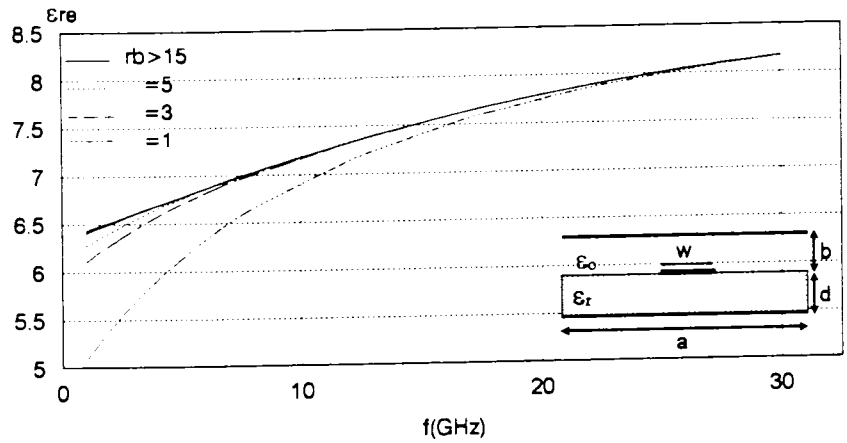

Fig. 4.15 Upper boundary effect on dispersion characteristics
d=1 mm; rw=2; ra=11; ε_r =9

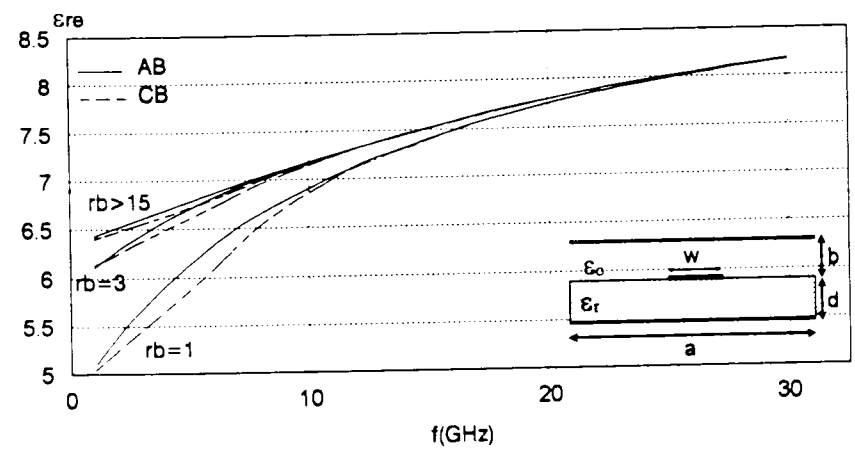

Fig. 4.16 Upper bound effect for AB-CB on dispersion curves
d=1mm ; rw=2; ra=11; ε_r =9

6. The Suspended microstrip

Fig. 4.17 shows the variation of the effective dielectric constant for the suspended stripline structure rb=b/d=2, and the suspended open microstrip line that correspond to $b_2/d>15$ as have been shown earlier in Fig. 4.15. It is observed that the effective dielectric constant is proportional to the ratio b_2/d.

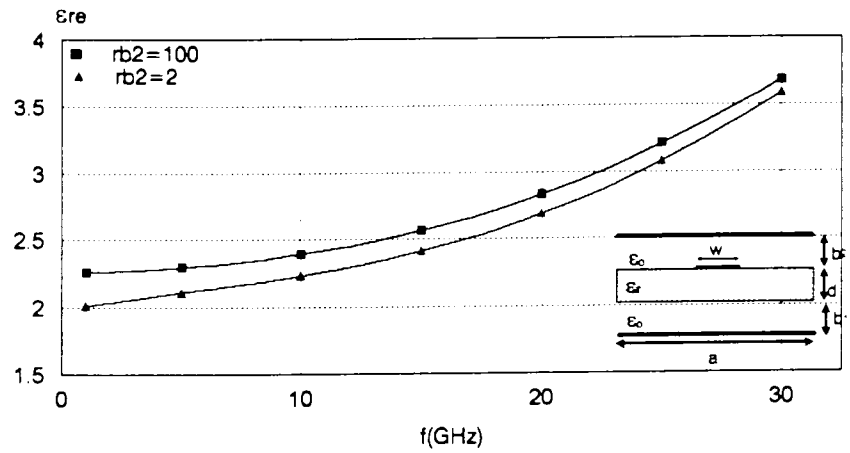

Fig. 4.17 Dispersion for suspended microstrip line
d=.6 mm; a=13 mm; rb_1=1; w=3 mm; ε_r =10.2

7. The edge-coupled microstrip structures

The dominant odd and even modes effective permittivities of an edge-coupled microstrip structure as a function of frequency are plotted in Figs. 4.18 and 4.19 for multiple ratios a/d. It may be observed from Fig. 4.18 that the dielectric constant for both modes increases as the ratio a/d increases. For a/d greater than 20, the dielectric constant remains approximately unchanged. This results for edge coupled structures are in accordance with the results of Fig.4.6 for the single microstrip. Moreover, the open structure is compared to the closed boundary case in Fig. 4.19, where it is shown that for a/d=20 the maximum error in the odd mode dielectric constant for both structures is of the order of 0.02% and of the order of 0.5% for the even mode constant.

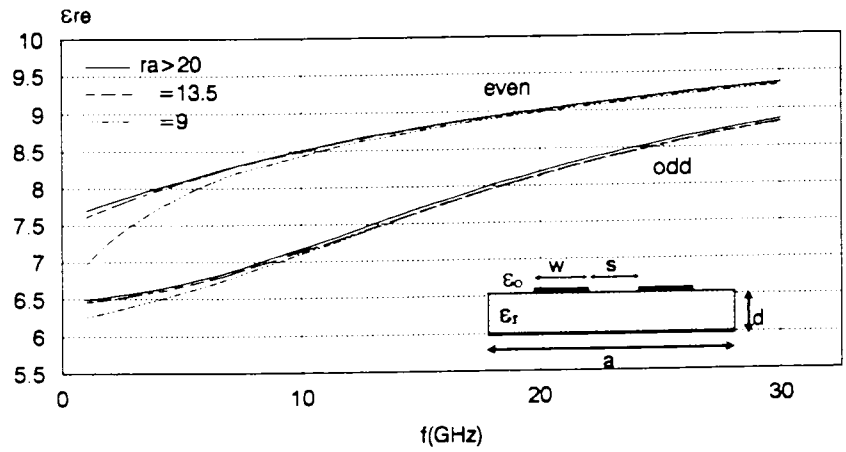

Fig. 4.18 Dispersion diagram. Effect of transverse dimension ra in edge-coupled strips
d=1mm; rw=1.5; rs=1.5; ra=[9 11.5 13.5 20]; rb=19; ε_r =10.2;

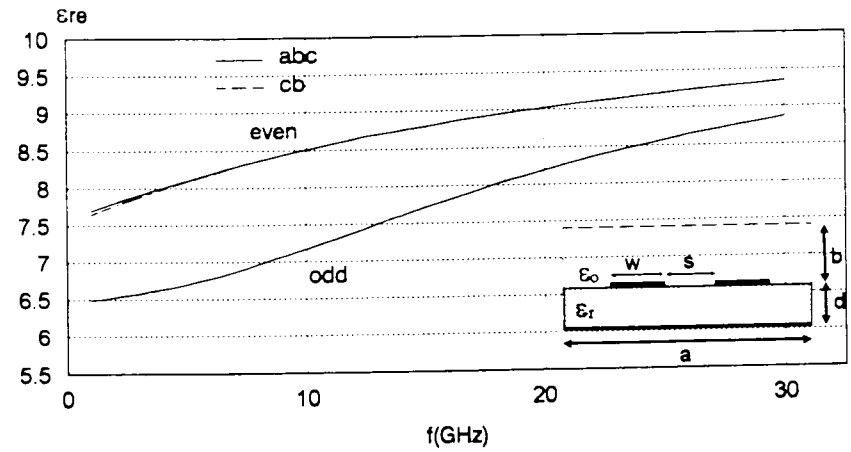

Fig. 4.19 Dispersion curve. Effect of CB in edge-coupled strips
d=1 mm; rw=1.5; rs=1.5; ra=20; rb=19; ε_r =10.2;

8. The Suspended edge-coupled lines

On the other hand, the suspended edge-coupled striplines characteristics are presented in Figs.4.20 and 4.21. A comparison of ABC to CB analysis is plotted in Fig. 4.20, where it is shown from this figure, that the effect of metallic walls on the odd mode dielectric constant is higher than that of the even mode. In addition to this, it is observed from Fig. 4.21 that the variation of the effective dielectric constant as a function of frequency increases as the ratio b_2/d increases.

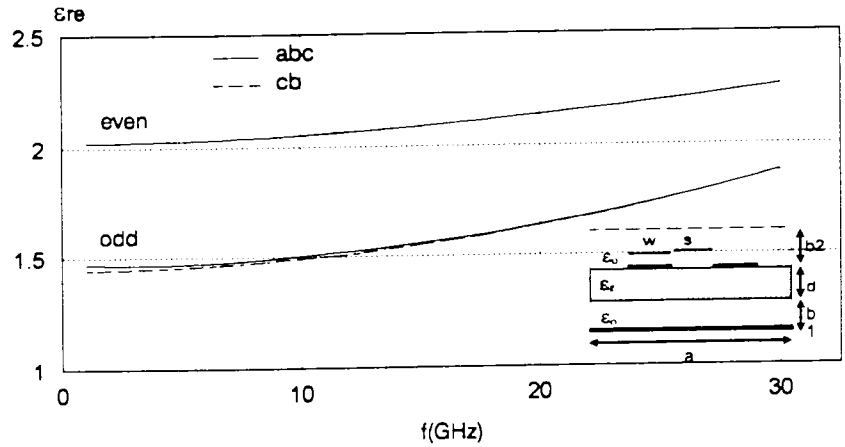

Fig. 4.20 Effective permittivity versus the frequency in edge-coupled strips
d=1 mm; w=1 mm; s=1 mm; a=15 mm; rb_1=2; rb_2=1; ε_r =3.78;

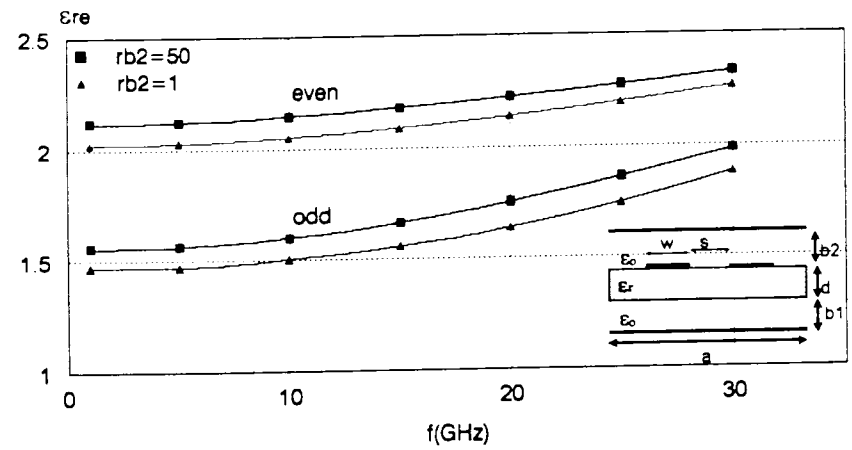

Fig. 4.21 Effective permittivity versus the frequency in edge-coupled strips
d=1mm; w=1mm; s=1mm; a=15mm; rb_1=2; rb_2=[1 50]; ε_r =3.78;

9. The Broadside-coupled suspended microstrip line

The variations of the dominant even and odd modes effective dielectric constants of a broadside-coupled suspended stripline as a function of frequency are depicted in Fig. 4.22. It shows that both modes increase slowly as the frequency increases compared to the edge-coupled structures, and the odd mode decreases more rapidly than the even mode by changing the ratio $rb_1=b_1/d$.

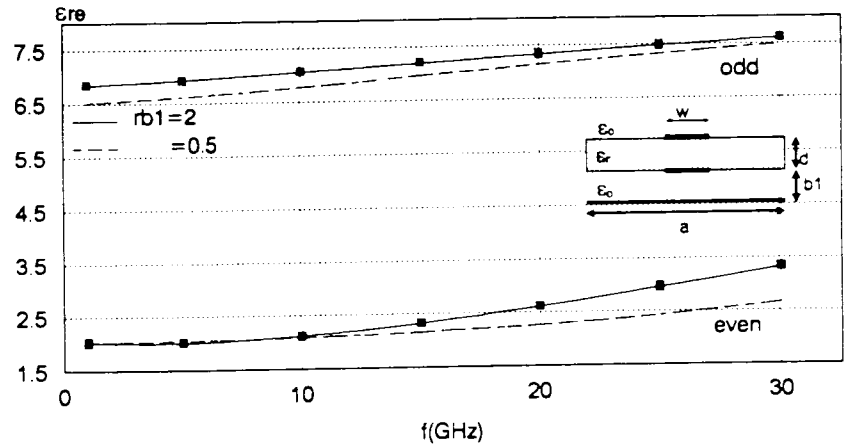

Fig. 4.22 Effective permittivity versus the frequency for the broardside-coupled strip
d=.6 mm; a=10.6 mm; ra=17.6667; rb_2=50; w=.6mm; rw=1; ε_r =9.6

10. The Broadside-Edge coupled suspended stripline

The variation of the effective dielectric constants for a broadside-edge coupled suspended microstrip line structure as a function of frequency are plotted in Figs. 4.23 to 4.25. Firstly, the effective permittivity is given as a function of frequency for the open type structure, where it is apparent that the rate of variation in the effective dielectric constant for the four modes is slow. Secondly, the effect of the upper boundary is introduced through a ground plane at $b_2/d=2$. Finally, in Fig. 4.25, the effective permittivity is shown to be decreasing as the ratio $rb_2=b_2/d$ decreases. The plotted results in Figs. 4.17 to 4.25 are compared to the results existing in reference [46] for closed boundaries analysis, and it has shown a good agreement within the accuracy of graphical data.

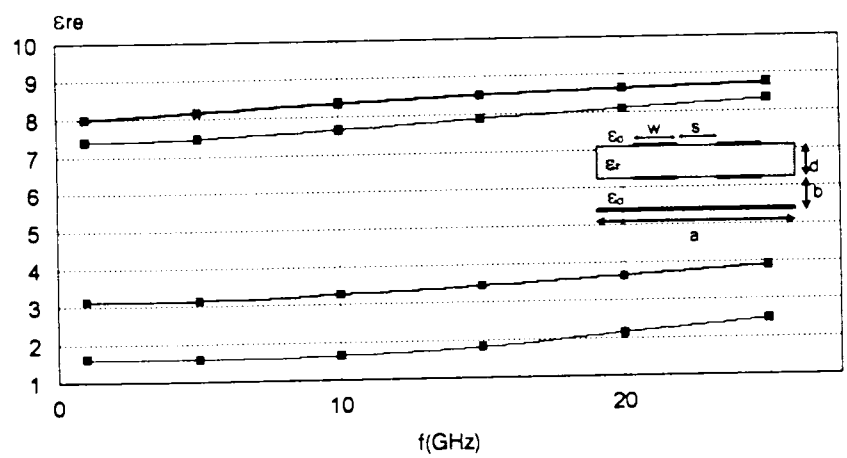

Fig. 4.23 Effective permittivity versus frequency for broardside-edge coupled strips
d=.6mm; a=12.2mm; rb_1=2; rb_2=100; w=1mm; s=1mm; M=5; ε_r =10.2

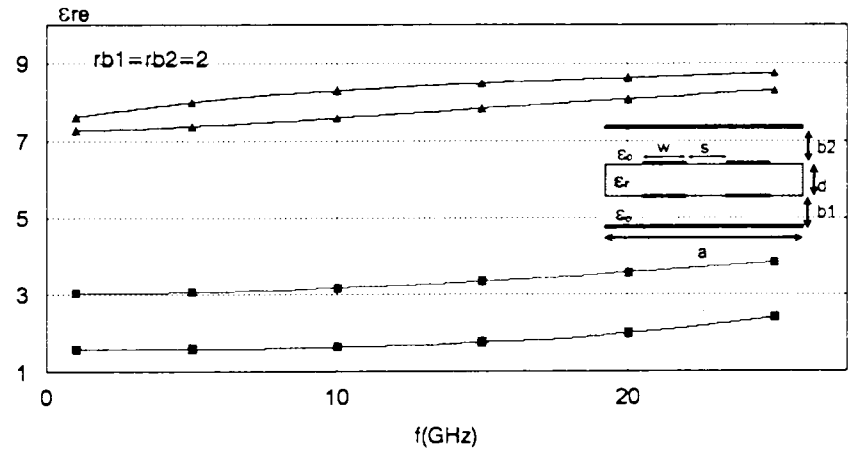

Fig. 4.24 Effective permittivity versus frequency for broardside-edge coupled strips
d=.6mm; a=12.2mm; rb_1=2; rb_2=2; w=1mm; s=1mm; M=5; ε_r =10.2

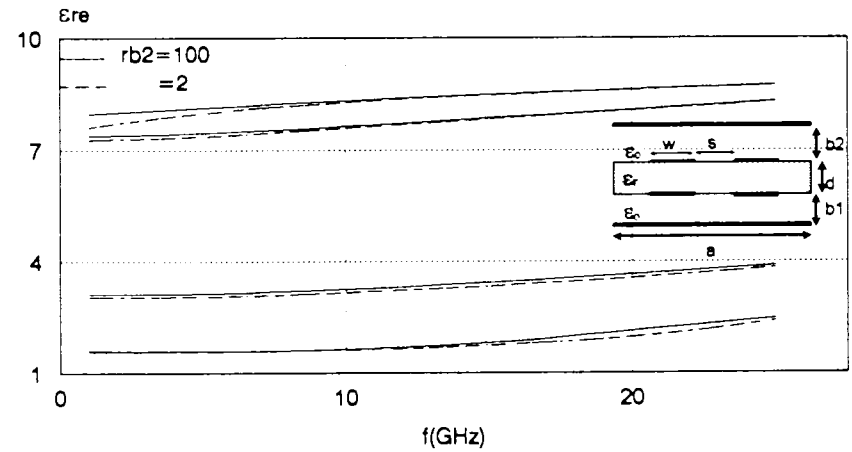

Fig. 4.25 Effective permittivity versus frequency for broardside-edge coupled strips
d=.6mm; a=12.2mm; rb_1=2; rb_2=[2 100]; w=1mm; s=1mm; M=5; ε_r =10.2

11. Fields and currents calculation for different structures

The electric field components and the current distributions, for both single and coupled line structures, are presented in Figs. 4.26 to 4.30. Concerning the field components and currents, the Figs. 4.26 and 4.27 of a single microstrip, show that only the *z*- component of the electric

field components that is highly affected by the existence of the metallic enclosure. In the CB structures, the z-component of the electric field vanishes to zero at the boundary due to the imposed Dirichlet-Dirichlet condition, however, for the open boundary case, this component has a non zero value due to the presence of ABC's. The foregoing figures are compared to graphical data in references [11,31] for both closed and open structures, where it has shown a total agreement.

Figs. 4.28 and 4.29 depict the current densities and the electric field components respectively for both even and odd modes of a two edge-coupled microstrip structure. An elaborated development can be handled in studying these curves, as an example, the investigation on the even or odd modes effects on the current density distributions.

As an example of multi-strip structures, the components of the electric field components E(x), E(y), and E(z) are given for a four edge-coupled microstirp configuration. Each of the Figs. 4.30 to 4.32 plots the related four modes of the corresponding electric field components.

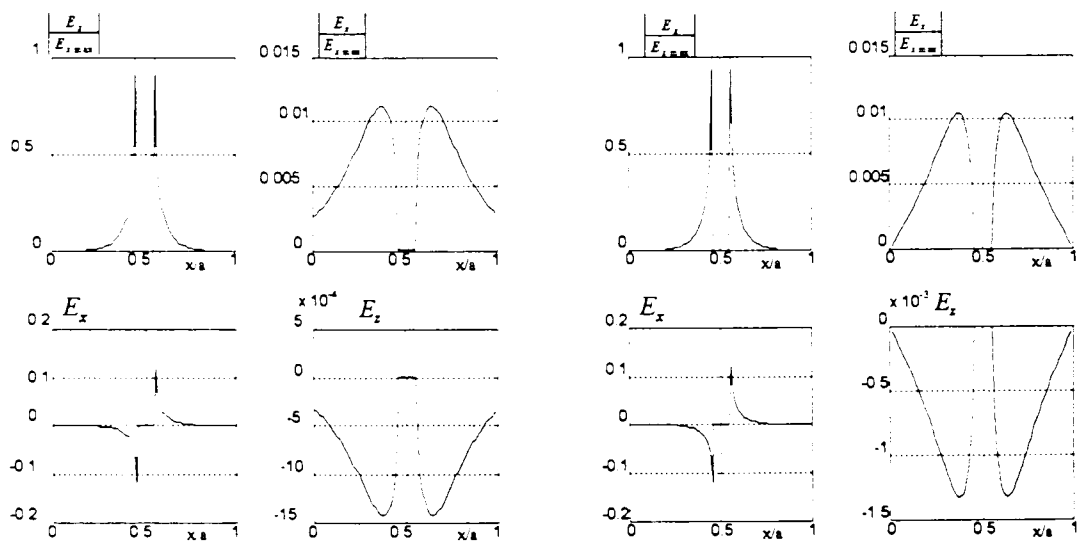

(a) ABC (b) CB

Fig. 4.26 Fields at a single microstrip interface. (a) ABC (b) CB
d=1mm; ra=10; rw=1; f=5GHz; ε_r =8.875; M=5.

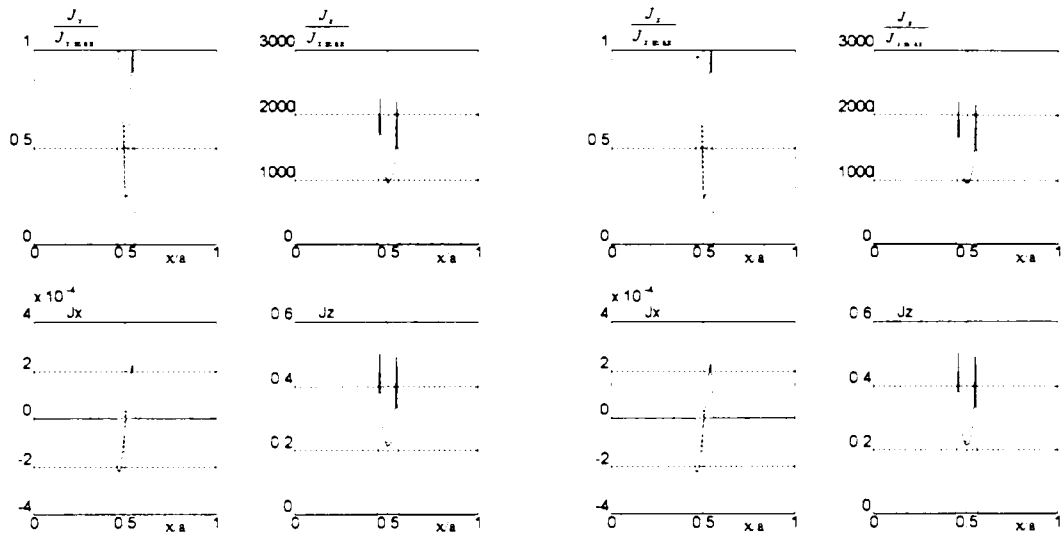

(a) ABC (b) CB

Fig. 4.27 Currents at a single microstrip interface. (a) ABC (b) CB.
d=1mm; ra=10; rw=1; f=5GHz; M=5.

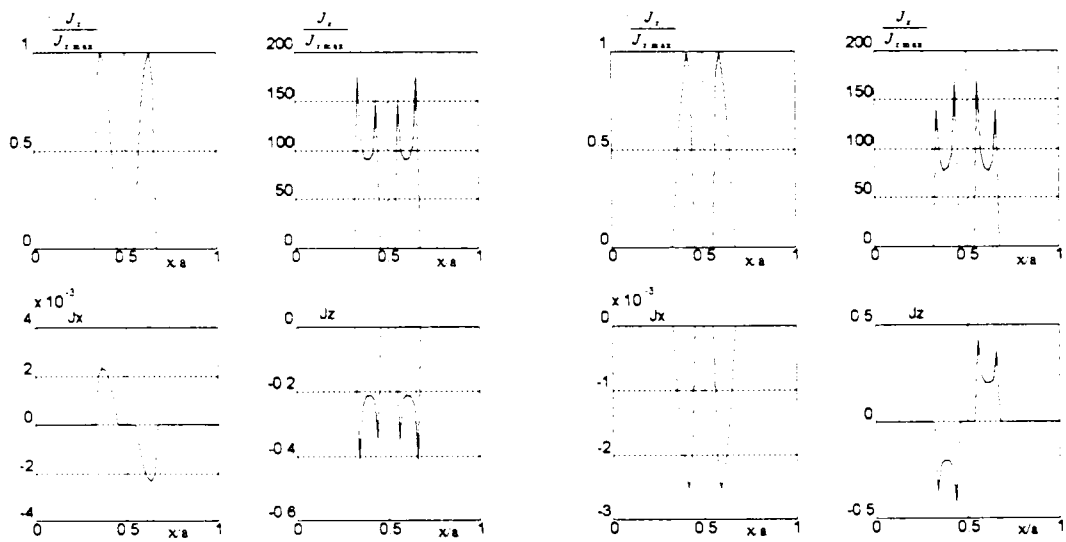

(a) even (b) odd

Fig. 4.28 Currents at an edge-coupled line interface. (a) even (b) odd
d=1mm; ra=13.5; rw=1.5; rs=1.5; f=5GHz; ε_r =8.875;

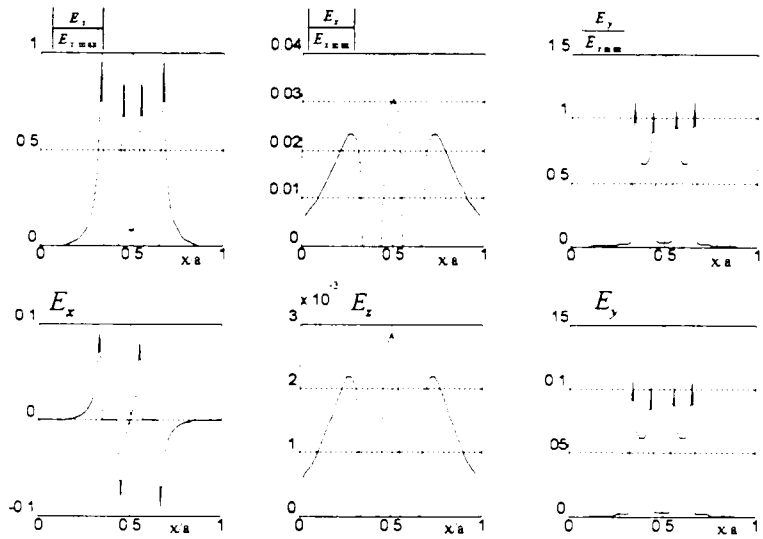

(a) even

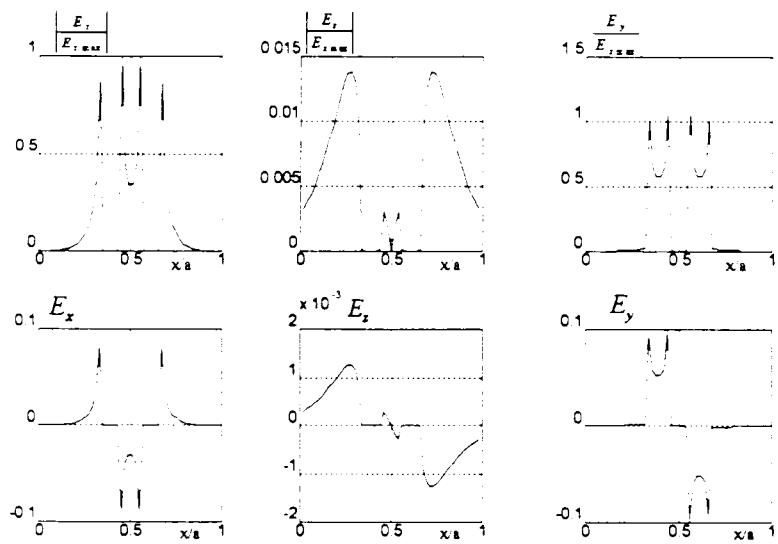

(b) odd

Fig. 4.29 Field components at an edge-coupled line interface.
d=1mm; ra=13.5; rw=1.5; rs=1.5; f=5GHz; ε_r =8.875;

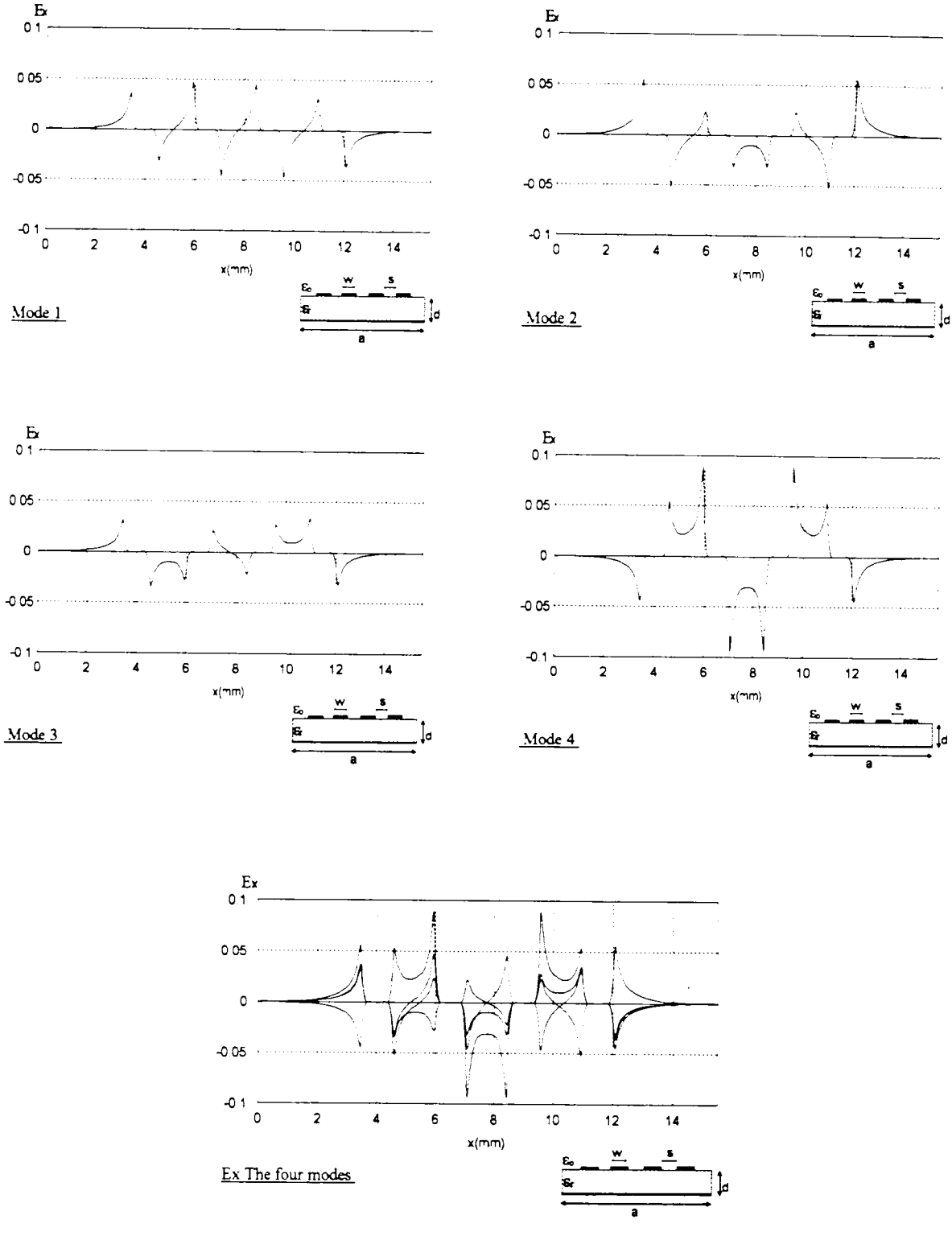

Fig. 4.30 Ex Electric field modes in a four edge-coupled strips
d=1mm; rw=1; rs=1.5; ra=15.5; rb=50; f=5GHz; ε_r =8.875;

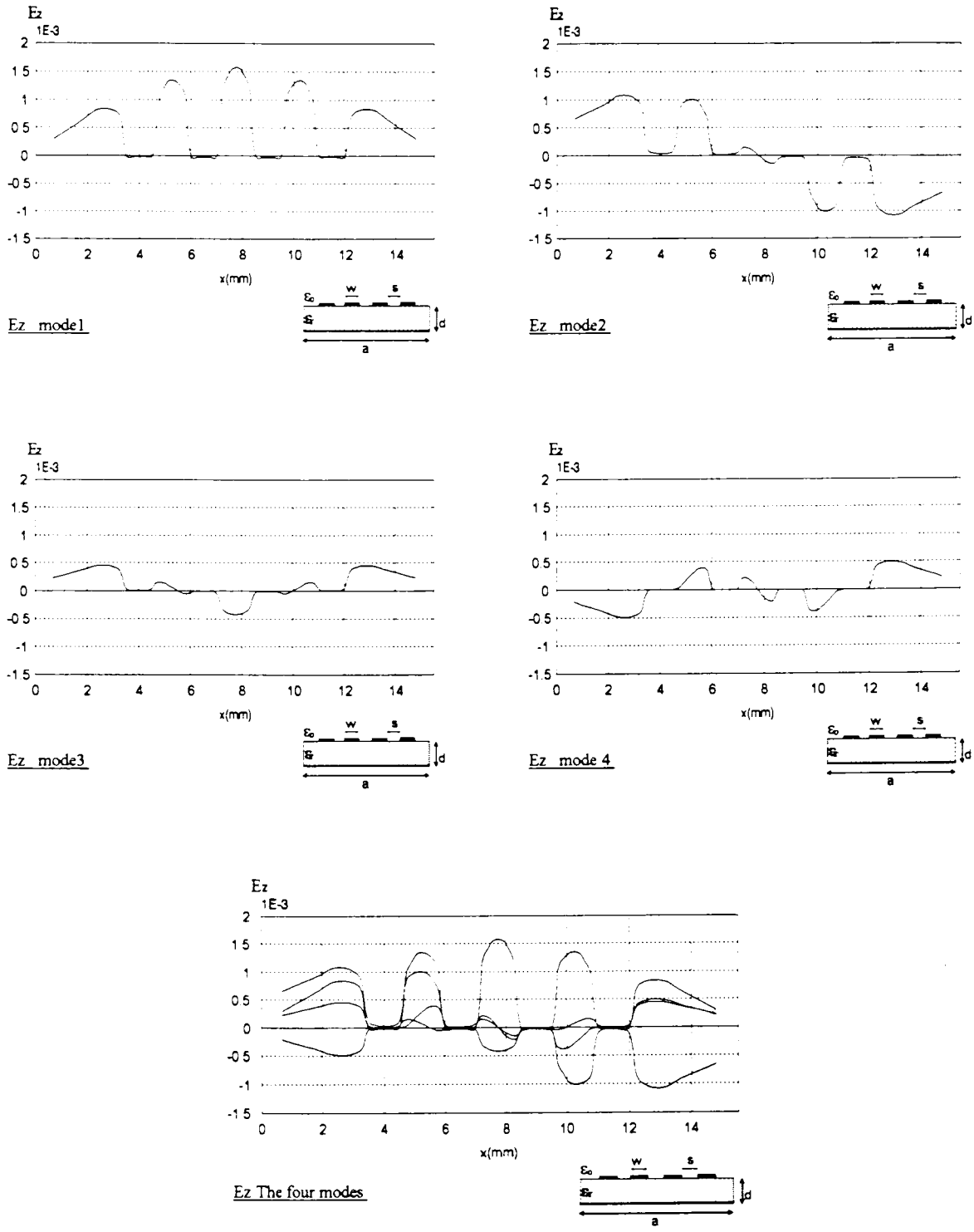

Fig. 4.31 Ez Electric field modes in a four edge-coupled strips
d=1mm; rw=1; rs=1.5; ra=15.5; rb=50; f=5GHz; ε^r =8.875;

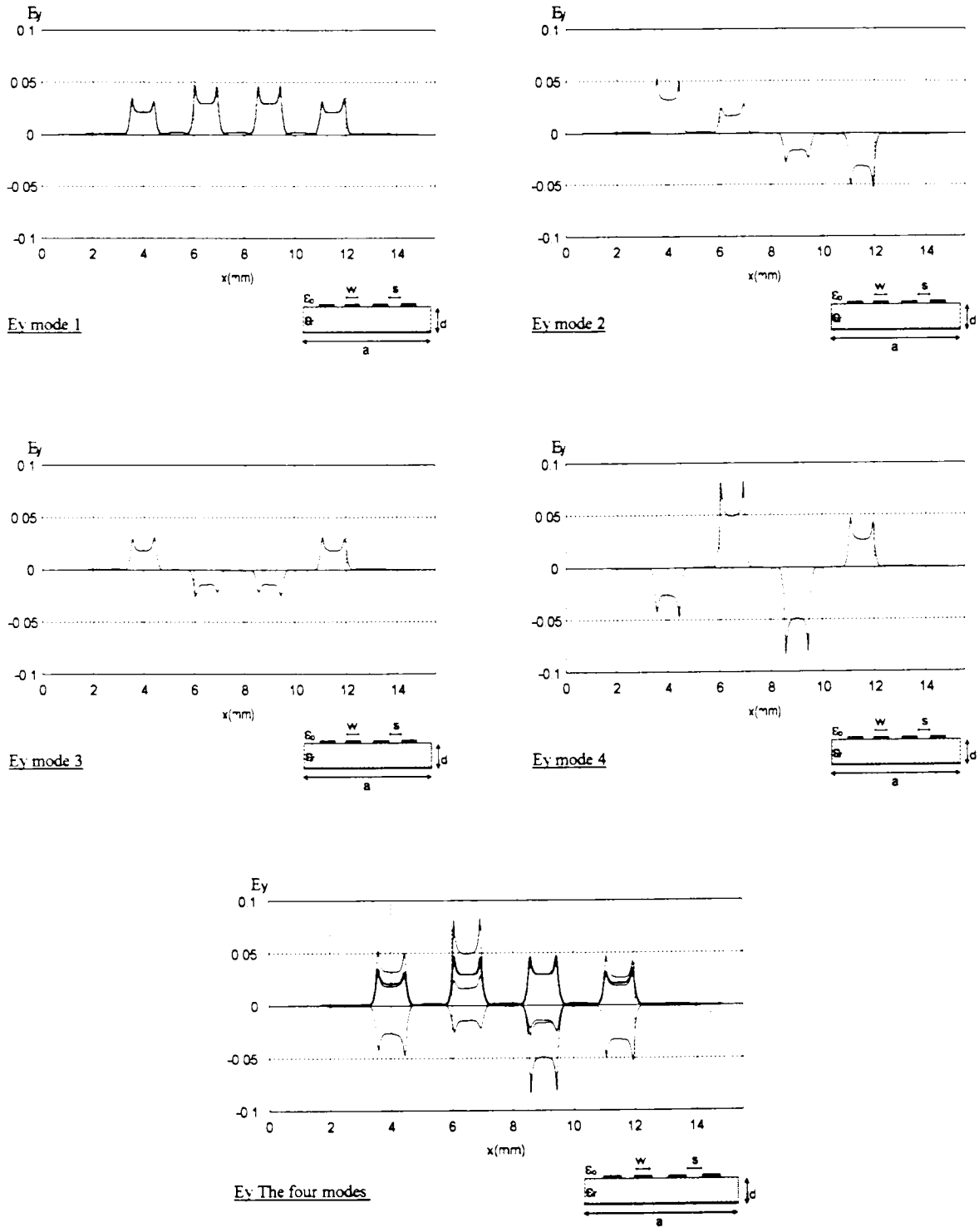

Fig. 4.32 Ey Electric field modes in a four edge-coupled strips
d=1mm; rw=1; rs=1.5; ra=15.5; rb=50; f=5GHz; ε_r =8.875;

4.5 CONCLUSION

In this chapter, the full-wave characterization of zero thickness open planar structures is achieved using the analysis developed in the former one. The characterization is performed through two steps. In the first step, a field transfer relation is defined between the interfaces of the same dielectric layer, that can be conducted in either transformed domain or original domain. In the second step, a more advanced analysis has been adopted in order to establish a general relation that links all the structure parameters, called the characteristic equation of the structure. Solving this equation, which is an indirect eigen value problem, leads to the calculation of the propagation constant. This last equation also, leads to the calculation of all the structure relatives. Consequently, a large set of structures can be characterized using this development starting from a single-layer single-microstrip to multi-layers multi-conductors zero thickness structures.

The results obtained through the simulation of the developed mathematical algorithm including dispersion, field components, and current densities have shown a total accordance with the previously published data.

The software developed can handle a variety of waveguiding structures such as, single microstrip, suspended microstrip, multiple edge coupled lines, multiple broadside coupled lines, and other complex zero thickness structures. It also considers both isotropic and anisotropic dielectric substrates.

Chapter 5

FULL WAVE ANALYSIS OF FINITE THICKNESS OPEN STRUCTURES WITH ISOTROPIC AND ANISOTROPIC SUBSTRATES

5.1 INTRODUCTION

In the previous chapter, we considered that the structures have strips with zero thickness or of infinitely thin thickness, which is of practical interest for many structures used in the field of microwaves. However, in most current MMIC structures, the finite thickness must be taken into consideration, as it is of the same order of magnitude as the width of the strip or of the slots between the strips. This is in fact, a natural result of the development of semiconductors technology.

The analysis of open structures with finite thickness strips is undoubtedly analogous to the closed boundary structures [47-51]. The distinct difference operators should be firstly developed, and then the fields transfer and matching equations are established.

5.2 MATHEMATICAL ANALYSIS

Consider the structure shown in Fig. 5.1, which consists of two different layers I and III. Between the two layers there is a microstrip of finite thickness t. Proceeding in the same way as in the case of the closed boundary structure from the interior side, and in the same manner as for the ABC for the two lateral sides. This results in a discretized structure similar to that of the closed case, however the two lateral conditions are substituted by the Absorbing Boundary Conditions operator instead of the closed boundary condition case.

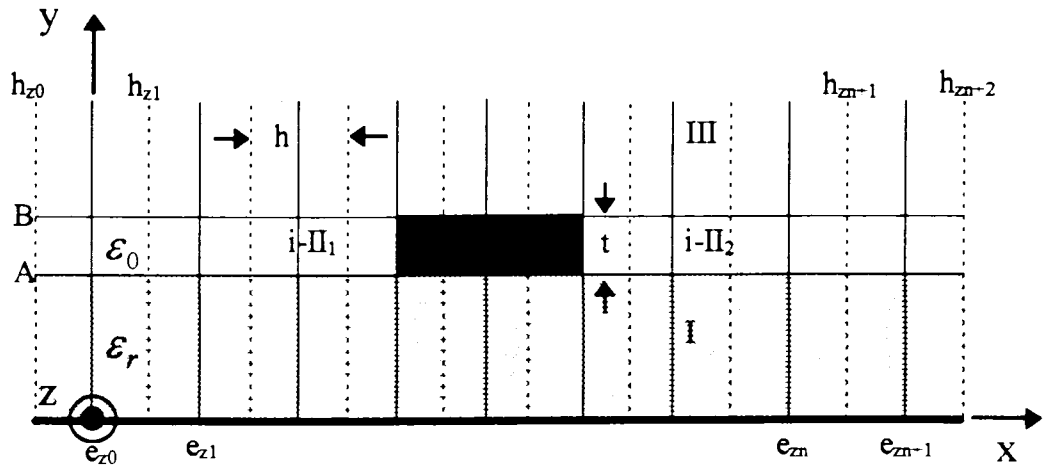

Fig. 5.1. Discretization scheme of an open finite thickness microstrip structure

Concerning the two homogeneous layers I and III, the analysis remains the same as it has been described in chapter 3, but care should be taken about the edge positioning at the finite strip edges. An electric field discretization line has to be put exactly on the edge of the finite metallization strip to satisfy the Dirichlet condition (see Fig. 5.1). The field behavior in layers I and III are fully described by eqs.(3.33) and (3.39) in the case of isotropic medium, and by eqs.(3.85) and (3.95) in the case of anisoptropic medium.

5.2.1 Difference Operators for Intermediate Regions

Consider the left side of the structure in the intermediate region i-II$_1$ (see Fig. 5.1), the left lateral boundary is an Open Boundary, where an ABC operator has to be applied, whereas at the right side, the Dirichlet boundary condition is already satisfied by the presence of the metallic boundary of the strip. Any analysis conducted through this intermediate region i-II$_1$ to identify the different operators will end up with a mixed ABC-CB operators or precisely in this special case ABC-Dirichlet difference operators.

Hence, for the left and right side intermediate subregions i-II$_1$ and i-II$_2$, the mixed boundary conditions will lead to a mixed systems of matrices that are symmetric in the lateral terms. The systems of mixed boundary conditions for both left and right intermediate regions can be given successively by

$$\begin{cases} i=1 \;\; : \; D_y^2 e_{z1} + (-h^{-2})(2+a)e_{z1} + (-h^{-2})(-1-b)e_{z2} + k_0^2 \varepsilon_d e_{z1} = 0 \\ \qquad\qquad \vdots \\ i>1 \;\; : \; D_y^2 e_{zi} + \left(\dfrac{e_{z(i-1)} - 2e_{z(i)} + e_{z(i+1)}}{h^2} \right) + k_0^2 \varepsilon_d e_{zi} = 0 \\ \qquad\qquad \vdots \\ i=n_1 \;\; : \; D_y^2 e_{zn_1} + \left(\dfrac{e_{z(n_1-1)} - 2e_{zn_1}}{h^2} \right) + k_0^2 \varepsilon_d e_{zn_1} = 0 \end{cases} \tag{5.1}$$

where n_1 is the number of lines at the left intermediate region, and

$$\begin{cases} i=1 \;\; : \; D_y^2 e_{z1} + \left(\dfrac{e_{z2} - 2e_{z1}}{h^2} \right) + k_0^2 \varepsilon_d e_{z1} = 0 \\ \qquad\qquad \vdots \\ i>1 \;\; : \; D_y^2 e_{zi} + \left(\dfrac{e_{z(i-1)} - 2e_{z(i)} + e_{z(i+1)}}{h^2} \right) + k_0^2 \varepsilon_d e_{zi} = 0 \\ \qquad\qquad \vdots \\ i=n_2 \;\; : \; D_y^2 e_{zn_2} + (-h^{-2})(2+a)e_{zn_2} + (-h^{-2})(-1-b)e_{z(n_2-1)} + k_0^2 \varepsilon_d e_{zn_2} = 0 \end{cases} \tag{5.2}$$

where n_2 (5.2) is the number of lines at the right intermediate regions.

These two systems can be written in matrix form as

$$\left[D_y^2 - (-h^{-2}) P_{ei} + k_0^2 \varepsilon_d I \right] \Psi_i^e = 0 \tag{5.3}$$

where the subscript i designates the number of intermediate subregions.

Equ.(5.3) is solved following the same procedure using the Method of Lines as described in section.3.4, where the tridiagonal matrices P_{ei} must be diagonalized using an appropriate transformation matrix T_{ei} in the case of the electric field. Equivalently, the procedure described above for the electric field is valid for the magnetic field analysis, from which we can deduce the first and second order difference operators for the mixed operators, as it follows in the two forthcoming subsections

5.2.1.1 ABC-DIRICHLET Boundary Conditions

By considering the subsystem (5.1) which characterizes the left intermediate subregion, the second order difference operators for both electric and magnetic field systems are given as

$$P_{en} = \begin{bmatrix} p_{11} & p_{12} & & & 0 \\ -1 & 2 & -1 & & \\ & \ddots & \ddots & \ddots & \\ & & -1 & 2 & -1 \\ 0 & & & -1 & 2 \end{bmatrix} \tag{5.4}$$

with

$$p_{11} = 2 + a \quad ; \quad p_{12} = -1 - b$$

and

$$P_{hn} = \begin{bmatrix} p_{11} & p_{12} & p_{13} & & 0 \\ -1 & 2 & -1 & & \\ & \ddots & \ddots & \ddots & \\ & & -1 & 2 & -1 \\ 0 & & & -1 & 1 \end{bmatrix} \tag{5.5}$$

with

$$p_{11} = 1 + a \quad ; \quad p_{12} = -1 - b - a \quad ; \quad p_{13} = b$$

where the subvariables a and b are those defined in chapter 2 for either isotropic or anisotropic substrates, from which we can deduce the first order operators as

$$D_{en} = \begin{bmatrix} 1+a & -b & & 0 \\ -1 & 1 & & \\ & \ddots & \ddots & \\ & & -1 & 1 \\ 0 & & & -1 \end{bmatrix} ; \quad D_{hn} = \begin{bmatrix} 1 & -1 & & 0 \\ & 1 & \ddots & \\ & & \ddots & -1 \\ 0 & & 1 & -1 \end{bmatrix} \tag{5.6}$$

5.2.1.2 DIRICHLET-ABC Boundary Conditions

Considering the subsystem (5.2), in the same way as above, which characterizes the right intermediate subregion, the second order difference operators for both electric and magnetic field systems can be expressed as

$$P_{ei} = \begin{bmatrix} 2 & -1 & & & 0 \\ -1 & 2 & -1 & & \\ & \ddots & \ddots & \ddots & \\ & & -1 & 2 & -1 \\ 0 & & & p_{12} & p_{11} \end{bmatrix} \tag{5.7}$$

with

$$p_{11} = 2 + a \quad ; \quad p_{12} = -1 - b$$

and

$$P_{hi} = \begin{bmatrix} 1 & -1 & & & 0 \\ -1 & 2 & -1 & & \\ & \ddots & \ddots & \ddots & \\ & & -1 & 2 & -1 \\ 0 & & p_{13} & p_{12} & p_{11} \end{bmatrix} \tag{5.8}$$

with

$$p_{11} = 1 + a \quad ; \quad p_{12} = -1 - b - a \quad ; \quad p_{13} = b$$

From which we can deduce the following first order difference operators

$$D_{ei} = \begin{bmatrix} 1 & & & 0 \\ -1 & 1 & & \\ & \ddots & \ddots & \\ & & -1 & 1 \\ 0 & & +b & -1-a \end{bmatrix} \; ; \quad D_{hi} = \begin{bmatrix} 1 & -1 & & 0 \\ & 1 & \ddots & \\ & & \ddots & -1 \\ 0 & & 1 & -1 \end{bmatrix} \tag{5.9}$$

5.2.2 Multi-Strip Configuration

In the case of two or more strips of finite metallizations at the interface, the analysis concerning the two lateral intermediate regions II_1 and II_3, (see Fig. 5.2), is similar to the one of the previous subsection. But, the subregions between the metallizations are considered as regions under the Dirichlet-Dirichlet boundary conditions, because of the two metallic walls of the strips. For the corresponding expressions of the difference operators, the complete analysis has been presented in chapter 1, that is directly applicable to such intermediate subregions. See Fig. 5.2.

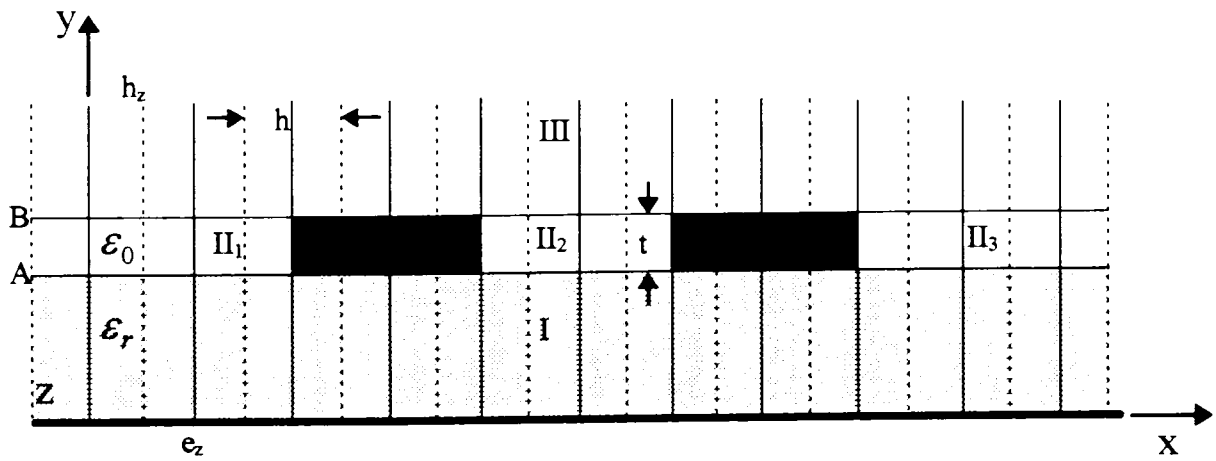

Fig. 5.2. Discretization scheme of a multi-finite thickness strip structure

Note that the discretization lines through the whole structure are identical. This is chosen as such to enable the continuity study to be handled at each interface. Note also that, the transformations in the three regions (I, II, and III) are distinct.

5.3 FIELD TRANSFER RELATIONS

Consider the structure shown in Fig. 5.3, it is composed of an arbitrary number of metallization strips laying between two dielectric layers. Using the analysis based on absorbing boundary conditions operators as described above, each dielectric layer and subregion in the structure will have its own transformation matrices, its first and second order difference operators, and hence, its diagonal and quasi-diagonal matrices. Therefore, the analysis must be carried out in the original domain by matching the field parameters at the layers interfaces of the whole structure.

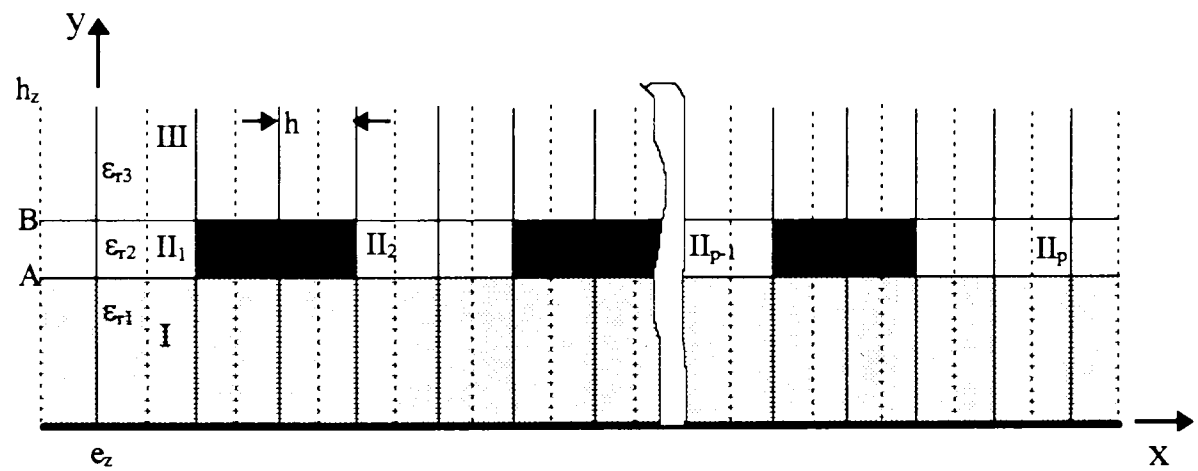

Fig. 5.3 Discretization scheme of a multi-strip interface

Following the procedure described in section.4.2, for the layer I and layer III, the field transfer equations are similar to those of eqs.(3.63) and (3.120) for isotropic and anisotropic layers respectively. Similarly, a field transfer equation can be established for each intermediate region (IIi) as

$$\eta_0 \begin{bmatrix} -j\overline{H}_{zA} \\ \overline{H}_{xA} \\ -j\overline{H}_{zB} \\ \overline{H}_{xB} \end{bmatrix}_{IIi} = \begin{bmatrix} \overline{y}_1^{IIi} & \overline{y}_2^{IIi} \\ \overline{y}_2^{IIi} & \overline{y}_1^{IIi} \end{bmatrix} \begin{bmatrix} \overline{E}_{xA} \\ -j\overline{E}_{zA} \\ -\overline{E}_{xB} \\ j\overline{E}_{zB} \end{bmatrix}_{IIi} \tag{5.10}$$

The quantities in the block matrices $\overline{y}_1^{IIi}$ and $\overline{y}_2^{IIi}$ in equ.(5.10) are defined by equ.(3.61) for isotropic medium, and by equ.(3.121) for the anisotropic medium. The representation of

equ.(5.10) is quite different from one intermediate region to another, due to the boundary conditions and to the number of discretization lines, especially, for λ and T which are again different for those of regions I and III. Using the notation, previously described in equ.(3.62), the subvectors of the field components at the intermediate regions interfaces are expressed as

$$\overline{H}_{A,BIIi} = \eta_0 \begin{bmatrix} -j\overline{H}_{zA,B} \\ \overline{H}_{xA,B} \end{bmatrix}_{IIi} \quad ; \quad \overline{E}_{A,BIIi} = \begin{bmatrix} \overline{E}_{xA,B} \\ -j\overline{E}_{zA,B} \end{bmatrix}_{IIi} \tag{5.11}$$

in the transformed domain.

Using equ.(5.11), equ.(5.10) can be written in short as :

$$\begin{bmatrix} \overline{H}_A \\ \overline{H}_B \end{bmatrix}_{IIi} = \begin{bmatrix} \overline{y}_1^{IIi} & \overline{y}_2^{IIi} \\ \overline{y}_2^{IIi} & \overline{y}_1^{IIi} \end{bmatrix} \begin{bmatrix} \overline{E}_A \\ -\overline{E}_B \end{bmatrix}_{IIi} \tag{5.12}$$

The relation between the transformed tangential fields components at the upper interface A of region I, can be written in the transformed domain as

$$\begin{bmatrix} -j\overline{H}_{zA} \\ \overline{H}_{xA} \end{bmatrix} = \begin{bmatrix} \overline{y}_{11}^{I} & \overline{y}_{12}^{I} \\ \overline{y}_{21}^{I} & \overline{y}_{22}^{I} \end{bmatrix} \begin{bmatrix} \overline{E}_{xA} \\ -j\overline{E}_{zA} \end{bmatrix} \tag{5.13}$$

The block matrices $\overline{y}_{ij}^{I}$ are determined according to the substrate type in eqs.(3.61) and (3.121). This equation, equ.(5.13), can be written as

$$\overline{H}_A = \overline{y}_1^{I}\, \overline{E}_A \tag{5.14}$$

Analogously, according to equ.(4.23), the following relation holds at the lower interface B of the region III in the transformed domain,

$$\begin{bmatrix} j\overline{H}_{zB} \\ -\overline{H}_{xB} \end{bmatrix} = \begin{bmatrix} \overline{y}_{11}^{III} & \overline{y}_{12}^{III} \\ \overline{y}_{21}^{III} & \overline{y}_{22}^{III} \end{bmatrix} \begin{bmatrix} \overline{E}_{xB} \\ -j\overline{E}_{zB} \end{bmatrix} \tag{5.15}$$

Where the matrices y_{ik}^{III} are given by equ.(3.61) or equ.(3.121). In short, equ.(5.15) can be written as

$$\overline{H}_B = -\overline{y}_1^{III}\, \overline{E}_B \tag{5.16}$$

5.4 FIELD MATCHING RELATIONS

Since the transformations mentioned before are different, the field matching at the interfaces A and B has to be done in the spatial domain. Knowing that both the tangential electric and magnetic field components vanish within a perfect conductor. Applying the fields continuity conditions at the interface of the intermediate region A, in the original domain for the magnetic field, we get

$$\begin{aligned} H_x &= J_z \\ H_z &= -J_x \end{aligned} \tag{5.17}$$

Using the above equalities and substituting them into the field components at the intermediate regions interface, we get for the interface A

$$E^I_{xA} = \begin{bmatrix} 0 \\ E^{II1}_{xA} \\ 0 \\ E^{II2}_{xA} \\ \vdots \end{bmatrix};\ E^I_{zA} = \begin{bmatrix} 0 \\ E^{II1}_{zA} \\ 0 \\ E^{II2}_{zA} \\ \vdots \end{bmatrix};\ H^I_{xA} = \begin{bmatrix} J^1_{zA} \\ H^{II1}_{xA} \\ J^2_{zA} \\ H^{II2}_{xA} \\ \vdots \end{bmatrix};\ H^I_{zA} = \begin{bmatrix} -J^1_{xA} \\ H^{II1}_{zA} \\ -J^2_{xA} \\ H^{II2}_{zA} \\ \vdots \end{bmatrix} \tag{5.18}$$

And similarly for the interface B

$$E^{III}_{xB} = \begin{bmatrix} 0 \\ E^{II1}_{xB} \\ 0 \\ E^{II2}_{xB} \\ \vdots \end{bmatrix};\ E^{III}_{zB} = \begin{bmatrix} 0 \\ E^{II1}_{zB} \\ 0 \\ E^{II2}_{zB} \\ \vdots \end{bmatrix};\ H^{III}_{xB} = \begin{bmatrix} J^1_{zB} \\ H^{II1}_{xB} \\ J^2_{zB} \\ H^{II2}_{xB} \\ \vdots \end{bmatrix};\ H^{III}_{zB} = \begin{bmatrix} -J^1_{xB} \\ H^{II1}_{zB} \\ -J^2_{xB} \\ H^{II2}_{zB} \\ \vdots \end{bmatrix} \tag{5.19}$$

In these equations (5.18) and (5.19) the subscripts 1,2,... in the current densities, designate the 1st, 2nd,... conductors and in the field components mark the 1st, 2nd,... intermediate regions. Transforming equ.(5.14) back to spatial domain and using equ.(5.18) we get

$$\begin{bmatrix} jJ_{xA}^{1} \\ -jH_{zA}^{II1} \\ jJ_{xA}^{2} \\ -jH_{zA}^{II2} \\ \vdots \\ J_{zA}^{1} \\ H_{xA}^{II1} \\ J_{zA}^{2} \\ H_{xA}^{II2} \\ \vdots \end{bmatrix} = \begin{bmatrix} T_h^I & \\ & T_e^I \end{bmatrix} \begin{bmatrix} \bar{y}_{11}^I & \bar{y}_{12}^I \\ \bar{y}_{21}^I & \bar{y}_{22}^I \end{bmatrix} \begin{bmatrix} T_h^{I\,-1} & \\ & T_e^{I\,-1} \end{bmatrix} \begin{bmatrix} 0 \\ E_{xA}^{II1} \\ 0 \\ E_{xA}^{II2} \\ \vdots \\ 0 \\ -jE_{zA}^{II1} \\ 0 \\ -jE_{zA}^{II2} \\ \vdots \end{bmatrix} \tag{5.20}$$

This system can be decomposed into two independent subsystems; one system describes the connection between the field components in the slot regions and the other allows the calculation of the currents. To achieve this decomposition, we introduce the following abbreviations,

$$H_A^{II} = \begin{bmatrix} -jH_{zA}^{II1} \\ -jH_{zA}^{II2} \\ \vdots \\ H_{xA}^{II1} \\ H_{xA}^{II2} \\ \vdots \end{bmatrix}; \quad E_A^{II} = \begin{bmatrix} E_{xA}^{II1} \\ E_{xA}^{II2} \\ \vdots \\ -jE_{zA}^{II1} \\ -jE_{ZA}^{II2} \\ \vdots \end{bmatrix}; \quad J_A = \begin{bmatrix} jJ_{xA}^{1} \\ jJ_{xA}^{2} \\ \vdots \\ J_{zA}^{1} \\ J_{zA}^{2} \\ \vdots \end{bmatrix} \tag{5.21}$$

together with the reduced transformation matrix recognized by the superscript *r*, and its complement recognized by the superscript *rc*,

$$T_I^r = \begin{bmatrix} T_h^{I\,r} & \\ & T_e^{I\,r} \end{bmatrix} \quad ; \quad T_I^{rc} = \begin{bmatrix} T_h^{I\,rc} & \\ & T_e^{I\,rc} \end{bmatrix} \tag{5.22}$$

The reduced transformation matrices consist of those rows, which belong to the lines in the slot. As an example, from the square matrix T_h^I, the non-square reduced matrix $T_h^{I\,r}$ and the

non-square complementary matrix $T_h^{I\,rc}$ can be obtained by partitioning of the rows. From equ.(5.20), we get the following equations

$$H_A^{II} = T_1^r \; \bar{y}_1^I \; T_1^{r-1} \; E_A^{II} \tag{5.23}$$

$$J_A = T_1^{rc} \; \bar{y}_1^I \; T_1^{rc-1} \; E_A^{II} \tag{5.24}$$

Analogously, we obtain from equ.(5.16) with the following abbreviations

$$H_B^{II} = \begin{bmatrix} -jH_{zB}^{II\,1} \\ -jH_{zB}^{II\,2} \\ \vdots \\ H_{xB}^{II\,1} \\ H_{xB}^{II\,2} \\ \vdots \end{bmatrix}; \quad E_B^{II} = \begin{bmatrix} E_{xB}^{II\,1} \\ E_{xB}^{II\,2} \\ \vdots \\ -jE_{zB}^{II\,1} \\ -jE_{ZB}^{II\,2} \\ \vdots \end{bmatrix}; \quad J_B = \begin{bmatrix} jJ_{xB}^1 \\ jJ_{xB}^2 \\ \vdots \\ J_{zB}^1 \\ J_{zB}^2 \\ \vdots \end{bmatrix} \tag{5.25}$$

the equations

$$-H_B^{II} = T_{III}^r \; \bar{y}_1^{III} \; T_{III}^{r-1} \; E_B^{II} \tag{5.26}$$

$$J_B = T_{III}^{rc} \; \bar{y}_1^{III} \; T_{III}^{rc-1} \; E_B^{II} \tag{5.27}$$

The inverse transformation to the original domain of equ.(5.12) yields

$$\begin{bmatrix} H_A^{IIi} \\ H_B^{IIi} \end{bmatrix} = \begin{bmatrix} T_{II}^i & \\ & T_{II}^i \end{bmatrix} \begin{bmatrix} \bar{Y}_1^{IIi} & \bar{Y}_2^{IIi} \\ \bar{Y}_2^{IIi} & \bar{Y}_1^{IIi} \end{bmatrix} \begin{bmatrix} T_{II}^i & \\ & T_{II}^i \end{bmatrix}^{-1} \begin{bmatrix} E_A^{IIi} \\ -E_B^{IIi} \end{bmatrix} \tag{5.28}$$

with

$$T_{II}^i = \begin{bmatrix} T_{hi}^{II} & \\ & T_{ei}^{II} \end{bmatrix} \tag{5.29}$$

Where T_{hi}^{II} and T_{ei}^{II} are the specific transformation matrices for each intermediate region i.

In order to achieve a combination of the equations of all slot regions II^i to only one equation, the vectors H^{IIi} and E^{IIi} must be divided in parts with x and z components and arranged in the same order as the components in the vectors of eqs.(5.21) and (5.25).

To this end, block matrices are constructed from the sub-matrices of $\bar{y}_1^{II_i}$ and $\bar{y}_2^{II_i}$ according to the following form with the subscript k = 1,2.

$$\begin{aligned} \bar{y}_{k,11}^{II} &= diag\left\{\bar{y}_{k,11}^{IIi}\right\} \\ \bar{y}_{k,22}^{II} &= diag\left\{\bar{y}_{k,22}^{IIi}\right\} \\ \bar{y}_{k,12}^{II} &= quasidiag\left\{\bar{y}_{k,12}^{IIi}\right\} \\ \bar{y}_{k,21}^{II} &= quasidiag\left\{\bar{y}_{k,21}^{IIi}\right\} \end{aligned} \tag{5.30}$$

These four matrices are now combined to only one block matrix for k = 1,2 as

$$\bar{y}_k^{II} = \begin{bmatrix} \bar{y}_{k,11}^{II} & \bar{y}_{k,12}^{II} \\ \bar{y}_{k,21}^{II} & \bar{y}_{k,22}^{II} \end{bmatrix} . \tag{5.31}$$

Now, we form block matrices from the individual transformations matrices according to

$$T_H^{II} = diag\left(T_{hi}^{II}\right) = \begin{bmatrix} T_{h1}^{II} & & & \\ & \ddots & & \\ & & T_{h2}^{II} & \\ & & & \ddots \\ & & & & T_{hp}^{II} \end{bmatrix} \tag{5.32}$$

and

$$T_E^{II} = diag\left(T_{ei}^{II}\right) = \begin{bmatrix} T_{e1}^{II} & & & \\ & \ddots & & \\ & & T_{e2}^{II} & \\ & & & \ddots \\ & & & & T_{ep}^{II} \end{bmatrix} \tag{5.33}$$

where the subscript p, designates the total number of slots (see Fig. 5.3).

Using the two blocks of eqs.(5.32) and (5.33), we get a single super block matrix defined as

$$T_{II} = diag\left(T_H^{II}, T_E^{II}\right) = \begin{bmatrix} T_H^{II} & \\ & T_E^{II} \end{bmatrix} \tag{5.34}$$

On the other hand, the complete equation can be written for the field components in the slot regions of the interface A and B in the following form

$$\begin{bmatrix} H_A^{II} \\ H_B^{II} \end{bmatrix} = \begin{bmatrix} T_{II} & \\ & T_{II} \end{bmatrix} \begin{bmatrix} \overline{Y}_1^{II} & \overline{Y}_2^{II} \\ \overline{Y}_2^{II} & \overline{Y}_1^{II} \end{bmatrix} \begin{bmatrix} T_{II} & \\ & T_{II} \end{bmatrix}^{-1} \begin{bmatrix} E_A^{II} \\ -E_B^{II} \end{bmatrix} \tag{5.35}$$

Substituting eqs.(5.23) and (5.26) into the left hand side of equ.(5.35), the indirect eigen value problem results,

$$\left(\begin{bmatrix} T_{II} & \\ & T_{II} \end{bmatrix} \begin{bmatrix} \overline{Y}_1^{II} & \overline{Y}_2^{II} \\ \overline{Y}_2^{II} & \overline{Y}_1^{II} \end{bmatrix} \begin{bmatrix} T_{II} & \\ & T_{II} \end{bmatrix}^{-1} - \begin{bmatrix} T_I^r & \\ & T_{III}^r \end{bmatrix} \begin{bmatrix} \overline{Y}^I & \\ & \overline{Y}^{III} \end{bmatrix} \begin{bmatrix} T_I^r & \\ & T_{III}^r \end{bmatrix}^{-1} \right) \begin{bmatrix} E_A^{II} \\ -E_B^{II} \end{bmatrix} = 0 \tag{5.36}$$

that can be simplified to

$$\left[Y(\varepsilon_{re}) \right] \begin{bmatrix} E_A^{II} \\ -E_B^{II} \end{bmatrix} = 0 \tag{5.37}$$

The homogeneous system (5.37) is an indirect eigen value problem, similar to the one described in the previous chapter for the zero thickness case, from which the propagation constant can be determined. The nonzero subvectors of the electric field vector E_A and E_B are then calculated to be the eigen vector corresponding to the eigen value ε_{re}. After that, the current density vectors J_A and J_B are obtained using eqs.(5.24) and (5.27). Organizing these vectors in their original form and introducing all the zero subvectors for both electric field and current density, all the electric or magnetic field components can be evaluated at each metallization interface i, after which they can be evaluated at all other dielectric interfaces at any position along each discretization line of the structure.

Note that, it is possible to develop a homogeneous system of equations (indirect eigen value system) similar to equ.(5.37) for the current densities on the metallizations, in the case of smaller strip widths rather than slot regions.

5.5 RESULTS AND DISCUSSION

In this part, using the developed mathematical procedure discussed earlier for the finite thickness case, some simulation examples are presented for the finite thickness open structures. The software developed for this purpose covers a large class of structures, of which single strip, coupled strips, edge-coupled strips, broadside coupled strips, and other multistrip structures.

1. Convergence behavior

Firstly, the convergence behavior is treated as a function of the number of discretization lines on the strip of finite thickness t. Fig. 5.4 shows the convergence behavior of a single finite thickness strip for an open structure. The effective dielectric constant is computed as a function of the number of discretization lines M on the strip for different normalized substrate thickness d/λ_0. Fig. 5.5 presents the variations in the dielectric constant as a function of the normalized discretization interval h/a. In Fig. 5.6, the rate of convergence is given in a form of an error $\varepsilon_{re}/\varepsilon_{re0}$, where ε_{re0} is the extrapolated solution for the effective dielectric constant at h=0. It shows that the higher the value of the normalized substrate thickness d/λ is, the faster is the convergence behavior. This presented results are in accordance with the published ones in references [11,48] for closed boundaries using the Method of Lines.

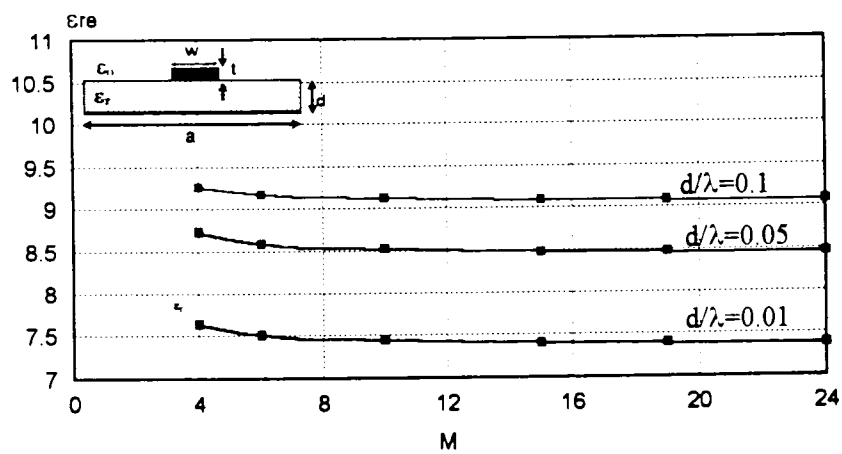

Fig. 5.4 Effective permittivity versus number of lines M on strip
d=1mm; rb=9; ra=16; rw=3; rt=0.1; ε_r=9.7

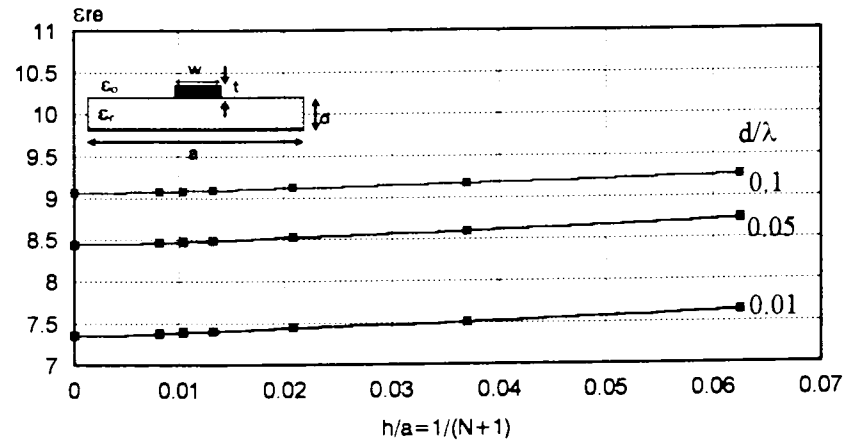

Fig. 5.5 Effective permittivity versus normalized discretization intervals (h/a)
d=1mm; rb=9; ra=16; rw=3; rt=0.1; ε_r=9.7

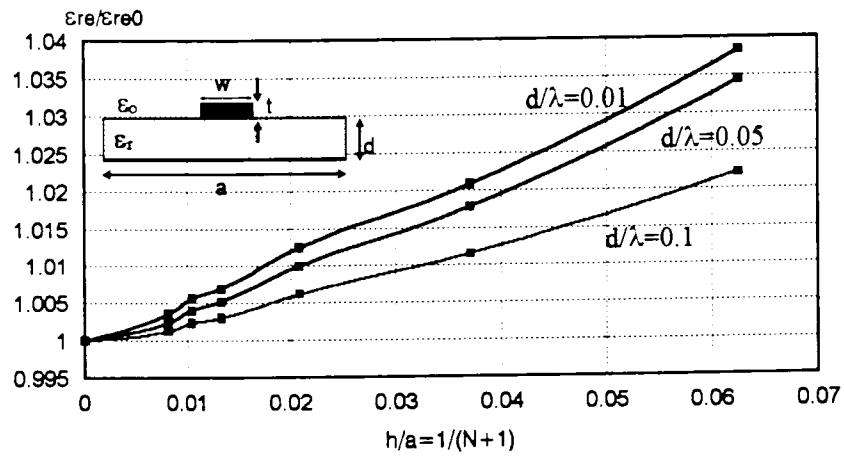

Fig. 5.6 Convergence error for different normalized substrate thickness d/λ
d=1mm; rb=9; ra=16; rw=3; rt=0.1; ε_r=9.7

2. Dispersion characteristics as a function of strip thickness t

The dispersion curves of a finite thickness microstrip line is shown in Fig. 5.7, in which the dielectric constant is given as a function of the metallization strip thickness t for different strip normalized widths w/d. It is found that increasing the strip thickness t leads to a decrease in the effective dielectric constant, which is in turn, is inversely related to the strip width w and to the normalized substrate thickness d/λ as it is clearly indicated in Fig. 5.8.

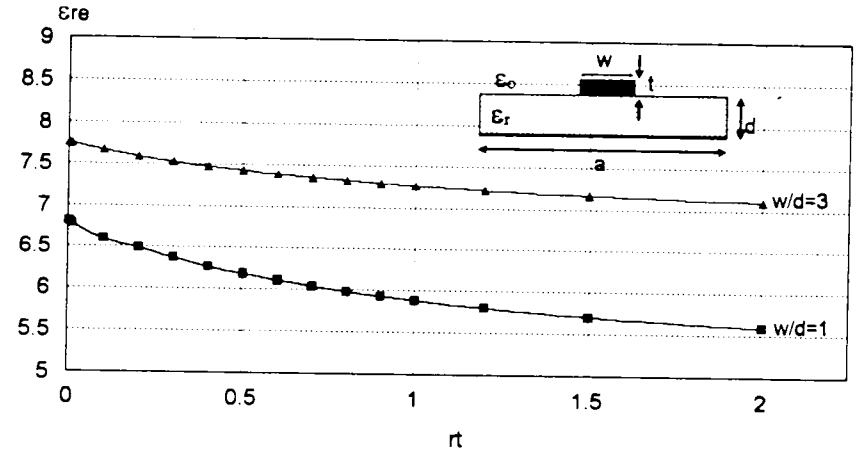

Fig. 5.7 Effective permittivity versus strip thickness rt=t/d
d=1mm; rb=9; ra=16; ε_r=9.7; f=5GHz.

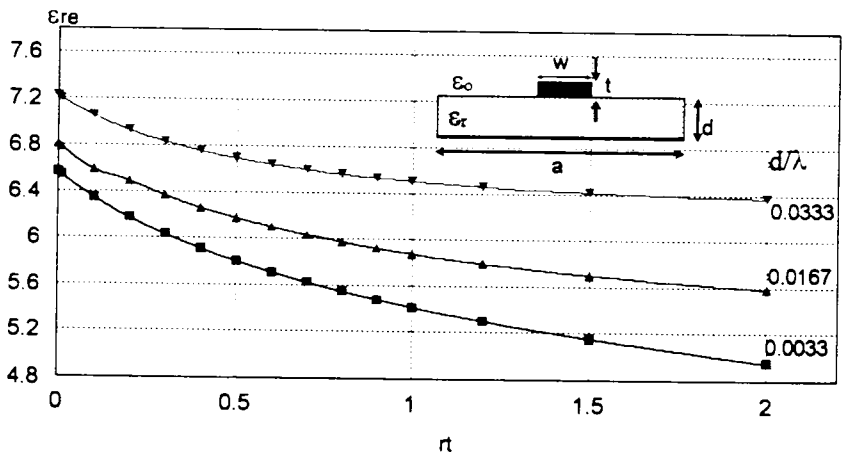

Fig. 5.8 Effective permittivity versus rt
d=1mm; rb=9; ra=16; rw=1; ε_r=9.7

In Fig. 5.9, the effective dielectric constant is considered for both ABC and CB analysis. The difference is apparent in the low frequency range, where the value of the effective dielectric constant is shown to be a bit greater using ABC's. Dispersion curves are also given for different normalized metallization strip widths w/d in Fig. 5.10, where an increase in this last parameter leads to an increase in the effective dielectric constant.

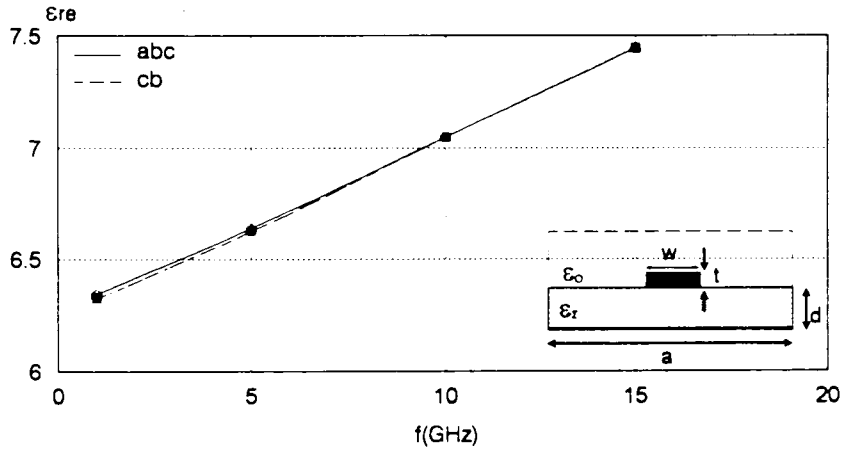

Fig. 5.9 Dispersion for both ABC and CB
d=1mm; rb=9; ra=16; rw=1; rt=0.1; ε_r=9.7

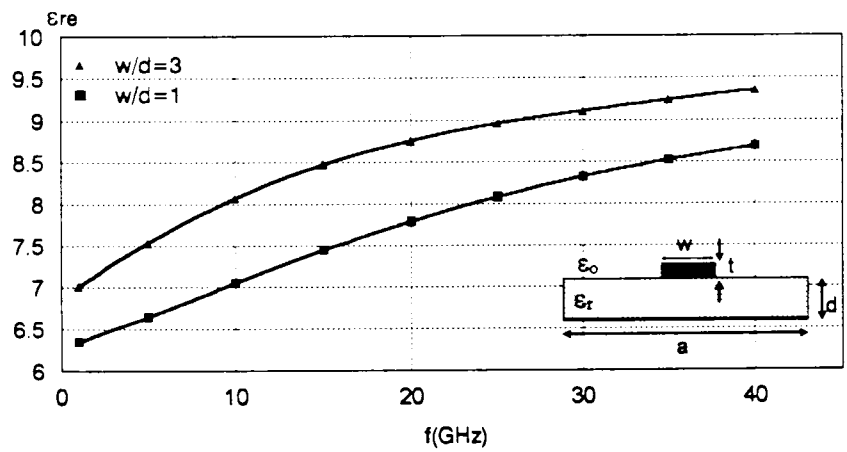

Fig. 5.10 Dispersion curves. Microstrip width effect
d=1mm; rb=9; ra=16; rt=0.1; t/w=0.3 and t/w=0.1; ε_r=9.7

3. The suspended and the suspended inverted microstrip line

The variations in the dispersion characteristics of a suspended microstrip line structure are shown in Fig. 5.11, where it is observed that the effective dielectric constant is inversely related to the finite metallization thickness t. On the other hand, the dispersion diagram of a suspended inverted microstrip line is presented in Fig. 5.12, where the same behavior observed in Fig. 5.11 holds.

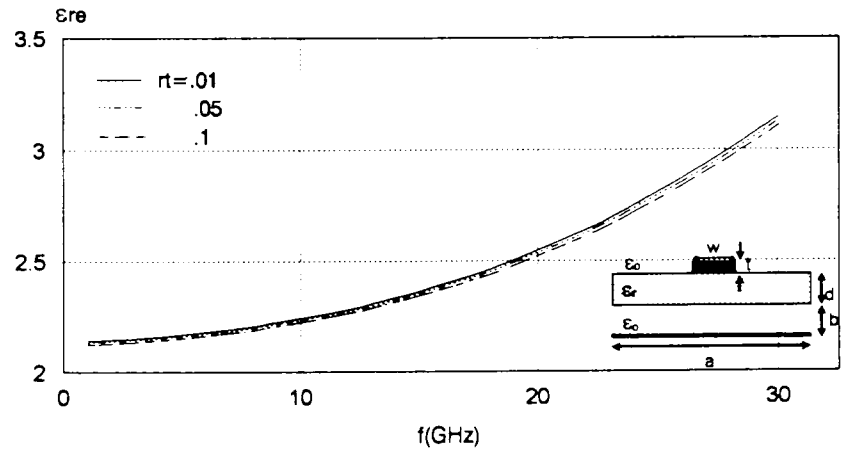

Fig. 5.11 Dispersion curves for a suspended microstrip line
d=.6mm; a=13mm; rb_1=1; rb_2=100; w=3mm; M=10; ε_r=8.875

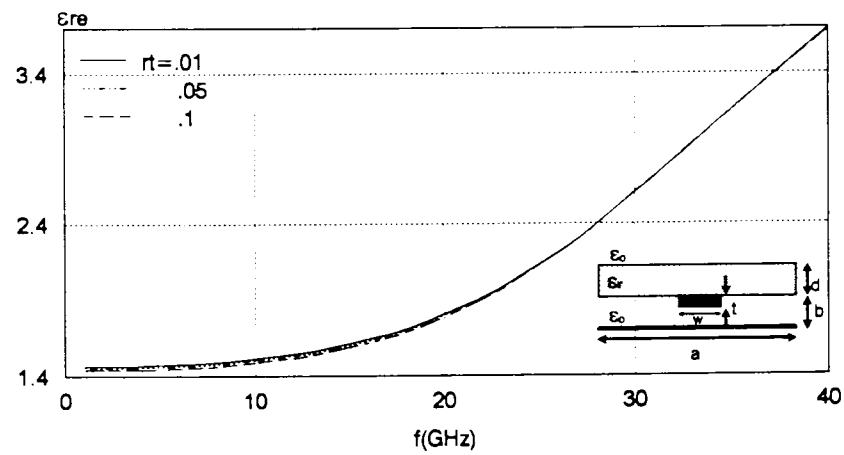

Fig. 5.12 Dispersion diagram for a suspended inverted microstrip line
d=.6mm; a=13mm; rb_1=1; rb_2=100; w=3mm; M=10; ε_r=8.875

4. The edge-coupled microstrip lines

The odd, even, and higher order modes effective permittivities of an edge-coupled microstrip lines are plotted in Figs. 5.13 and 5.14 for two different metallization strip widths rt=0.01 and rt=0.1 respectively. The dispersion effect of this structure is characterized by the existence of higher order modes at relatively low frequencies, mainly, with increasing metallization thickness t. A comparison between the dominant modes for the two distinct metallization thickness rt=0.1 and rt=0.01 is given in Fig. 5.15. It is observed from this last figure that, with increasing metallization thickness t, the effective dielectric constant decreases. It is also apparent that the decrease rate for the odd mode is greater than the decrease rate of the even mode.

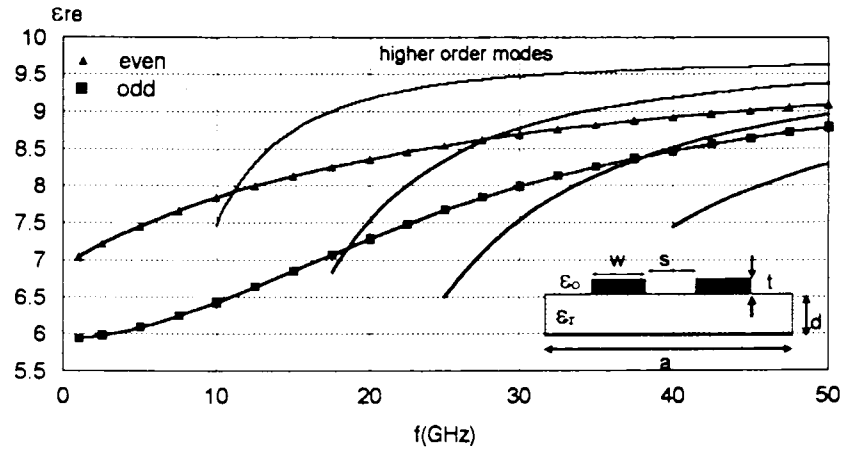

Fig. 5.13 Dispersion characteristics for an edge-coupled microstrip lines
d=1mm; rw=1; rs=1.5; ra=13.5; rb=50; rt=0.01; ε_r=9.7;

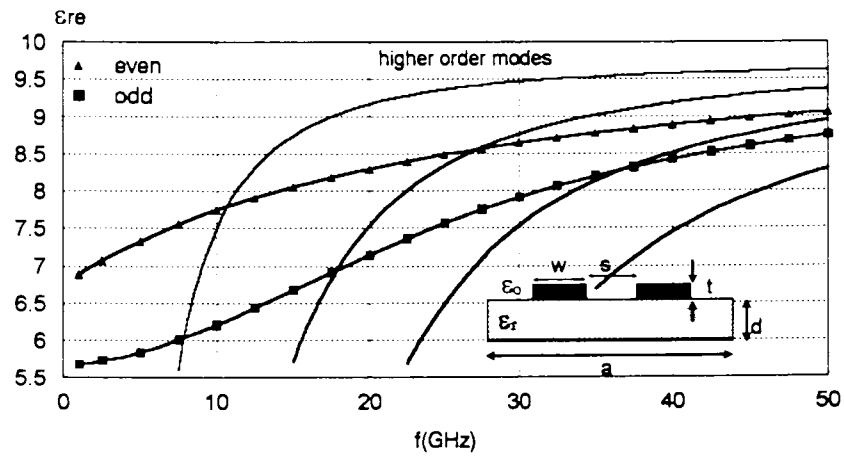

Fig. 5.14 Dispersion characteristics for an edge-coupled microstrip lines
d=1mm; rw=1; rs=1.5; ra=13.5; rb=50; rt=0.1; ε_r=9.7;

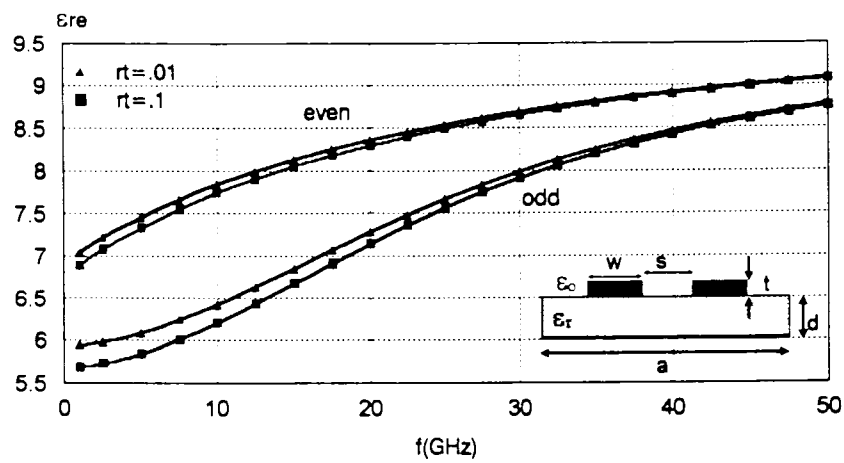

Fig. 5.15 Effect of metallization thickness t for an edge-coupled microstrip lines
d=1mm; rw=1; rs=1.5; ra=13.5; rb=50; ε_r=9.7

5. The suspended edge-coupled microstrip

The dispersion diagrams of the suspended edge-coupled microstrip lines is presented in Figs. 5.16 to 5.18. The two dominant even and odd modes for the effective permittivity of Fig. 5.16, show an inverse dependence to the dimension b of the introduced air layer as compared to the results of Fig.5.15. The effect of closed boundaries, which is presented in Fig. 5.17, is shown to affect highly the odd mode rather than the even mode. In Fig. 5.18, the upper ground plane effect is introduced for the edge-coupled stripline configuration, where the ratio b_2/d is found to be proportional to both the even and the odd modes effective dielectric constants.

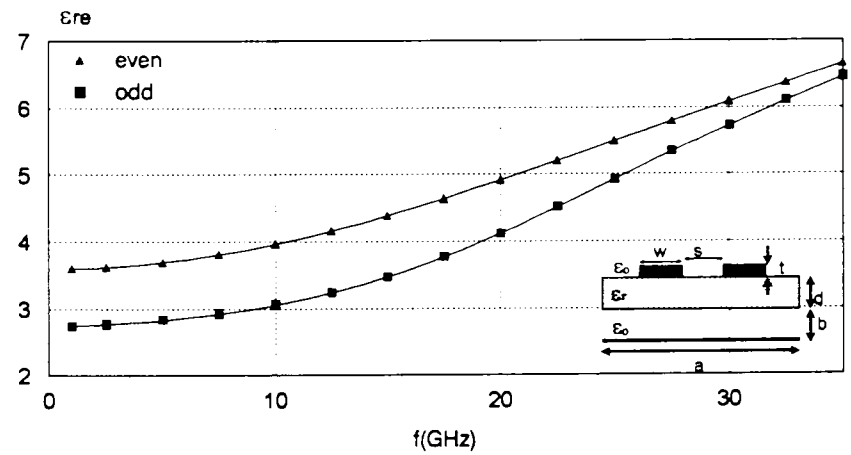

Fig. 5.16 Dispersion for suspended edge-coupled microstrips
d=1mm; rw=3; rs=1.5; ra=17.5; rb=0.5; rt=0.01; ε_r=10.2

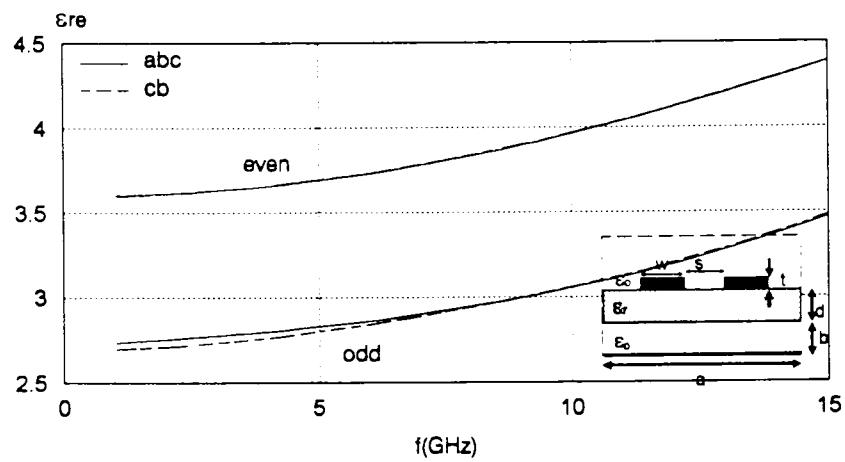

Fig. 5.17 Dispersion diagram for ABC and CB suspended edge-coupled strips
d=1mm; rw=3; rs=1.5; ra=17.5; rb=0.5; rt=0.01; ε_r=10.2

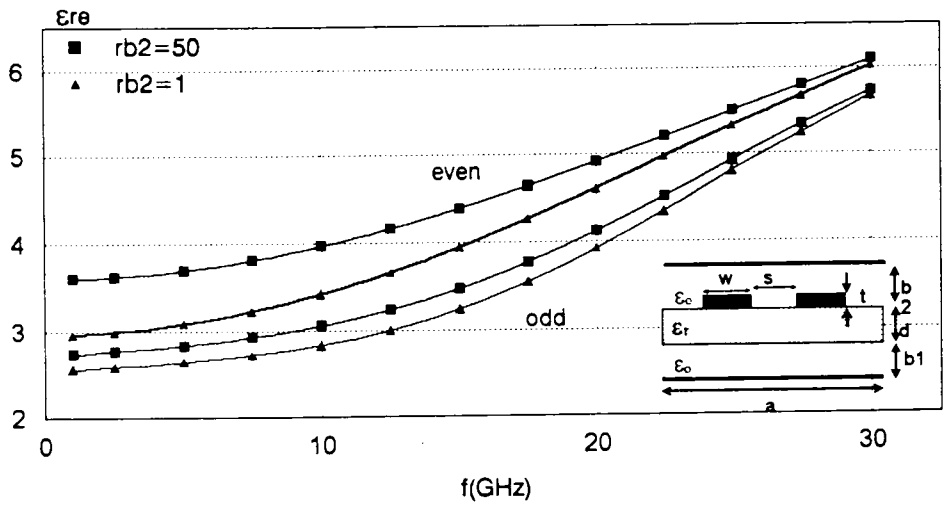

Fig. 5.18 Effect of upper bound on effective permittivity edge-coupled strips
d=1mm; rw=3; rs=1.5; ra=17.5; rb_1=0.5; rt=0.01; ε_r=10.2;

6. The broadside and the broadside-edge coupled suspended strip lines

Two more examples of interest are given in Figs. 4.19 and 4.20. The first one depicts the variation of the dominant odd and even modes effective dielectric constants of a broadside-coupled suspended striplines for rb_2=1, and rb_2=100 which simulates the open structure. The latter, shown in Fig. 5.20, reveals the variations of the four modes effective permittivity constants of a broadside-edge coupled suspended microstrip structure as a function of frequency for both open and stripline configuration with rb_2=2. From these two figures, it is observed that, as the ratio b_2/d increases the effective dielectric constant increases. The variation in the effective dielectric constant for both cases is also observed to be very small. A similar behavior has been already encountered during the analysis of the zero thickness case.

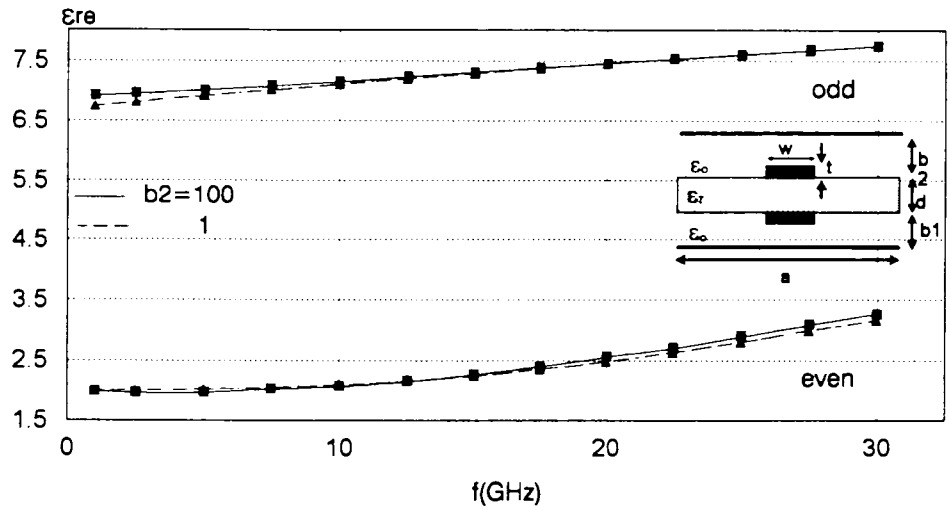

Fig. 5.19 Dispersion curve for broardside-coupled strips
d=.6mm; a=10.6mm; ra=17.6667; rb_1=2; rt=0.01; rw=1; ε_r=9.6

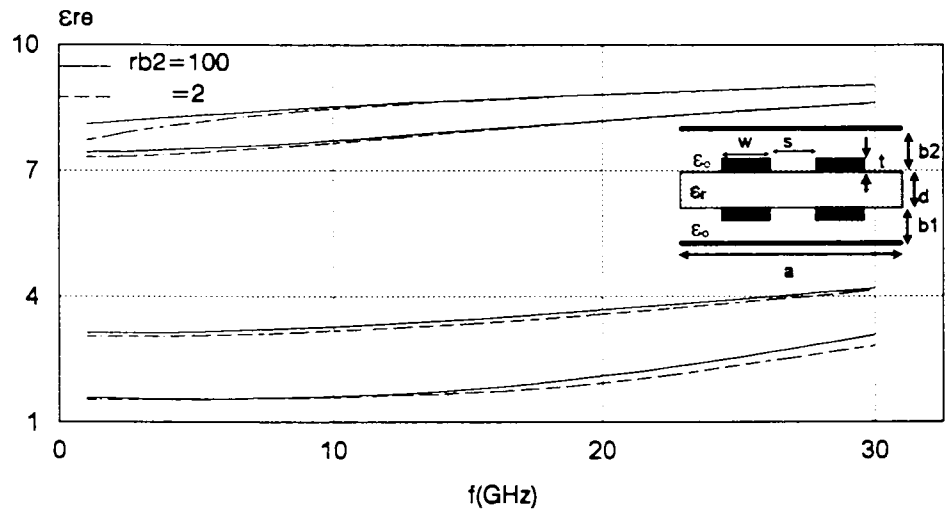

Fig. 5.20 Dispersion diagram for broardside-edge coupled strips structures
d=.6mm; a=12.2mm; rb_1=2; rt=0.01; w=1mm; s=1mm; M=5; ε_r=10.2

5.6 CONCLUSION

In this chapter, the Method of Lines has been extended to the full-wave characterization of finite thickness metallizations open MIC and MMIC structures. Due to the nature of the discretization scheme of this method, a new set of difference operators are introduced to describe the field behavior in the slot regions at the level of the metallizations thickness. This new mixed difference operators are the result of the existence of both absorbing boundary and closed boundary conditions. Using this development, a large class of structures can be efficiently handled.

On the other hand, we have developed a software package that can handle the characterization of a variety of finite thickness metallizations structures such as, single microstrip, suspended microstrip, edge-coupled lines, broadside-coupled lines, and other complex finite thickness structures with both isotropic and anisotropic dielectric substrates.

The results obtained through the simulation of the developed mathematical algorithm have shown their efficiency and a total accordance compared with the published data in the literature has been observed

GENERAL CONCLUSION

The work presented in this thesis is the reflection of an extensive study of open planar and quasi-planar MIC and MMIC structures using the Absorbing Boundary Conditions. The Method of Lines is used as a numerical tool, which has shown a very good efficiency in calculations and ease in handling through both analysis and software realization.

The development of the necessary mathematical tools and transformations is firstly carried out for the Full-Wave characterization of both zero-thickness and finite-thickness metallization strips open structures. The study done is exhaustive and general, it involves various kinds of MIC and MMIC structures, starting form a single metallization with a single dielectric substrate to multiple metallization interfaces with multiple dielectric substrate structures. Both isotropic and anisotropic dielectric layers are considered with both uniform and nonuniform discretization schemes.

Secondly, we have developed the needed algorithms for the implementation of a software package for simulating the forgoing theory. The software we have developed is based on the MATLAB programming, which is found to be very convenient in handling such indirect eigen value problems. It handles a complete characterization of the studied structures, of which, the effective dielectric constant, the electric and magnetic fields, the current elements, and the characteristic impedance that can be easily computed for both isotropic and anisotropic substrate with zero and finite thickness strips.

A wide class of structures such as,

- Microstrip line structures
- Suspended microstrip structures
- Suspended inverted microstrip structures
- Multi-conductors edge-coupled structures
- Broadside-coupled structures
- Broadside-edge coupled structures

and some others of their combinations can be completely characterized. The software is designed to be adaptable to other complex structures.

The results obtained are in accordance with the results previously published in papers and references using other methods of analysis. Some of the results are compared with those obtained using Closed Boundaries, because of the lack of data for open type structures for both zero thickness and finite thickness metallization.

Through the present work, using the Absorbing Boundary conditions, the Method of Lines has been extended to the analysis of open planar and quasi-planar waveguiding structures, where the computational domain can be further reduced. This leads to a reduced number of discretization lines, and so, it saves great time and memory requirements. One disadvantage using the Absorbing Boundary development is sensed for the case of multi-layered structures, due to the nature of the conducted analysis concerning the field matching between different dielectric interfaces, which has to be done in the original domain.

REFERENCES

[1] T. C. Edwards, Foundations for microstrip circuit design, New York : J. Wiley & Sons, 2nd Ed, 1992.

[2] I. Kasa, Microwave Integrated Circuits, Studies in Electrical and Electronic : Elsevier, 1991.

[3] E. Yamashita, Analysis Methods for Electromagnetic Wave Problems, Boston : Artech House, 1990.

[4] M. N. O. Sadiku, Numerical Techniques in Electromagnetics, Florida : CRC Press, 1992.

[5] V.N. Faddeeva, " The Method of Lines applied to certain boundary value problems ," *Tr. matem. in-ta im. V.A. Steklova*, 28, 73-103, 1949.

[6] A. Liskovets, "The method of lines, Review," *Differential'nye Uravneniya*, Vol.1, no.12 pp 662-1678, 1965.

[7] U. Shulz and R. Pregla, " A New technique for the Analysis of the Dispersion Characteristics of Planar waveguides ," AEÜ, band. 34, Half 4, pp. 169-173, 1980.

[8] U. Schulz and R. Pregla, " A New Technique for the analysis of the Dispersion Characteristics of Planar waveguides and its Application to Microstrip with Tuning Septums ," Radio Science 16, No. 6, pp. 1173-1178, 1981.

[9] A. C. Keen, M. J. Wale, M. I. Sobhy and A. J. Holden, " quasi-static analysis of elctrooptic modulators by the method of lines, " J. Lightwave Technol., vol.8, pp. 42-50, 1990.

[10] U. Rogge and R. Pregla, " The Method of Lines for the Analysis of Strip-Loaded Optical Waveguides, " ,1991.

[11] R. Pregla and W. Pasher, " The method of lines " in Numerical Techniques for Microwave and Millimeter wave Passif Structures, T. Itoh, Ed. New-York : Wiley, 1989, pp. 381-446.

[12] S. B. Worm and R. Pregla, " Hybrid Mode Analysis of Arbitrary Shaped Planar Microwave Structures by the Method of Lines," *IEEE Trans.*, MTT-32, No. 6, pp. 633-638, 1984.

[13] R. H. Diestel, " Analysis of Planar Multiconductor Transmission-line Systems with the Mehod of Lines ," Arch. Elecktron. & Ubertragungstech., 41, pp. 169-175, 1987.

[14] W. Veit, H. R. Diestel, and R. Pregla, " Coupling of Crossed Planar Multiconductor systems," *IEEE Trans.*, MTT-38, No. 3, pp. 265-269, 1990.

[15] F. Gardiol, Microstrip Circuits, New York : J. Wiley & Sons 1994.

[16] B. Engquist and A. Majda, "Absorbing boundary conditions for the numerical simulation of waves," Math. Comput., vol. 31, pp. 629-651, July 1977.

[17] R. Clayton and B. Engquist, "Absorbing boundary conditions for acoustic and elastic wave equations," Bulletin of the seismological society of America, vol. 67, No. 6, pp. 1529-1540, 1977.

[18] U. Schulz, " On the Edge condition with the method of Lines in Planar Waveguides ", Arch. Elekron. Uebertragungstech., 34, pp. 176-178, 1980.

[19] J. Meixner, " The Behavior of Electromagnetic fields at edges ", IEEE Ap-20, pp. 442-446, 1972.

[20] D. Mirshekar-Syahkal, Spectral Domain Method for Microwave Integarted Circuits, Research Studies Press, New York : J. Wiley & Sons 1990.

[21] H. Diestel and S. B. Worm, " Analysis of Hybrid Field Problems by the Method of Lines with nonequidistant Discretization ", *IEEE Trans.*, MTT-32, No. 6, pp. 633-638, 1984.

[22] W. C. Chew, Electromagnetic fields in nonhomogeneous media. New York : VNR, 1990.

[23] T. G. Moore, J. G. Blaschak, A. Taflove, G. A. Kriegsmann, "Theory and application of radiation boundary operators," IEEE Trans. Antennas Propagat., vol. AP36, PP.11797-1812, DEC. 1988.

[24] A. Sommerfeld, Partial Differential Equations in Physics. New York: Academic Press, 1967.

[25] A. Bayliss, and E. Turkel, "Radiation boundary conditions for wave-like equations," Commun. Pure Appl. Math. Vol. 23, pp. 707-725, 1980.

[26] G. A. Kriegsmann, and C. S. Morawetz, "Numerical solutions of exterior problems with the reduced wave equation," J. Comput. Phys., Vol. 28, pp. 181-197, 1979.

[27] S. N. Karp, "A convergent far-field expansion for two-dimensional radiation function," Commun. Pure Appl. Math. Vol. 14, pp. 427-434, 1961.

[28] A. Bayliss, M.Gunzburger, and E. Turkel, "Boundary conditions for the numerical solution of elliptic eqautions in exterior regions," SIAM J. Appl. Math., Vol. 42, pp. 430-451, 1982.

[29] L. Halpern, and L. N. Trefethen, "Wide-angle one way wave equations," Dept. Math., Mass. Inst. Technol., Cambridge, Numerical Analysis Rep. 86-5, July 1986.

[30] L. N. Trefethen, and L. Halpern, "Well-posedness of one way wave equations and absorbing boundary conditions," Math. Comput., vol. 47, pp. 421-435, October 1986.

[31] A. Dreher, and R. Pregla, "Analysis of planar waveguides with the method of lines and absorbing boundary conditions," IEEE Microwave and Guided Wave Letters, vol. 1, No. 6, PP. 138-140, 1991.

[32] A. Dreher, and R. Pregla, " Full-wave analysis of radiating planar resonators with the method of lines," *IEEE trans.*, MTT-41, No. 8, pp. 1361-1368, 1993.

[33] R.E. Collin , Field Theory of Guided Waves, Mc Graw-Hill, New-York, 1960.

[34] A. J. Baden Fuller, Microwaves, An introduction to Microwave Theory and Techniques, Oxford : Pergamon press 1979.

[35] A. OUADI, Hybrid-Mode Analysis of Microwave and Millimeter-wave structures of Realistic Configuration, Magister Thesis, INELEC, No. 03/95, 1995.

[36] B. M. Sherill and N. Alexopoulos, " The method of lines applied to a finline/strip configuration on an anisotropic substrate, " *IEEE Trans.*, MTT-35, pp. 568-575, 1987.

[37] N.G. Alexopoulos, " Integrated-circuit structures on anisotropic substrates, " *IEEE Trans.*, MTT-33, pp. 847-881, 1985.

[38] M. Kobayashi, " Analysis of the Microstrip and the Electrooptic light Modulator ", *IEEE Trans.*, MTT-26, N.2, pp. 119-126Feb. 1978.

[39] A. Nakatani and N. G. Alexopoulos, " Toward a generalized algorithm for the modeling of the dispersive properties of integrated circuit structures on anisotropic substrates, "*IEEE Trans.*, MTT-33, No. 12, pp. 1436-1441, 1985.

[40] B. E. Kretch and R. E. Collin, " Microstrip dispersion including anisotropic substrates, "*IEEE Trans.*, MTT-35, pp. 710-718, 1987.

[41] Z. Chen, and B. Gao, "Full-wave analysis of multiconductor coupled lines in MICs by the Method of Lines," IEE Proceedings, vol. 136, Pt. H, No. 5, PP. 399-404, October. 1989.

[42] Jansen R. H., " Fast Accurate Hybrid mode Computation of Non-Symetrical Coupled Microstrip Characteristics ", Proc. 7 th European Microwave Conf., pp. 135-139, 1977.

[43] R. R. Mansour and R. H. Macphie, " A unified hybrid-mode analysis for planar transmission line with multilayer isotropic/anisotropic substrates," *IEEE trans.*, MTT-35, pp. 1382-1391, 1987.

[44] T. Itoh and R. Mittra, " Spectral-Domain approach for Calculating the Dispersion Characteristics of Microstrip Lines ", *IEEE Trans.*, MTT, pp. 496-499, July 1973.

[45] X. H. Yang, and L. Shafai, " Extension of method of lines to unboundede regions by using co-ordinate transformation ", Electronics Letters, , vol. 27, No. 23, PP. 2108-2109, 1991.

[46] B. Bhat, S. Koul, Stripline-Like Transmission Lines for Microwave Integrated Circuits, New York : J. Wiley & Sons 1989.

[47] Kowalski G. and Pregla R., " Dispersion Characteristics of Sheilded Microstrip with Finite Thickness ", AEÜ pp. 193-196, 1971.

[48] R. Pregla and F. J. Scmükle, " The method of lines for the analysis of planar wave structures with finite metallization thickness, " *Kleinheubacher Berichte*, Vol.31, 431-438, 1988.

[49] J. Gerdes, K. H. Helf and R. Pregla, " Full-wave analysis of traveling-wave electrodes with finite thickness for electro-optic modulators by the method of lines, " *IEEE Trans.*, MTT-9, pp.461-467, April 1991.

[50] Jansen R. H., " High-speed Computation of the Single and Coupled Microstrip Including Dispersion, High-order modes, Loss and Finite strip Thickness ", *IEEE Trans.*, MTT-26, pp. 75-82, 1978

[51] T. Kitazawa, " Metallization thickness effect of striplines with anisotropic media : quasi-static and hybrid-mode analysis," *IEEE trans.*, MTT-35, pp. 769-775, April 1989.

[52] P.Bhartia, I. J. Bahl, Millimeter Wave Engineering and Application, New York : J. Wiley & Sons 1984.

[53] R. S. Elliot, An Introduction to Guided Waves and Microwave Circuits, New Jersey : Prentice Hall 1993.

[54] R. E. Collin, *Foundation for microwave engineering*, McGraw-Hill, pp. 34-37, 1966.

A N N E X E

Liste et composition du Jury en vue de la soutenance de mémoire de Magister en Ingenierie des Systemes Electroniques par ***Mr DAHMANI Samir.***

PRESIDENT/ : *Dr A. FARAH,* Maitre de Conference, E.N.P - ALGER

RAPPORTEUR/: *Dr H. BOURDOUCEN,* Maitre de Conference, I.N.E.L.E.C- BOUMERDES

MEMBRES/: *Dr R. AKSAS,* Maitre de Conference, E.N.P - ALGER
Dr k. BENAISSA, Maitre de Conférence, I.A.P- BOUMERDES
Dr M. YAGOUB, Maitre de Conférence,U.S.T.H.B- ALGER